NSG-1063

OPTICAL LINE RADIATION FROM URANIUM PLASMAS

BY

EDWARD LOUIS MACEDA

B.S., Manhattan College, 1970

M.S., University of Illinois, 1972

THESIS

Submitted in partial fulfillment of the requirements
for the degree of Doctor of Philosophy in Nuclear Engineering
in the Graduate College of the
University of Illinois at Urbana-Champaign, 1977

Urbana, Illinois

DEDICATION

This thesis is dedicated to my wife Bettiann who put up with me while I worked on this thesis.

ABSTRACT

The radiative-energy current due to line radiation is calculated in a U^{235} plasma over a temperature range of 5000°K to 8000°K. Also a variation in the neutron flux of $2x10^{12}$ neutrons/(cm^2-sec) to $2x10^{16}$ neutrons/(cm^2-sec) is considered. The plasma forms a cylinder with a diameter and height of one meter.

To calculate the radiative-energy current, a knowledge of the atomic state densities within the plasma is necessary. A rate equation formalism is developed to solve for the atomic state densities along with a model for the energy levels in neutral and singly-ionized uranium.

Because the electron states in uranium lie below 5eV, recombination is the principle excitation mechanism. At and above 6000°K, inversions were found and at all temperatures the line radiation at line center was greater than the corresponding black-body radiation. An example of this is the 28763 cm^{-1} to 5762 cm^{-1} transition in neutral uranium, where the Planck function at 5000°K is $6.49x10^{-6}$ ergs/cm^2 and the calculated radiative-energy current was $1.49x10^{-4}$ ergs/cm^2. There are negligible differences in the radiative-energy current at 6000°K for variations in the neutron flux. Also the average opacity, which varied from 100 to 10^5 gm/cm^2, over the frequency range of line radiation is calculated.

ACKNOWLEDGMENT

The author wishes to express sincere gratitude to Professor George H. Miley, his advisor, without whose guidance and invaluable suggestions the present work would not have been possible.

The author wishes to thank his thesis committee, especially Professor J. Verdeyen whose class on Quantum Electronics provided information for the solution to the radiative transport problem. Many of the author's colleagues, Dr. C. Bathke, R. Chilausky, R. Miller, H. Towner, and Dr. Chan Choi, to name a few, provided beneficial criticism and helpful suggestions which expedited the completion of this work. In addition, the author is grateful for the financial support from the NASA-AEC Space Power Office under Grant US NASA NSG 1063.

The author wants to express appreciation for the moral support provided by his parents and his wife Bettiann.

The author thanks Norma Elliott for the excellent typing of the thesis manuscript.

TABLE OF CONTENTS

Page

CHAPTER I. DISCUSSION OF THE PROBLEM

In a gaseous core reactor non-equilibrium radiation will be emitted from the plasma due to the presence of a non-Maxwellian electron flux and rapid recombination caused by the relatively low electron temperature. The frequency distribution and intensity of the emitted radiation are important because of the potential applications for energy conversion and chemical processing as well as the material constraints they put on the reactor design. This study is concerned with the line radiation emitted over a range of operating conditions envisioned for a gaseous core uranium reactor.[1] Thus a uranium plasma at a pressure of one atmosphere with temperatures ranging from 5000°K to 8000°K, (the boiling point of uranium being 4407°K at 1 atm) will be investigated.

Normal treatments of the problem are insufficient because of the physical parameters of this unique plasma. A "coronal" model, where the principal method of depopulating excited states is through spontaneous decay, is inadequate because of the large collisional rates due to the large electron population. An equilibrium model, where the collisional processes completely dominate state relaxation, is also inappropriate because the large non-equilibrium excited state densities lead to non-negligible radiative relaxation from excited states. Hence, the state densities are explicitly calculated using a rate equation approach[2,3] and then the emitted radiation is evaluated.

The plasma conditions cited above are characteristic of a subcritical uranium plasma. Critical reactors have higher temperatures (center line temperatures of 40,000°K) and pressures (approaching 500 atmospheres[4]). However, the results of these calculations should be applicable to the

outer layers of a critical reactor. Also, this temperature range encompasses the 6000°K temperature of the proposed 5 Megawatt Los Alamos experimental reactor.[5]

In addition to the effect of a temperature variation, a change of the neutron flux of 2×10^{12} to 2×10^{16} neutrons/(cm^2-sec) is considered. Finally, the effect of the size of the plasma on the emitted radiation is studied. The sizes of interest range from a cylinder 4-cm diameter and 18-cm long[6] to a larger size corresponding to the Los Alamos experimental[7] plasma of 105.5-cm long and 102.4 cm in diameter.

A. Previous Work Related to the Problem

NASA has been interested in a gaseous core reactor for space propulsion purposes for approximately ten years. Much of the early work was carried out by workers at United Aircraft[8] who assumed the plasma emission had a black-body spectrum. The first detailed calculation for uranium was carried out by Parks et al[9] at General Atomic. The underlying assumption in their work was that equilibrium statistics can be used to determine state densities within the plasma. However, recent studies[10,11] have shown that a gas in the presence of a neutron-induced source will not have a Boltzmann distribution of excited states. This is because a non-Maxwellian electron flux is produced within the plasma. Also, at the high ion and electron densities, recombinational excitation becomes an important mechanism.[12]

An early treatment of radiation transport in a plasma was done by Holstein[13,14] in which he considered trapping of resonance radiation. His results are significant because he showed the importance of considering the frequency dependence of the absorbing medium. However, an exact

calculation of the density of excited states and non-equilibrium excitation mechanisms were ignored in his analysis. A later analysis[15] assumed an excitation temperature for a transition and then used a thermodynamic source term for the emitted radiation. Pomraning[16] formulated the source term through a rate equation formulation, and then did some sample calculations in a slab geometry. Later the concept of multi-temperature electrons was used by Eddy[17,18] where a finite number of excitation temperatures was used.

In the present analysis a rate equation approach is used to calculate the excited state densities. Unlike previous calculations, the radiative-energy intensity is evaluated and then substituted into the rate equations. This allows state densities to be calculated when neither collisional nor radiative processes dominate relaxation within the plasma. Also, state densities can be calculated when either collisional or radiative processes dominate relaxation. From these state densities the radiative-energy current is calculated. Another feature of the present analysis is that it can treat a non-uniform plasma (i.e., variations in temperature, pressure or flux).

B. Physical Applications

Well referenced discussions of the uses of gaseous core reactors exist in the literature,[19,20] hence an extensive list of references is not included here.

The initial impetus for research on a gaseous core reactor was to develop a nuclear rocket engine. Shorter transit time for space flights, (80 days for a round trip to Mars as opposed to 200 days using conventional propulsion systems), and savings in weight, (up to an order of magnitude over chemical propellants on long flights), make nuclear rocket engines

desirable. Another advantage of the nuclear rocket is that the propulsion system can be adapted to simultaneously provide power for the space craft after take off. In this application the emitted radiation is important because it is used to heat the propellant.

Several characteristics of the gaseous core reactor also make it attractive for terrestrial power production. Thermodynamic cycle efficiencies of approximately 65% can be attained in a plasma core-MHD device at 5000°K.[21] Because of the lower densities in a gas core reactor, smaller inventories of nuclear fuel would have to be maintained at the plant site thus reducing production costs. This reduced inventory would also decrease the amount of radioactive waste at the plant site. Finally, because the fuel is a gas, refueling could be done continuously, eliminating the need for lengthy reactor shutdowns.

In addition to normal power plant uses, because of its high thermal-neutron flux-density, the gas core reactor could be used as a breeder of U^{233} from thorium. Non-thermal energy-conversion cycles could be developed utilizing the non-Maxwellian electron flux and fast recombination rate for direct nuclear pumping of lasers.[22,23] Further, radiation at a desired frequency could be produced by the selection of an appropriate seed gas to be used in chemical processing.

Any of the processes dealing with light, lasers, or chemical processing require a detailed knowledge of the emitted radiation energy spectrum and intensity. Also in any gaseous core configuration the radiation must be transmitted through a semitransparent wall. Absorption in this "window", which can cause extensive heating, is frequency dependent. These considerations motivated the present study.

C. Terminology

Several terms, namely gain, directed radiative-energy intensity, total radiative-energy intensity and radiative-energy current are defined here.

The gain, γ, describes the amplification, (or absorption), of photons in the plasma. This can be expressed[24,25]

$$\gamma = A_{ij} \frac{c^2}{8\pi\nu^2} g(\nu) \left[N_i - \frac{g_i}{g_j} N_j \right] - \frac{8e^6 N_e N_t}{3(mc^2)kT} \sqrt{\frac{mc^2}{2\pi h}} \frac{\exp\left(\frac{-h\nu}{kT}\right)}{m\nu^2}, \quad (I\text{-}1)$$

where A_{ij} is the spontaneous transition probability, c, the speed of light, ν, the frequency of the transition, $g(\nu)$, the line shape, N_i, the upper state density, N_j, the lower state density, N_e, the density of electrons within the plasma, N_t, the density of ions within the plasma, g_i/g_j, the ratio of the upper state to lower state degeneracies, e, the electron charge, m, the electron mass, k, Boltzmann's constant, h, Planck's constant, and T is the temperature of the plasma. The units of gain are cm^{-1} conforming to the CGS units used throughout this work.

If the plasma is homogeneous, the intensity at a distance s from the origin due to an attenuated intensity at the origin can be written as

$$I(s,\nu) = I(0,\nu)\exp(\gamma(\nu)s) . \quad (I\text{-}2)$$

The directed radiative-energy intensity, $I_\nu(\theta,\phi)$ is the energy per unit time per unit area per steradian per unit frequency at frequency ν. From this quantity the total radiative-energy intensity, $F_\nu(s)$, can be calculated by integrating the directed radiative-energy intensity over all angles as follows:

$$F_\nu(s) = \int I_\nu(\theta,\phi)d\Omega, \qquad \text{(I-3)}$$

where the units for $F_\nu(s)$ are the same as $I_\nu(\theta,\phi)$ with the angular dependence integrated out. The total radiative-energy intensity combined with the Einstein B coefficient for absorption or stimulated emission gives the reaction rates for these processes within the plasma and can be written

$$R(s) = \frac{1}{c} BF_\nu(s). \qquad \text{(I-4)}$$

To calculate the radiative energy-spectrum emitted at the surface of the plasma, the radiative-energy current, J_ν, must be known. This is obtained by multiplying the directed radiative energy flux times $\hat{\Omega} \cdot \hat{\Omega}'$ where $\hat{\Omega}$ is the direction the current is being evaluated and integrating this quantity over all $\hat{\Omega}'$. Hence

$$J_\nu(\Omega) = \int I_\nu(\theta,\phi)\hat{\Omega}'\cdot\hat{\Omega}\, d\Omega' \quad . \qquad \text{(I-5)}$$

This result has the same dimensions as the total radiative-energy intensity.

In Chapter II a theoretical formalism for rate equations that describes the state densities within the plasma is discussed along with the radiation transport problem. The gain of Eq. (I-1) and the total radiative-energy intensity of Eq. (I-3) are used in Chapter II. Chapter III describes the computer code developed using this formalism and Chapter IV describes the plasma and the physical quantities that are used in the analysis. In Chapter V the results of these calculations are presented and discussed. Chapter VI contains the conclusions drawn from this work and suggestions future research.

CHAPTER II. RADIATION TRANSPORT PROBLEM

A. Physical Parameters

Electron-ion recombination and non-Maxwellian electron excitation lead to non-equilibrium radiation emission by a plasma. This study deals with the radiation emitted by such a plasma. The plasma processes that lead to the emission are illustrated in Fig. (II-1). The electron flux is produced by fission fragments within the gas. This flux in turn excites the constituents of the plasma leading to line radiation. The radiation is absorbed or amplified by the medium leading to a shift in the excited-state densities of the gas. This shift in excitated state densities will be significant when the line radiation they produce is large enough to contribute to the rate equations. The interplay between the radiation and state densities within the plasma results in a non-linear problem.

To solve for the emitted radiative current, the excited-state densities within the plasma are first calculated in the absence of any radiation and then the radiation intensity is computed. The state densities are recalculated using the computed radiative intensity. Then the radiative intensity is evaluated with the new state densities. This process is repeated until the solution for the radiative intensity converges. In this manner the nonlinear problem is solved.

In this work a cylindrical plasma is assumed because this most nearly models the configuration planned for the Los Alamos gaseous-core experiments[7] as well as the design proposed by United Aircraft[6] for prototype models of gaseous-core rocket engines. In this analysis the plasma is broken up into concentric rings. This is done so any temperature,

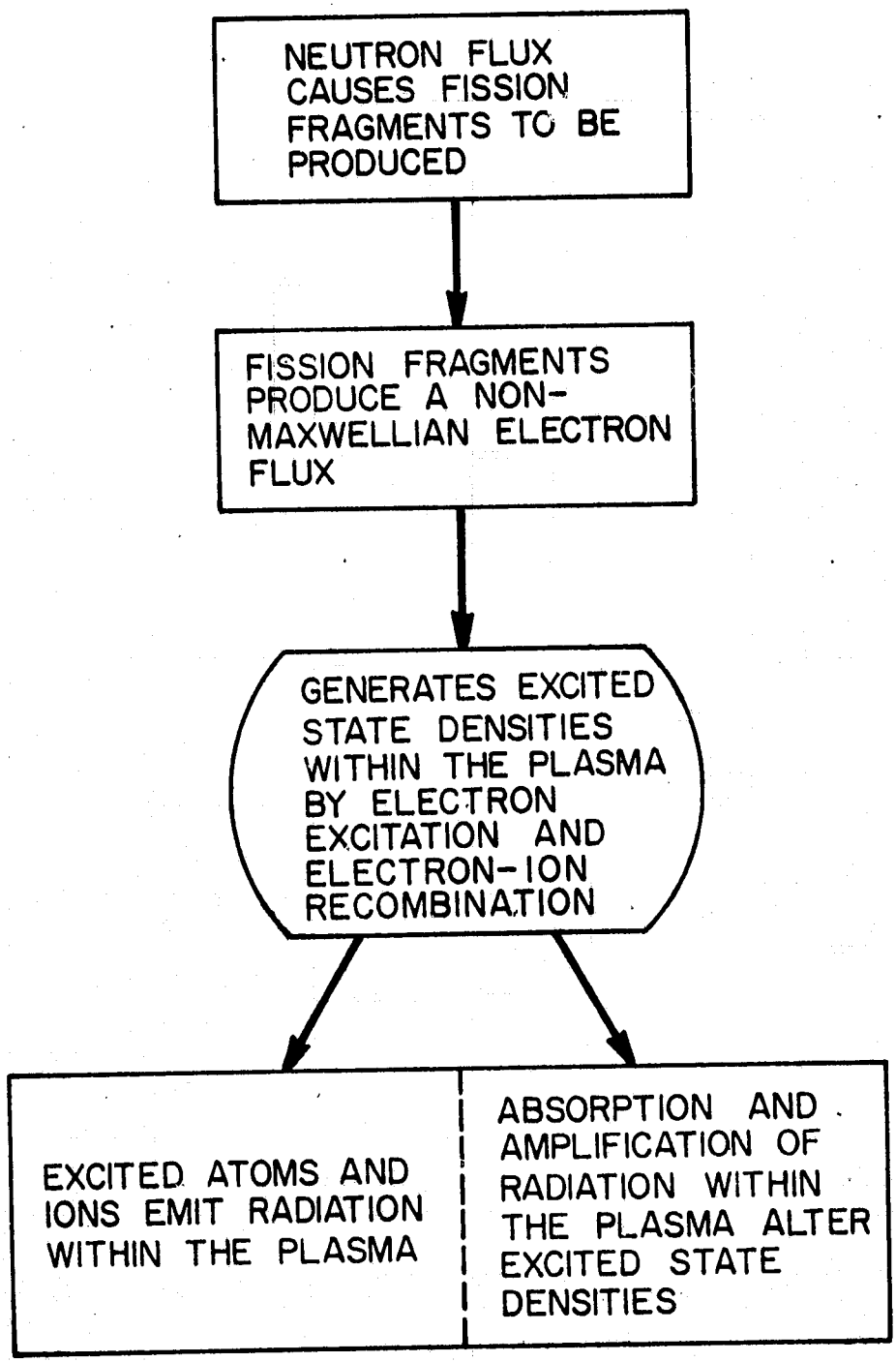

Figure II-1. Flow diagram of physical processes within the plasma.

flux or density gradients within the plasma can be included. Within a given region all physical properties of the plasma are assumed to be constant but these properties change from ring to ring to account for gradients. This model presupposes constant physical properties along the axis of the cylinder.

B. Rate Equations

The rate equations are a system of equations[2,3] that describe the atomic-state densities within the plasma. They have the form

$$\sum_{p} C_{pq} N_p = D_q , \qquad \text{(II-1)}$$

where N_p is the state density of the p^{th} state of the atom, C_{pq} is the collisional-radiative matrix coefficient and D_q is a collisional constant describing recombination. Figure (II-2) gives a schematic representation of the processes that determine the coefficients in the rate equations. C denotes collisional processes between states, i.e. excitation and de-excitation rates. R denotes radiative processes. Both radiative and collisional processes will take electrons from the upper to lower state and from the lower to the upper state. Hence, the paths in Fig. (II-2) have arrows at both ends but each path is labeled only once for simplicity. In this work the first subscript of the matrix element is the designation of the initial atomic state and the second subscript is that of the final atomic state.

Photon absorption is the process that takes electrons from a lower state to an upper state while spontaneous and stimulated emission account for the radiative processes that take electrons from an upper state to a lower state. Stimulated emission is when a photon with energy equal to

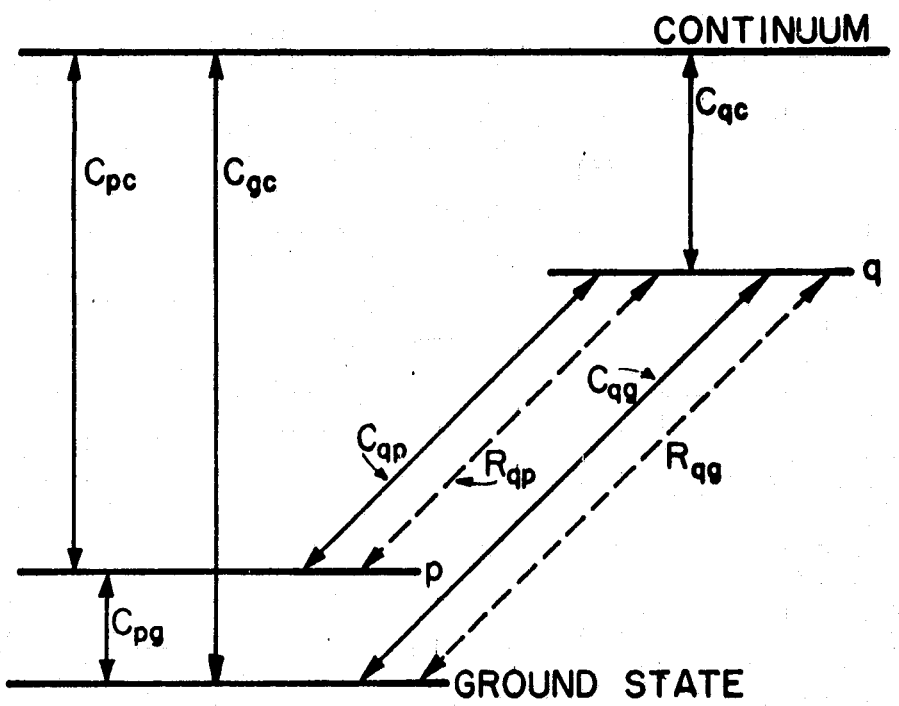

Figure II-2. Schemetic representation of the process that determine the state densities of states p and q.

the difference in the state energies collides with an excited atom causing it to de-excite emitting a photon in phase with the original photon. Ionization causes bound electrons to become part of the continuum while recombination is the inverse process. Since recombination takes free electrons from the continuum into atomic states in the plasma it is represented by the right hand side of Eq. (II-1). The states used in this work are described in the model in Chapter IV. In uranium three-body processes dominate ionization and recombination thus no radiative channels are seen from any bound state to the continuum in Fig. (II-2). Also, as will be described in Chapter IV, there are no radiative processes within the families of upper states and lower states as illustrated by no radiative processes between the ground state and state p.

Processes that are considered in the present study are listed below and discussed in Chapter IV.

1. Spontaneous Emission of Radiation:

$$X(q) \rightarrow X(p) + h\nu, \qquad \text{(II-2)}$$

where p and q represent different energy levels and ν is the frequency of this transition. The spontaneous transition probability is A_{qp} with dimensions of sec^{-1}, and is equal to the dipole moment for the transition.

2. Absorption of Radiation:

$$X(p) + h\nu \rightarrow X(q). \qquad \text{(II-3)}$$

The rate for this interaction is $\rho(\nu)\ B_{pq}$ where $\rho(\nu)$ is the radiation density at ν per unit ν and B_{pq} is the Einstein B coefficient. Where B has dimensions of $cm^3\text{-}sec^{-2}\text{-}ergs^{-1}$ and ρ has dimensions of $ergs\text{-}sec\text{-}cm^{-3}$.

3. Stimulated Emission of Radiation:

$$X(q) + h\nu \rightarrow X(p) + 2\ h\nu. \qquad \text{(II-4)}$$

The rate for this interaction is $\rho(\nu)\ B_{qp}$.

4. Electron Excitation:

$$X(p) + e \rightarrow X(q) + e. \qquad \text{(II-5)}$$

The rate for this process is given by $\int \sigma_{qp}(E)\ \phi_e(E)\ dE$ where $\sigma_{pq}(E)$ is the excitation cross section and $\phi_e(E)$ is the electron flux per unit energy. The flux has units of cm^{-2}-sec^{-1} and the cross sections has units of cm^2. All cross-sections are zero for energies below threshold. These cross sections are for all states including the ground state.

5. Electron De-Excitation:

$$X(q) + e \rightarrow X(p) + e. \qquad \text{(II-6)}$$

The rate for this process is given by $\int \sigma_{qp}(E)\ \phi_e(E)\ dE$.

6. Ionization of State q:

$$X(q) + e \rightarrow X^+ + 2e. \qquad \text{(II-7)}$$

The rate for this process is given by $\int \sigma_{qi}(E)\ \phi_e(E)\ dE$ where $\sigma_{qi}(E)$ is the ionization cross-section.

7. Recombination into State q:

i) Two-body recombination

$$X^+ + e \rightarrow X(q) + h\nu. \qquad \text{(II-8)}$$

ii) Three-body recombination

$$X^+ + 2e \rightarrow X(q) + e. \qquad \text{(II-9)}$$

The total (i.e., combined) rate for these processes can be written $\int n_e(E)\ n_i(E)\ \alpha^q_{eff}(E)\ dE$ where $n_e(E)$ and $n_i(E)$ are the electron and ion number densities at E per unit E and $\alpha^q_{eff}(E)$ is the "effective" two-body

recombinational branching coefficient to state q[2,3]. The effective two-body recombinational branching can be written as

$$\alpha^q_{eff}(E) = \alpha^q_2(E) + n_e(E)\ \alpha^q_3(E), \qquad \text{(II-10)}$$

where α^q_2 is the two-body recombinational branching rate to state q and α^q_3 is the three-body recombinational branching rate to state q. The branching ratio is the fractional part of the recombination coefficient that accounts for recombination into state q.

All of the above processes are taken into account for the constituents of the uranium plasma. If another plasma is to be considered, these process will have to be re-examined to see which ones are important. In this analysis, atom-atom and atom-ion collisions have been neglected because they do not contribute significantly to excitation and ionization at thermal energies due to the small cross sections in this energy range.[26] Direct fission fragment excitation is also neglected due to the low fragment density.[27]

When the processes described by Eq. (II-2) through Eq. (II-9) are combined and an infinite medium is assumed so diffusion losses can be neglected, the rate equation obtained for state q becomes:

$$\begin{aligned}\frac{dN_q}{dt} = &- \sum_{p<q} (A_{qp}+\rho(\nu)\ B_{qp})\ N_q + \sum_{p>q} (A_{pq}+\rho(\nu)\ B_{pq})\ N_p \\ &- \sum_{p>q} \rho(\nu)\ B_{qp}\ N_q + \sum_{p<q} \rho(\nu)\ B_{pq}\ N_p \\ &- \sum_{p\neq q} N_q \int \sigma_{qp}(E)\ \phi_e(E)dE + \sum_{p\neq q} N_p \int \sigma_{pq}(E)\ \phi_e(E)dE \\ &- N_q \int \sigma_{qi}(E)\ \phi_e(E)dE + \int n_e(E)\ n_i(E)\ \alpha^q_{eff}(E)dE. \qquad \text{(II-11)}\end{aligned}$$

To describe specific plasma conditions, the sum over all state densities of a given atomic species should equal the total number of atoms of that species. This can be written:

$$N_T = \sum_p N_p . \qquad \text{(II-12)}$$

The total radiative-energy intensity, $F_\nu(0)$, enters into the rate equations because it is proportional to $\rho(\nu)$. This proportionality is

$$\rho(\nu) = \frac{F_\nu(0)}{c} , \qquad \text{(II-13)}$$

here $F(\nu)$ has units of ergs/cm^2.

Equation (II-11) can be simplifed in the case of a steady state. When $\frac{dNq}{dt}$ is set equal to zero, Eq. (II-11) has the form of Eq. (II-1) where

$$D_q = -\int n_e(E)\ n_i(E)\ \alpha^q_{eff}(E)\ dE , \qquad \text{(II-14)}$$

and

$$C_{pq} = \begin{cases} (A_{pq} + \rho(\nu)\ B_{pq}) + \int \sigma_{pq}(E)\ \phi_e(E)dE, & p > q \\ -\sum_{p<q} (A_{qp} + \rho(\nu)\ B_{qp}) - \sum_{p\neq q}\int \sigma_{qp}(E)\ \phi_e(E)dE & \\ -\int \sigma_{qi}(E)\ \phi_e(E)dE - \sum_{p\neq q} \rho(\nu)\ B_{qp}, & p = q \\ \int \sigma_{pq}(E)\ \phi_e(E)dE + \rho(\nu)\ B_{pq}. & p < q \end{cases} \qquad \text{(II-15)}$$

With the coefficients in Eq. (II-15), Eq. (II-1) can be solved to give the atomic state densities of the various energy levels in the plasma

under consideration. Once these state densities are known, the emitted radiation from the plasma is calculated.

C. Radiation Transport

1. Plasma Source and Attenuation

The volumetric source of radiation per unit frequency per unit time within the plasma is evaluated utilizing the atomic state densities calculated from the rate equations. This source has two components and can be written:

$$f(\nu) = f_L(\nu) + f_p(\nu), \tag{II-16}$$

where f_L is the source of line radiation due to atomic transitions and f_p is the source of continuum radiation due to bremsstrahlung within the plasma. The first term is given by[24]

$$f_L = \frac{AN_u h\nu\, g(\nu)}{4\pi}\ \delta(\nu-\nu_o), \tag{II-17}$$

where A is the spontaneous transition probability, h is Planck's constant, ν is the frequency of the transition, $g(\nu)$ is the line shape and N_u is the atomic state density of the upper level of the transition calculated from the rate equations and $\delta(\nu-\nu_o)$ is the delta function. Units for the volumetric source are ergs/cm^3.

The continuum source is given by[25]

$$f_p = \frac{4e^6 N_e N_i}{3\pi m^2 c^4}\ \sqrt{\frac{mc^2}{2\pi h\nu}}\ \exp\left(\frac{-h\nu}{kT}\right), \tag{II-18}$$

where e is the electronic charge, m is the mass of the electron, c is the speed of light, k is Boltzmann's constant, T is the temperature of the plasma, N_e is the electron density in the plasma, and N_i is the ion density

of the plasma. Equation (II-18) neglects contributions due to free-bound transitions (recombination events). The photons emitted during recombination events represent a small contribution to the source at the frequencies considered in this work and this allows the plasma emission to be of the form of Eq. (II-18).[9,25]

The attenuation at a given frequency per unit frequency per unit length for this radiation can be written

$$\gamma(\nu) = \gamma_L(\nu) + \gamma_p(\nu) , \qquad \text{(II-19)}$$

where γ_L is the attenuation due to the atomic-state densities[24] within the plasma and γ_p is the plasma absorption coefficient.[25] The atomic attenuation is due to bound-bound transitions in the atoms while the plasma absorption coefficient is due to free-free transitions. Free-bound transitions are neglected because their contribution to the attenuation are negligible. The attenuation due to atomic-state densities can be written[24] as:

$$\gamma_L = A_{ij} \frac{c^2}{8\pi\nu^2} g(\nu) \left[N_i - \frac{g_i}{g_j} N_j \right], \qquad \text{(II-20)}$$

where A_{ij} is the spontaneous transition rate (Einstein A coefficient), c is the speed of light, $g(\nu)$ is the line shape, N_i is the state density of the upper state, N_j is the state density of the lower state and g_i/g_j is the ratio of the degeneracies of state i to state j. The corresponding expression for the plasma absorption[25] is

$$\gamma_p = \frac{8e^6 N_e N_i}{3(mc^2)kT} \sqrt{\frac{mc^2}{2\pi h\nu}} \frac{\exp\left[\left(\frac{-h\nu}{kT}\right)\right]}{m\nu^2} . \qquad \text{(II-21)}$$

Once the source rate and attenuation of radiation are known within a the plasma, the directed radiative-energy intensity along path length s can be calculated.

2 General Relationships for the Total Radiative-Energy Flux and the Radiative-Energy Current

To do these calculations an expression for the directed radiative-energy intensity must first be derived. Figure (II-3) shows a cylindrical volume element, along path length s, that has surface area dA normal to s and length ds. Within this volume element there is a volumetric source $f(\nu,s)$, corresponding to the source in Eq. (II-16) and an attenuation of radiation, $\gamma(\nu,s)$, through the element. The divergence of the direct radiative-energy intensity is defined by $d\Omega$ about Ω, where Ω is the angle s makes with the origin.

The energy incident upon the surface can be written as

$$I(\nu,s)\, d\nu\, dt\, dA, \tag{II-22}$$

where $I(\nu,s)$ is a directed radiative-energy intensity, $d\nu$ is the frequency interval, dt is the time interval and $s = s(\Omega)$. Similarly the radiative-energy intensity leaving the volume is $I(\nu,s) + dI(\nu,s)$ and the energy leaving is

$$[I(\nu,s) + dI(\nu,s)]\, d\nu\, dt\, dA. \tag{II-23}$$

Inside the volume element, the radiative-energy intensity will be incremented due to the volumetric source, which can be written as

$$f(\nu,s)\, dV\, d\nu\, dt, \tag{II-24}$$

where $dV = dA\, ds$. The radiative-energy intensity will be attenuated along path length s, which can be written as

$$I(\nu,s)\, \gamma(\nu,s)\, ds\, d\nu\, dt\, dA. \tag{II-25}$$

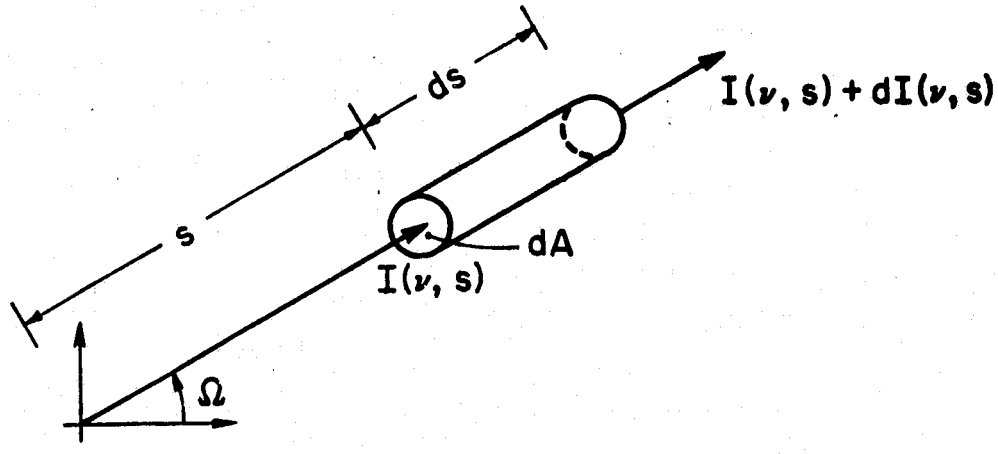

Figure II-3. Cylindrical volume element with surface area dA and length ds.

Combining Eqs. (II-22) through (II-25), the expression for the intensity becomes

$$\frac{dI(\nu,s)}{ds} = \gamma(\nu,s)\ I(\nu,s) + f(\nu,s). \qquad \text{(II-26)}$$

Equation (II-26) can be integrated over the path length s to obtain the integral form of the transport equation[28]

$$I(\nu,s) = I(\nu,o)\ \exp\left\{\int_o^s \gamma(\nu,s')ds'\right\} + \exp\left\{\int_o^s \gamma(\nu,s')ds'\right\} \int_o^s f(\nu,s')\ ds'\ \exp\left\{-\int_o^{s'} \gamma(\nu,x')dx'\right\}. \qquad \text{(II-27)}$$

Equivalently Eq. (II-27) can be rewritten to express the directed radiative-energy intensity at the origin when the directed radiative-energy intensity at s is zero as

$$I(\nu,o) = \exp\left\{\int_o^s \gamma(\nu,s')ds'\right\} \times \int_o^s f(\nu,s')\ ds'\ \exp\left\{-\int_o^{s'} \gamma(\nu,x)\ dx\right\}. \qquad \text{(II-28)}$$

In Appendix A expressions for the radiative-energy current and the total radiative-energy intensity will be derived in terms of the directed radiative-energy intensity. Analytic expressions for these quantities will be obtained for two simple geometries. The general expressions from Appendix A can be expressed for a cylindrical geometry as follows:

When θ is the azimuthal angle and ϕ is the angle made with the x-axis, the radiative-energy current at the origin in a direction $\hat{\Omega}'$ is written

$$J_\nu(o,\hat{\Omega}') = \int_o^{2\pi} d\phi \int_{-1}^{1} d(\cos\theta)\ \ (\hat{\Omega}\cdot\hat{\Omega}')I_\nu(\theta,\phi), \qquad \text{(II-29)}$$

where $\hat{\Omega}$ and $\hat{\Omega}'$ are unit vectors in their respective directions and

$$I_\nu(\theta,\phi) \equiv I(\nu, s[\theta,\phi]). \tag{II-30}$$

Also the total radiative-energy intensity can be written

$$F_\nu(o) = \int_0^{2\pi} d\phi \int_{-1}^{1} d(\cos\theta)\ I_\nu(\theta,\phi). \tag{II-31}$$

These expressions will be used in the subsequent development of the radiation transport problem.

3. Radiation Transport in a Cylinder

Since the total radiative-energy intensity is used in the rate equations for each region, Eq. (II-31) will form the basis for the following analysis.

In order to handle any density and temperature gradients involved, the cylindrical plasma is divided into regions within which the state densities and volumetric source are approximately constant (Fig. II-4). The simplest case is when the plasma is homogeneous (i.e., there are no gradients in the electron flux or density of the plasma and it can be characterized by a single temperature). In this case the plasma can be described by two regions. The inner region, whose radius is half the plasma radius, so the average state densities within the gas can be calculated, will account for the radiative-energy intensity to be used in the rate equations. The calculation employs an iterative technique. The convergence of the total radiative-energy intensity at the surface implies the convergence of the radiaitve-energy current, which will ultimately be calculated.

If the plasma is non-homogeneous, then the number of regions is

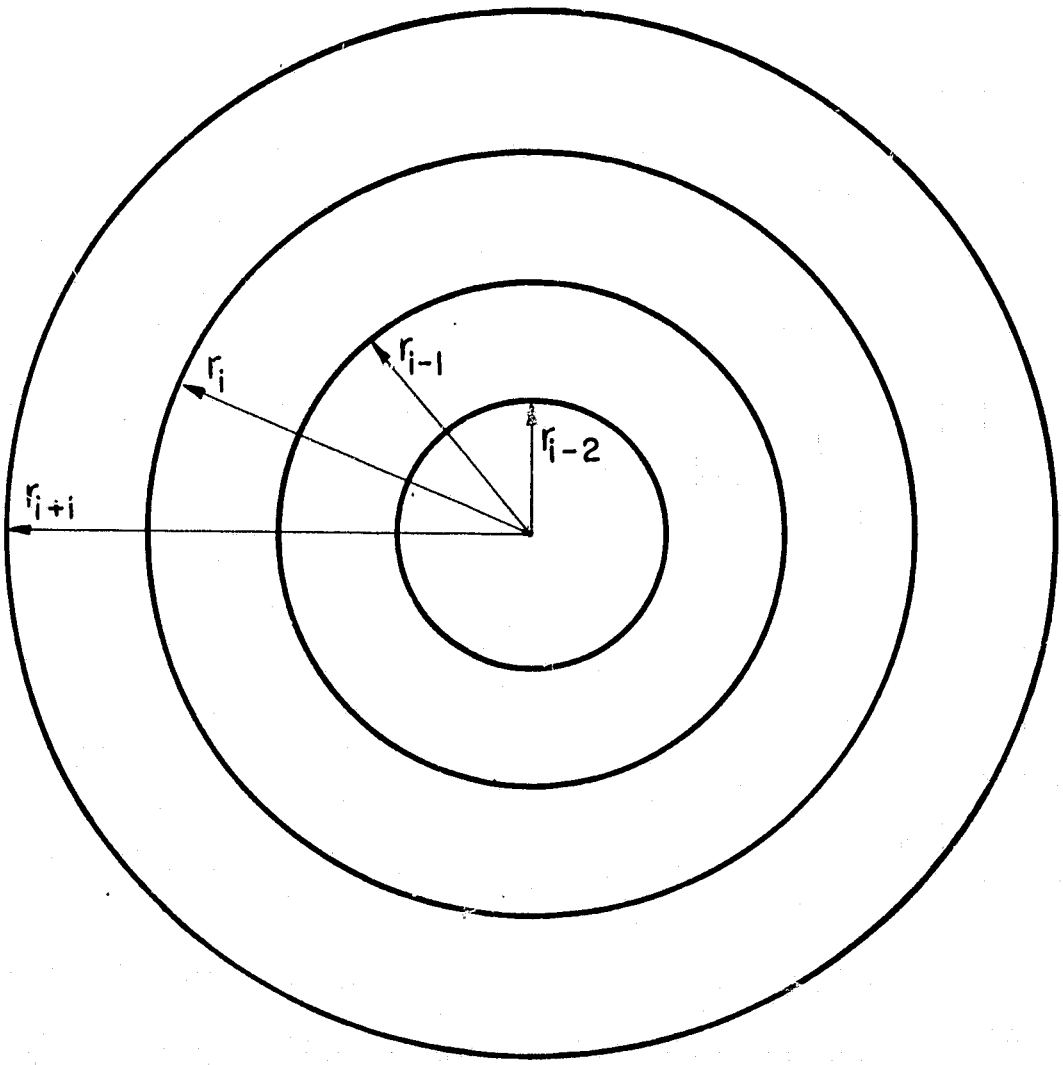

Figure II-4. Cross-sectional cut of a cylindrical plasma that is divided into four different regions. Excited state densities are assumed to be constant over each region.

determined by the gradients. For example, if the core region is at 7000°K and the outer region is at 6000°K, then there would be three regions. The inner region would describe the core while the outer two regions would allow the calculation of the state densities and emitted radiation for the 6000°K region. This process of subdividing the plasma can be repeated to obtain a given accuracy for larger gradients in physical properties, as in the cases of the actual rocket engine configuration where the temperature goes from a value of 100,000°K at the center to 10,000°K at the plasma surface.[19]

To calculate the total radiative-energy intensity emitted from the plasma an appropriate boundary condition on the outer surface is required. Since only the emitted radiation is of interest, the appropriate initial condition on $I(\nu,s)$ is that the inward directed radiative-energy flux is zero. This condition can be written as

$$I(\nu,s_{max}) = 0 \quad , \tag{II-32}$$

where s_{max} indicates the path originates on the surface of the plasma. In the method used in these calculations, the origin is shifted from region to region to evaluate the total radiative-energy intensity within each region. Hence, in the following analysis $F_\nu(0)$ is of central importance.

Now the geometry of the problem must be considered. First the boundaries of the cylindrical shells must be known (Fig. II-5). The equation for a cylindrical shell of radius r_j with its central axis displaced along the x-axis by a distance r_i is

$$r^2 \sin^2\theta - 2\, r\, r_i \sin\theta \cos\phi + (r_i^2 - r_j^2) = 0. \tag{II-33}$$

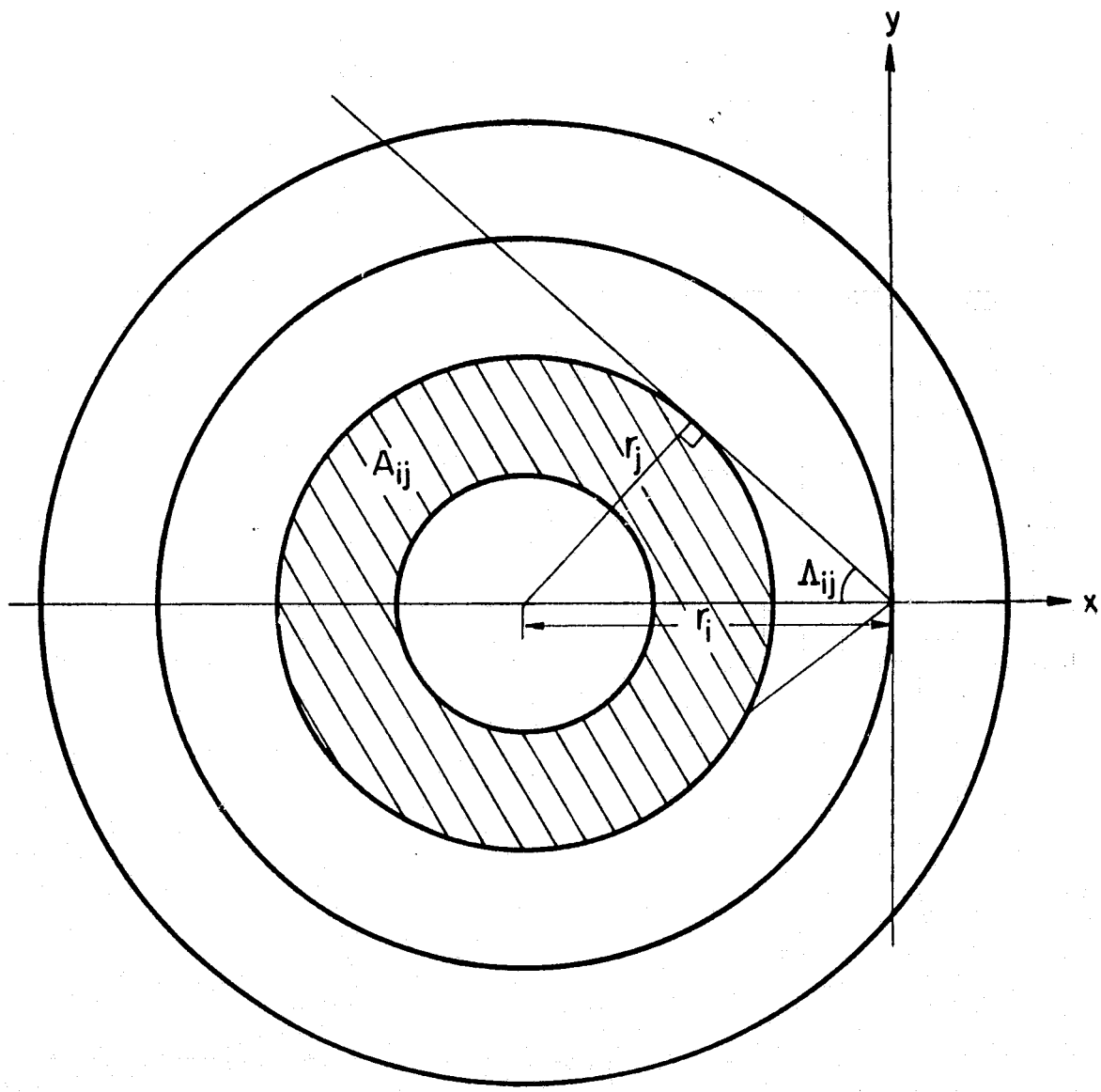

Figure II-5. Cross section of cylinder with origin of coordinate system displaced by a distance $-r_i$ along the x-axis. Here the z-axis is perpendicular to the plane of the slice shown.

In Fig. (II-5) $\Lambda = 180° - \phi$ and θ is not shown because the z-axis is perpendicular to the plane of the slice shown. Equation (II-34) can be solved for the roots of r to give

$$r_{\pm} = \frac{r_i \cos\phi \pm \sqrt{r_j^2 - r_i^2 \sin^2\phi}}{\sin\theta} , \qquad \text{(II-34)}$$

where r_+ is the longer distance and r_- is the shorter distance to the cylindrical shell from the origin for a given θ and ϕ. Another quantity of important is the angle Λ_{ij} (Fig. II-5). Sin Λ_{ij} can be written as

$$\sin \Lambda_{ij} = \frac{r_j}{r_i} , \qquad \text{(II-35a)}$$

or, solving for Λ_{ij},

$$\Lambda_{ij} = \arcsin\left(\frac{r_j}{r_i}\right) . \qquad \text{(II-35b)}$$

Because the mathematical form of the path length varies when the path tranversed by a ray originates on the top and the side of the cylinder, two explicit forms of $I_\nu(\theta,\phi)$ must be obtained. In this formulation of the problem all calculations will be made for the plane that cuts the cylinder in half in the x-y plane. The length of the cylinder is 2b and its radius is a (Fig. II-6). To solve the problem, two different volumes must be considered. The forward volume to the right of the origin, $\phi\varepsilon\left[-\frac{\pi}{2}, \frac{\pi}{2}\right]$ and the backward volume to the left of the origin, $\phi\varepsilon\left[\frac{\pi}{2}, \frac{3\pi}{2}\right]$ where ϕ is the angle measured from the x axis in the x-y plane. This division is made because in the backward volume a path s can cross the same cylindrical boundary twice while in the forward volume the crossing will only happen once (Fig. II-7). With this division of the cylinder, Eq. (II-31) can be written

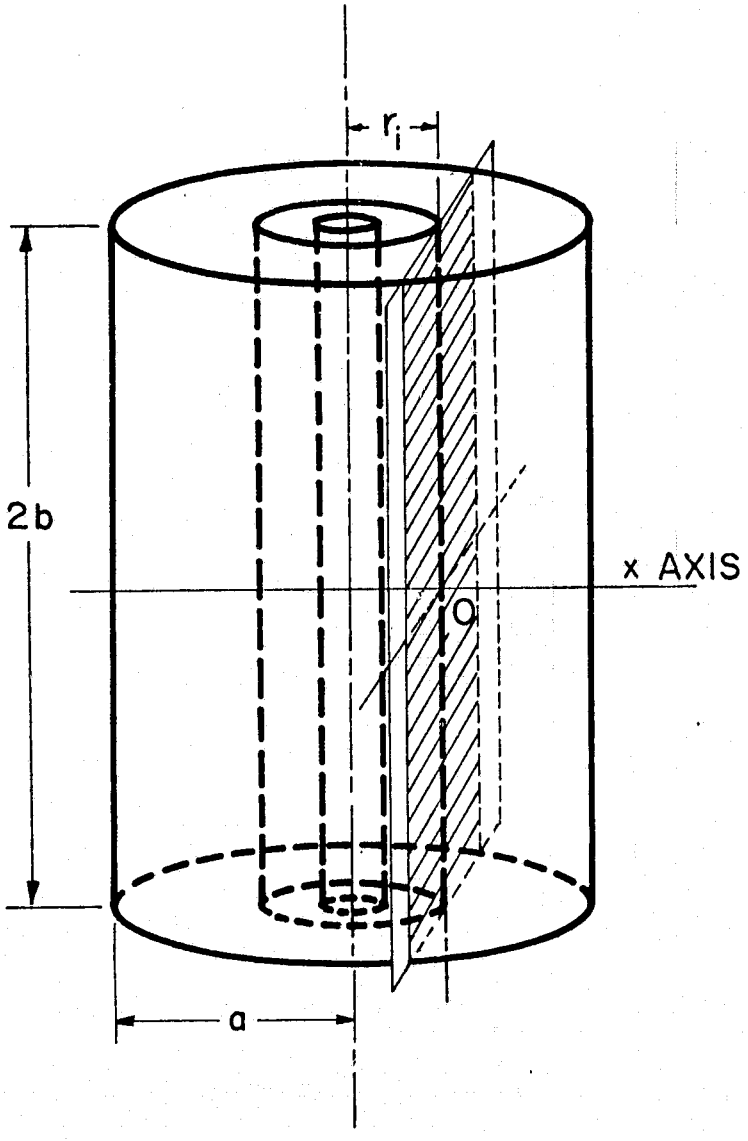

Figure II-6. Side view of cylinder with origin displaced a distance r_i. The forward volume is to the right and the back volume is to the left of the shaded plane.

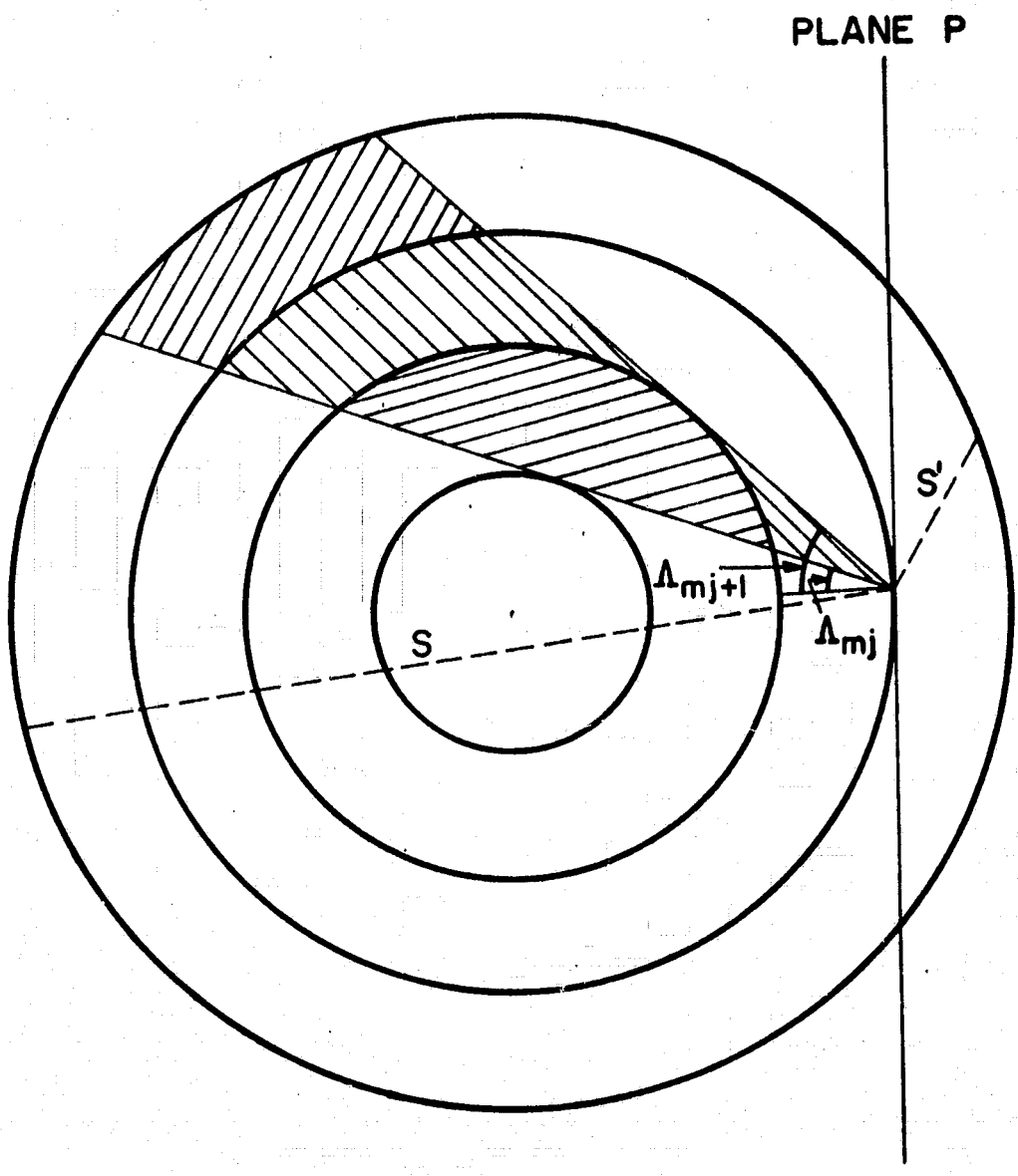

Figure II-7. Cross section of cylinder with forward path s' and backward path s. Plane P divides the cylinder into foward and backward volumes.

$$F_\nu(o) = F^+(o) + F^-_\nu(o) \qquad \text{(II-36)}$$

$F^+_\nu(o)$ and $F^-_\nu(o)$ are the forward and backward total radiative-energy intensities defined by

$$F^+_\nu(o) \equiv \int_{-\pi/2}^{\pi/2} d\phi \int_{-1}^{1} d(\cos\theta)\ I_\nu(\theta,\phi)\,, \qquad \text{(II-37a)}$$

and

$$F^-_\nu(o) \equiv \int_{\pi/2}^{3\pi/2} d\phi \int_{-1}^{1} d(\cos\theta)\ I_\nu(\theta,\phi)\,. \qquad \text{(II-37b)}$$

The + or - sign indicate the integration is done over the forward or backward volume of the plasma. Let the plasma be divided into n regions and let $F_\nu(0)$ be evaluated at the m^{th} boundary ($m \leq n$). To evaluate $F^+(0)$ along path s', that starts on the side of the cylinder (Fig. II-7), the directed radiative-energy intensity is needed and is written as

$$I^+_{\nu s}(\theta,\phi) = \sum_{i=m}^{n} \frac{f_i}{\gamma_i}\left[e^{\gamma_i(s_{i+1}-s_i)} - 1\right] \prod_{j=m}^{m+i-1} e^{\gamma_j(s_{j+1}-s_j)}\,, \qquad \text{(II-38)}$$

where

$$s_j = \begin{cases} 0 & j = m \\ \dfrac{r_m\cos - \sqrt{r_j^2 - r_m^2\sin^2\phi}}{\sin\theta} & j \neq m \end{cases} \qquad \text{(II-39)}$$

If this expression is integrated over the side of the cylinder, one obtains

$$F^+_{\nu s}(o) = 4\int_0^{2\pi} d\phi \int_0^{b/\sqrt{b^2+d^2}} d(\cos\theta)\ I^+_{\nu s}(\theta,\phi)\,, \qquad \text{(II-40)}$$

where $d = a - r_m$ and a is the radius of the plasma. When the path s' orginates on the top surface, different regions are denoted by different s' (Fig. II-8).

$$\cos\theta_{j,m} = \frac{b}{\sqrt{b^2 + s_{j,m}^2}} \quad , \tag{II-41}$$

where

$$s_{j,m} = \frac{r_m\cos\phi - \sqrt{r_i^2 - r_m^2 \sin^2\phi}}{\sin\theta} \quad . \tag{II-42}$$

here the directed radiative-energy intensity is:

$$I_{\nu t}^{+} = \sum_{i=m}^{k} \frac{f_i}{\gamma_i}\left[e^{\gamma_i(s_{i+1}-s_i)}-1\right] \prod_{j=m}^{m+i-1} e^{\gamma_j(s_{j+1}-s_j)} \tag{II-43}$$

where $k \equiv m + n$, n is the number of boundaries crossed to define $\theta_{j+1,m}$, and

$$s_j = \begin{cases} b/\cos\theta & j = k \\ 0 & j = m \\ \dfrac{r_m\cos\phi - \sqrt{r_j^2 - r_m^2\sin^2\phi}}{\sin\theta} & j \neq m,k. \end{cases} \tag{II-44}$$

If this expression is integrated over the top of the cylinder, we obtain

$$F_{\nu t}^{+}(0) = 4 \sum_{\cos\theta_j = \frac{b}{\sqrt{b^2+a^2}}}^{1} \int_0^{\pi/2} d\phi \int_{\theta_j}^{\theta_{j+1}} d(\cos\theta)\, I_{\nu t}^{+}(\theta,\phi) \, , \tag{II-45}$$

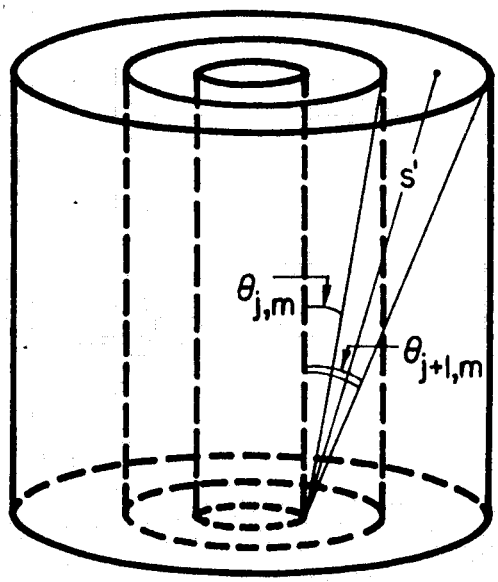

Figure II-8. Angles $\theta_{j,m}$, $\theta_{j+1,m}$ are defined by the j^{th} and $j^{th}+1$ surfaces on the top of the cylinder with the origin at the m^{th} cylinder.

Equations (II-40) and (II-45) add up to give $F_\nu^+(0)$.

To obtain the backward contribution to $F_\nu(0)$, it is simpler to write the angular dependence in terms of θ and Λ since these are the quantities that define the boundary regions of interest. Hence $F_{\nu s}^-(0)$ can be written as

$$F_{\nu s}^-(0) = 4 \sum_{\Lambda_{j,m=0}}^{\pi/2} \int_{\Lambda_{j,m}}^{\Lambda_{j+1,m}} d\Lambda \int_0^{\sqrt{b^2+a^2}} d(\cos\theta)\, I_{\nu s}^-(\theta,\Lambda) \,, \qquad \text{(II-46)}$$

where $d = a + r_m$ and

$$I_{\nu s}^-(\theta,\Lambda) = \sum_{i=m}^{m+n-2k-1} \frac{f_i}{\gamma_i} \left[e^{\gamma_i (s_{i+1}-s_i)} - 1 \right] \prod_{}^{i-1} e^{\gamma_j (s_{j+1}-s_j)} . \qquad \text{(II-47)}$$

Here k ≡ number of cylinders that are crossed twice, and we define

$$s_j = \begin{cases} \dfrac{r_m \cos\Lambda + \sqrt{r_j^2 - r_m^2 \sin^2\Lambda}}{\sin\theta} & j \geq m+n-2k \\ 0 & j = m \\ \dfrac{r_m \cos\Lambda - \sqrt{r_j^2 - r_m^2 \sin^2\Lambda}}{\sin\theta} & \begin{matrix} j \neq m \\ j < m+n-2k \end{matrix} \end{cases} ,$$

and

$$\gamma_i = \gamma_j + n - 2k + 1 . \qquad \text{(II-48)}$$

Equations (II-46) through (II-48) give the contribution to $F_\nu^-(0)$ from the side. To obtain the contribution from the top, the cylinder will be divided into angular regions as seen in Fig. (II-8) and defined by Eq. (II-3). Hence,

$$F_{\nu t}^{-}(0) = 4 \sum_{\cos\theta_j = \frac{b}{\sqrt{b^2+a^2}}}^{1} \int_0^{\pi/2} d\Lambda \int_{\theta_j}^{\theta_{j+1}} I_{\nu t}^{-}(\theta,\Lambda)\, d(\cos\theta) \,, \qquad \text{(II-49)}$$

and

$$I_{\nu t}^{-}(\theta,\Lambda) = \sum_{i=m}^{k} \frac{f_i}{\gamma_i} \left[e^{\gamma_i (s_{i+1}-s)} - 1 \right] \prod_{j=m}^{i=1} e^{\gamma_j (s_{j+1}-s_j)} \,, \qquad \text{(II-50)}$$

where k = m + number of boundaries along path at angle θ_j. Also, in this case,

$$S_j = \begin{cases} b/\cos\theta & j = k \\ \dfrac{r_m\cos\Lambda + \sqrt{r_j^2 - r_m^2 \sin^2\Lambda}}{\sin\theta} & j > n,\ j \neq k \\ \dfrac{r_m\cos\Lambda - \sqrt{r_j^2 - r_m^2 \sin^2\Lambda}}{\sin\theta} & j \leq n,\ j \neq m \\ 0 \,, & j = m \end{cases} \qquad \text{(II-51)}$$

and

$$\gamma_j = \gamma_{k-n} \,. \qquad \text{(II-52)}$$

The sum of Eqs. (II-46) and (II-49) give $F_\nu^-(0)$. Therefore the sum of Eqs. (II-40), (II-45), (II-46) and (II-49) give $F_\nu(0)$.

The only place it is of interest to calculate the current is on the surface of the plasma. Here $J_\nu(0,\hat{n}) = J_\nu^+(0,\hat{n})$ so the previous analysis for calculating the total radiative-energy flux in the backward region

is correct when Eqs. (II-46) and (II-49) are multiplied by $\hat{\Omega}\cdot\hat{\Omega}'$. When the current is calculated along the x axis

$$\hat{\Omega} \cdot \hat{\Omega} = \sin\theta \cos\phi \ . \qquad \text{(II-53)}$$

A numerical integration is carried out to obtain the current in this manner.

When the core emits black-body radiation but the outer region remains semitransparent, the preceding analysis is correct for the shaded area in Fig. (II-9) because the path-lengths through this region do not go through the black body emitting core. However, for path lengths that pass through the core region, the directed radiative-energy intensity in Eq. (II-47) and Eq. (II-50) will become

$$I(0,\Lambda) = I_\nu^B \prod_{j=m}^{2} e^{\gamma(s_{j+1}-s_j)} + \sum_{i=2}^{m} \frac{f_i}{\gamma_i} \left(e^{\gamma_i(s_{i+1}-s_i)} - 1 \right) \prod_{j=m}^{i} e^{\gamma_j(s_{j+1}-s_j)} \ , \qquad \text{(II-54)}$$

where

$$I_\nu^B = \frac{2h^3}{c^2} \left(e^{h\nu/kT} - 1 \right)^{-1} \ , \qquad \text{(II-55)}$$

and

$$s_j = \frac{r_m \cos\Lambda - \sqrt{r_j^2 - r_m^2 \sin^2\Lambda}}{\sin\theta} \ . \qquad \text{(II-56)}$$

With the above form of the directed radiative-energy intensity for paths that transverse the black-body core, the previous analysis can be used to calculate the total radiative-energy intensity.

Now that the radiative energy-flux has been calculated it can be substituted into the rate equations to re-evaluate the state densities

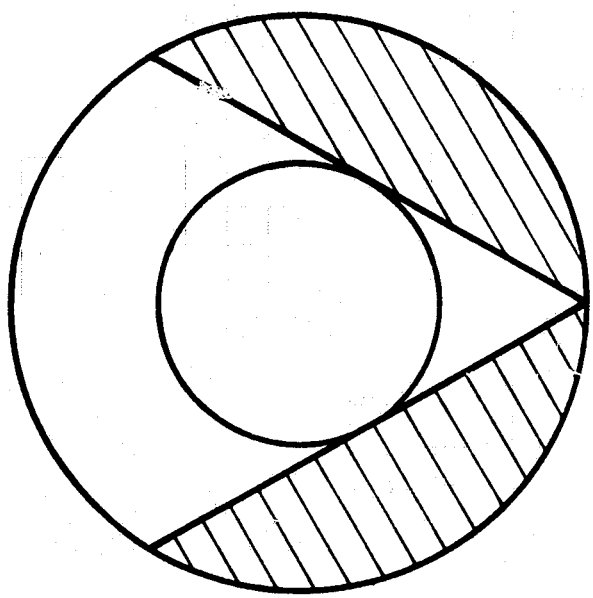

Figure II-9. Two region core with central region emitting black-body radiation.

within the plasma. The radiative flux can then be recalculated and this process is repeated out until convergence is obtained. Basically the non-linear coupling of the total radiative-energy flux and the state densities makes this iteration procedure necessary.

In this chapter the rate equation formalism was first developed. Then the expression for the directed radiative-energy intensity was derived. Finally, expressions for the total radiative-energy intensity in a cylindrical geometry were obtained.

CHAPTER III. CODE DESCRIPTION AND TESTING

A. Discussion of Code

1. General Description

A computer code was developed to solve the complex, non-linear problem described in the previous chapter. In this code the rate equations Eq. (II-11) and the total radiative-energy intensity Eq. (II-31) are treated as separate problems. The rate equations are first solved to give the source function and the attenuation for the radiative-energy intensities, then the radiative intensities are substituted back into the rate equations to recalculate the state densities. This process is repeated until convergence for the radiative energy intensities is obtained. A flow chart for this procedure is given in Fig. (III-1). The logic of the code is divided into four major sections and each section will be individually discussed.

The first section initializes the data to be used in solving the problem. The next two sections evaluate the state densities and radiative-energy intensities, respectively. Finally the solutions are checked for convergence to determine if the problem is solved.

2. Sectional Discussion of the Code

In initializing the problem in the first section, the plasma must be described by its constituents and geometry. Also the number of the iteration must be given to allow for radiative energy-fluxes to be used from previous calculations if convergence was not obtained.

Parameters describing the atomic composition of the plasma and the geometry of the system are input in the first section of the computer code.

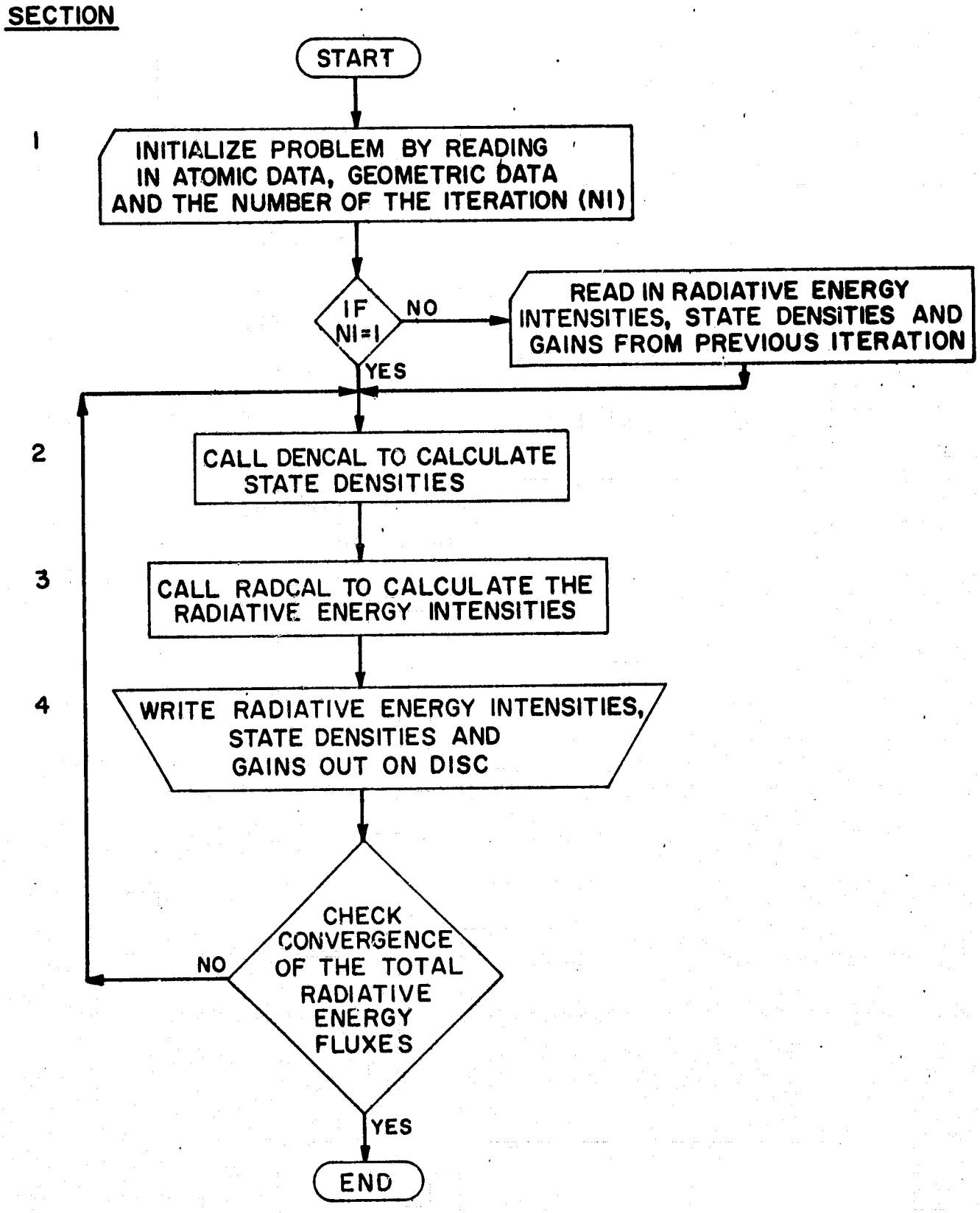

Figure III-1. Flow chart of principal sections of computer code. The excited state densities and total radiative-energy intensities are calculated in DENCAL and RADCAL, respectively.

The atomic data consists of the terms to be substituted into the rate equations, e.g. Eq. (II-11). Here the data can be global or local. Global data consists of factors that are uniform throughout the volume of plasma. These terms include the Einstein A and B coefficients, energy levels of the plasma components and the frequencies of the various transtions. Local data describe conditions that exist within the specific regions of the plasma. Here the collisional reaction rates and line widths are found.

Next the geometry of the system must be described. Cylindrical geometry is used in the present analysis. Thus the half height of the cylinder as well as the number of regions and their radii must be input into the computer code. The final step in the initialization process is to read in the number of the iteration and, if necessary, the electron state densities from the previous iteration.

The rate equations Eq. (II-11) can be solved once the plasma properties are entered into the program. This is described in section two. A flow chart of the subroutine involved, RATE1, is shown in Fig. (III-2). First the collisional-radiative terms are combined into the form of Eq. (II-15) to be used in the matrix formulation of the rate equations. Next the coefficients are scaled down to the order or unity and the system of equations is closed using Eq. (II-12).

With the state densities evaluated in GAUSS1, the radiative-energy intensities can be calculated in RADCAL. Figure (III-3) shows the subroutines contained in CGYPAC where the calculations in RADCAL are actually done. Each of the subroutines in Fig. (III-3) computes the different representatives of the directed radiative-energy intensity within the

RATE1

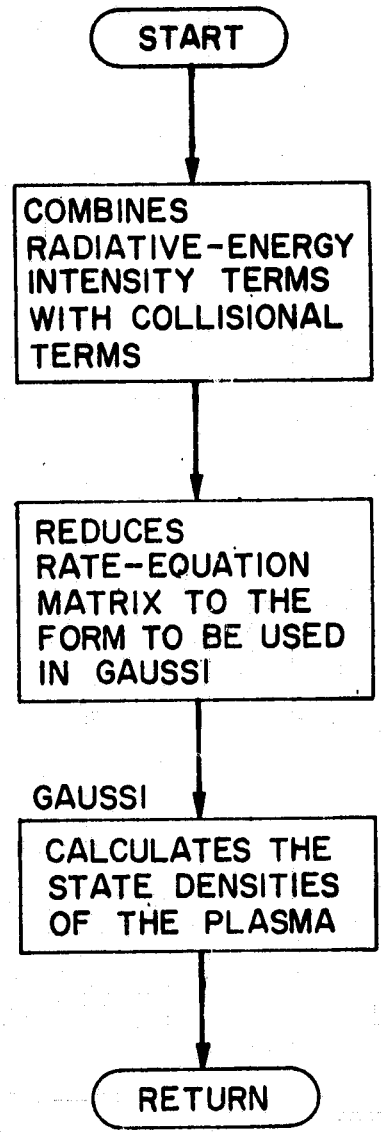

Figure III-2. Flow chart of subroutine RATE1. This is the subroutine in DENCAL in which the excited state densities within the plasma are calculated.

CGYPAC

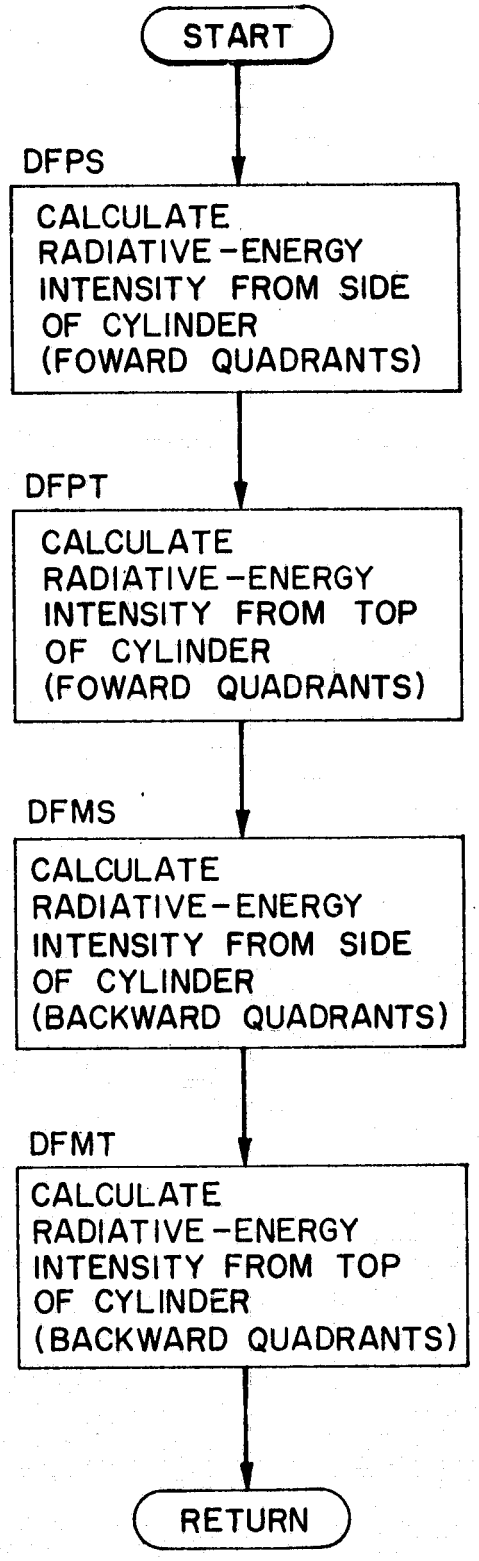

Figure III-3. Flow chart of subroutine CGYPAC. This is the subroutine in RADCAL in which the total radiative-energy intensities are calculated.

plasma and DFPS evaluates the directed intensity along paths that originate on the side of the cylinder and are in the forward area. The form of the directed intensity is that of Eq. (II-38). DFPT calculates the directed intensity from the top of the cylinder in the forward volume and the form of this intensity is that of Eq. (II-43). In the backward volume DFMS computes the directed flux from the side of the cylinder and its form is that of Eq. (II-47). Finally DFMT evaluates the directed intensity from the top of the cylinder in the backwards direction and was the form of Eq. (II-50). Each of these must be integrated over the quadrants where they apply. Thus an integrating routine to do double integrals containing a functional dependence for the inner integration had to be developed. A ten-point Gaussian-quadrature routine is used to do both the inner and outer integrals. To ensure intermediate data is not lost between iterations, the results of CYGPAC and RATE1 are written on disks.

The radiative-energy intensities are chosen to determine if the solutions converge. Because of their complex dependence on the state densities, the radiative-energy intensities converge more slowly than the state densities. The criteria used in these calculations are that no more than one percent of the solutions can diverge by more than 15 percent and only ten percent of the solutions can diverge between five and fifteen percent. Once these criteria are met the calculation stops and final solutions are printed out.

B. Tests of the Code

Within the computer code described in the previous section two major calculations are performed. The first is the calculation of the state densities in RATE1 and then the computation of the radiative-energy

intensities in CYGPAC. Thus each calculation section was internally checked to determine if they were functioning properly. Then the entire code which contains both of these subroutines was tested to decide if it functioned properly.

RATE1 was first successfully tested on a system of three equations. Then to see if a system with multiple electron states could be treated, a low-pressure helium plasma was treated.[10] Helium was chosen in order to take advantage of the availability of electron cross-sections and state lifetimes. At this low pressure, 10 torr, the radiative-energy intensities in the plasma do not contribute significantly to the rate equations. These calculations illustrated the importance of the metastable states as was observed in experiments.[29]

To test the internal consistancy of CYGPAC a transition was chosen with a frequency of 4×10^{14} sec^{-1}, with an inverse lifetime of 4×10^{8} sec^{-1}, an upper-state density of $1.5 \times 10^{13}/cm^3$, a line width of 1.6×10^{11} sec^{-1}, and an attenuation of 0.3 cm^{-1}. The cylinder had a height and diameter of 20 cm in these calculations. The first check involved varying the number of regions within the cylinder to determine how this affected the calculated radiative-energy flux at the edge of the cylinder on the centerline. The results of these calculations are seen in Table (III-1) for 1 to 5 regions within the plasma. The solution changes only 1.6 percent with the variation in the number of regions. This difference arises because the mesh of the integrations over the volume of the cylinder becomes finer as the number of regions is increased, thus the solution becomes more accurate. If a large multi-region problem were to be treated using this code then a better integration routine over

Number of Regions	$F_\nu(0)$ evaluated at the surface
1	38.5 ergs/cm^2
2	38.5 ergs/cm^2
3	38.3 ergs/cm^2
4	38.2 ergs/cm^2
5	38.0 ergs/cm^2

Table III-1. Comparison of the Radiative-energy Flux at the Surface of a Cylinder For a Variable Number of Interior Regions.

the azimuthal angle would be necessary to obtain accuracy. For example, instead of a 10-point Gaussian-quadrature integration, a 96-point quadrature could be used.

As a further check, these results were compared to results for inscribed and circumscribed spheres. The latter should provide lower and upper bounds on the total radiative-energy intensity and represent cases where an analytic solution is possible. As shown in Appendix A, the total radiative-energy intensity for a sphere is:

$$F_\gamma(0) = \frac{2\pi f}{\gamma}\left[\frac{1}{2\gamma a}\left(e^{2\gamma a} - 1\right) - 1\right], \qquad \text{(III-1)}$$

where

$$f = \frac{ANh\nu g(\nu)}{4\pi}, \qquad \text{(III-2)}$$

and a is the radius of the sphere.

The radiative-energy intensity of the surface of an inscribed sphere containing the same plasma as in Table (III-1) is 21.9 ergs/cm^2 while a circumscribed sphere has a radiative-energy intensity of 178.3 ergs/cm^2. Thus, the result from the code is indeed bracketed by these values. The reason for the large difference in the results for the two spheres is that the attenuation along the path length changes for each of these cases. In the case of the inscribed sphere the maximum path length is 20 cm, while the circumscribed sphere's maximum path length is 28.3 cm compared to a maximum path length of 22.4 cm for the actual cylinder. The ratio of the radiative-energy intensities is approximately 1:2:18 for the inscribed sphere to the cylinder to the circumscribed sphere. If just the exponential attenuation, $e^{\gamma s}$, is considered for the maximum path lengths in the plasma this ratio is approximately 1:2:22. Thus, CYGPAC is functioning properly.

The previous tests prove that the results from each of the major calculational subroutines are correct. Now the code with both of these subroutines must be examined. The model used in these tests is a two species plasma in which species one is a four-level atom and species two is a three-level atom with 3 and 2 optical transitions, respectively. This simple model allows the state densities of the first iteration to be pre-calculated by hand as an additional check for the code. In the initial test in this series a case where there were high absorptions for all the transitions in the plasma was investigated. The high absorptions guarantee the total radiative-energy intensities will be small. Hence, the solutions will rapidly converge. Table (III-2) shows the state densities and radiative-energy intensities for this case. A converged solution is obtained in two iterations and the total radiative-energy intensities are small.

Table (III-3) presents the state densities and calculated radiative-energy intensities for a case where a high gain is assumed. In this case the solutions rapidly converge because the saturation radiation intensity I_s is realized[30,31]; that is:

$$I_s = \frac{c(C_u C_L)}{(C_U + C_L - A)B} \quad , \qquad \text{(III-3)}$$

where c is the speed of light, C_U and C_L are the inverse collisional life-times of the upper and lower state, respectively; A is the transition probability and B is the Einstein B coefficient for the transition.

The final test in this series is a case where there are non-saturated gains present in the plasma. Table (III-4) shows the state densities and

	Species 1		Species 2	
	Iteration		Iteration	
	1	2	1	2
State Densities #/cm^3	1.37×10^{17}	1.37×10^{17}	1.0×10^{17}	1.0×10^{17}
	1.13×10^{17}	1.13×10^{17}	1.0×10^{16}	1.0×10^{16}
	1.0×10^{16}	1.0×10^{16}		
Radiation Intensity ergs/cm^2	8.20×10^{-4}	8.20×10^{-4}	4.44×10^{-5}	4.44×10^{-5}
	8.68×10^{-4}	8.68×10^{-4}	1.81×10^{-5}	1.81×10^{-5}
	3.52×10^{-4}	3.52×10^{-4}		

Table III-2. State densities and radiative-energy intensities for a case with large absorption.

	Species 1		Species 2	
	Iteration		Iteration	
	1	2	1	2
State Densities #/cm^3	5.48×10^{16}	7.50×10^{16}	4.88×10^{16}	4.99×10^{16}
	4.52×10^{16}	6.18×10^{16}	6.11×10^{16}	6.00×10^{16}
	1.60×10^{17}	1.28×10^{17}	1.12×10^{15}	1.10×10^{15}
	1.00×10^{17}	9.44×10^{16}		
Radiation Intensity ergs/cm^2	2.66×10^{6}	2.66×10^{6}	1.03×10^{-4}	9.92×10^{-5}
	1.46×10^{5}	1.46×10^{5}	8.38×10^{4}	8.38×10^{4}
	2.62×10^{3}	2.62×10^{3}		

Table III-3. State densities and radiative-energy intensities for atoms with large gains.

	Species 1				Species 2			
	Iteration				Iteration			
	1	2	3	4	1	2	3	4
State	5.48×10^{13}	7.36×10^{13}	7.28×10^{13}	7.28×10^{13}	4.88×10^{13}	4.99×10^{13}	4.99×10^{13}	4.99×10^{13}
Densities	4.52×10^{13}	6.06×10^{13}	6.00×10^{13}	6.00×10^{13}	6.11×10^{13}	6.01×10^{13}	6.01×10^{13}	6.01×10^{13}
$\#/cm^3$	1.60×10^{14}	1.27×10^{14}	1.26×10^{14}	1.26×10^{14}	1.12×10^{12}	1.10×10^{12}	1.10×10^{12}	1.10×10^{12}
	1.00×10^{14}	9.86×10^{13}	1.01×10^{14}	1.01×10^{14}				
Radiation	1.97×10^{3}	1.83×10^{1}	3.64×10^{1}	3.61×10^{1}	1.03×10^{-4}	9.92×10^{-5}	9.92×10^{-5}	9.92×10^{-5}
Intensity	2.66×10^{6}	2.66×10^{6}	2.66×10^{6}	2.66×10^{6}	8.39×10^{4}	8.39×10^{4}	8.39×10^{4}	8.39×10^{4}
$ergs/cm^2$	3.81×10^{2}	2.15×10^{1}	3.56×10^{1}	3.54×10^{1}				

Table III-4. State densities and radiative-energy intensities for atoms with non-saturated gains.

total radiative-energy fluxes for this case. Four iterations are required before an acceptable solution is obtained because now there are large radiative-energy intensities that are not saturated.

C. Conclusion

In this chapter the computer code developed from the analysis in Chapter II was discussed. Then the tests of the principal computational subroutines were presented showing that the calculations produce results that are correct. Finally, the tests of the entire code were discussed proving that the code would treat all possible attenuations that are found in a uranium plasma.

CHAPTER IV. URANIUM PLASMA MODEL

A. Introduction

The first step in formulating a plasma model is to identify the principle constituents of the plasma. For the plasma under consideration, this entails identifying the concentrations of the various ions of uranium present. Calculations have been done at the University of Illinois by C. Bathke[27] to determine the fractional densities of various species in the plasma and the resulting electron flux. He calculated the constituents of the plasma using the Saha equation as applied by Krascella[4] to uranium. Results quoted in the present work for the electron flux and plasma constituents are taken from Bathke's work at a pressure of one atmosphere.

The atomic constituents of the plasma change when the plasma temperature changes as is shown in Table (IV-1). The ionization fraction ranges from 10^{-2} at 5000°K to 0.5 at 8000^{0} K. Doubly ionized uranium can be neglected as a source of radiation in these calculations because of its low density. Although the neutron flux dramatically alters the high-energy electron flux, it does not significantly change the densities of the plasma constituents. This is because at these temperatures thermal effects are the main cause of ionization rather than the high energy electrons.

In the modeling of the plasma both global and local properties must be considered. Global properties are those properties that are constant for a given species throughout the plasma. Examples of these are the spontaneous decay lifetimes of the atomic states. Local properties are constant for a species only within a given region of the plasma. An example is the electron flux which changes in each region.

T Temp (1000°K)	N_o	N_+	N_{++}
5	1.39×10^{18}	3.56×10^{16}	3.51×10^{10}
6	9.86×10^{17}	1.15×10^{17}	2.78×10^{12}
7	5.77×10^{17}	2.32×10^{17}	6.56×10^{13}
8	2.58×10^{17}	3.26×10^{17}	7.18×10^{14}

Table IV-1. The atomic densities (#/cm^3) of the various species of uranium present in the plasma for various temperatures at a pressure of 1 Atm.[27] N_o is the density of neutral uranium. N_+ and N_{++} are the densities of singly and doubly ionized uranium.

B. Radiation Data

Electron energy levels must be identified in each of the radiating constituents to develop a model. This can be accomplished if the transitions in both neutral, U°, and singly ionized, U^{+}, are identified. Then by describing the transitions by their inverse lifetimes (Einstein A coefficients), absorption and stimulated emission can be calculated.

The Einstein A coefficient is sufficient to describe radiative processes within the plasma because absorption and stimulated emission can be described by the Einstein B coefficients. The ratio of the Einstein A coefficient to the Einstein B coefficient is

$$\frac{A_{ij}}{B_{ij}} = \frac{8\pi h\nu^3}{c^3} , \qquad \text{(IV-1)}$$

where A_{ij} is the inverse lifetime, B_{ij} is the Einstein B coefficient describint stimulated emission, h is Planck's constant, ν is the frequency of the transition and c is the speed of light; also

$$\frac{B_{ij}}{B_{ji}} = \frac{g_j}{g_i} , \qquad \text{(IV-2)}$$

where B_{ji} describes absorption and g_i/g_j is the ratio of the lower to upper state degeneracies.

The radiative term in the rate equation corresponding to absorption or stimulated emission is of the form

$$R = B_{ij} \frac{F_{\nu}(0)}{c} . \qquad \text{(IV-3)}$$

Thus once the inverse lifetimes are known, the radiative processes within the plasma can be described.

The first reported data[32] describing transitions in uranium was from an experiment at the National Bureau of Standards (N.B.S.) where the plasma temperature was 5000°K. Intensities for two hundred and eighty-five transitions in U° and two hundred and seventy-eight transitions in U^{+} were reported. These workers did not, however, report lifetimes. Thus it is necessary to estimate A coefficients as follows. From the measured intensities, relative inverse lifetimes (i.e., A_1/A_2) can be obtained using the relation:

$$\frac{A_1}{A_2} = \frac{I_1}{I_2} \frac{\nu_2}{\nu_1} \frac{N_2}{N_1} \quad , \qquad \text{(IV-4)}$$

where I is the relative intensity, ν is the transition frequency, N is the atomic-state density of the emitter and 1 and 2 refer to transition 1 and 2. Since the atoms were in thermodynamic equilibrium, Boltzmann statistics is assumed valid, in which case N_2/N_1 becomes:

$$\frac{N_2}{N_1} = e^{-E/kT} \quad , \qquad \text{(IV-5)}$$

where E is the difference in energy between state 2 and 1.

In uranium the transitions are governed by j-j selection rules as opposed to l-s selection rules in hydrogen. Figure (IV-1) shows the range[33] of known levels in U° and U^{+}. In neutral uranium a single family of upper states is identified that has even parity. These states emit radiation to two families with lower energies that have odd parity. The same situation exists in singly ionized uranium but here there are three lower energy families with odd parity and one high-energy family with odd parity that can emit radiation to the lower lying even parity states

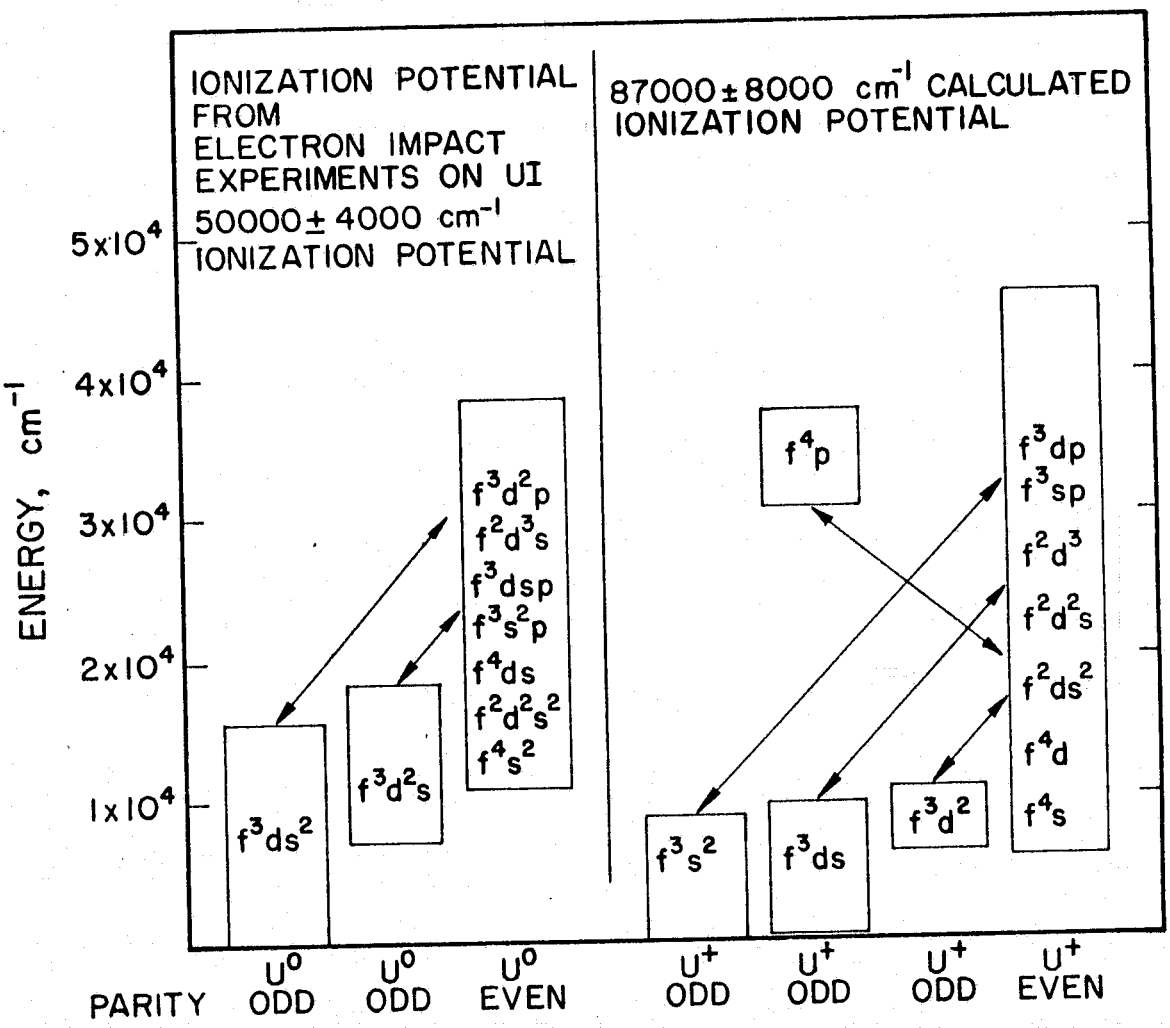

Figure IV-1. Range of energies for known states in neutral and singly ionized uranium[33].

(e.g. $f^4p \rightarrow f^4d$). In this figure the state energies were given in cm^{-1}, the conversion between cm^{-1} and eV being

$$1 \text{ eV} = 8066.1 \text{ cm}^{-1}. \qquad \text{(IV-6)}$$

Later experiments at Los Alamos[33,34] provided additional data on other transitions in uranium. Although many more transitions were identified in these works, most of them could not be used because data on the conditions of the plasma were not described, (i.e., equilibrium vs non-equilibrium). Consequently, only transitions that originated from the same upper state, making $N_2/N_1 = 1$ in Eq. (IV-4) could be added to the existing A values with any confidence. This process added 982 transitions to U° and 298 transitions to U^+. The data are summarized in Appendix B (Tables B-1 and B-4).

Thus the N.B.S. experiment[32] identified a set of basic transitions in uranium and the Los Alamos experiments[33,34] provided data for additional transitions. An example of this identification process can be seen in Table (IV-2) for some transitions in U°. Here the number of transitions positively identified by their lifetimes increased by a value of 370% using the LASL data, but some A values are still uncertain. This inability to include all the possible transitions is one of the major shortcomings of the present work. Still, the omission does not seem to be overly crucial, since the intensities of the missing lines were not predominant in the experimental observations.

Absolute A values must be known for the calculations. To obtain these from the ratios, one of the lifetimes in each atom must be known. For U^o the relative inverse lifetimes are converted to an absolute scale using the 27887 to 0 cm^{-1} absolute A value of 1.37×10^8 sec^{-1} obtained

		FINAL STATE										
		0	620	3801	3868	4276	4453	5762	5991	6249	7006	7104
INITIAL STATE	28444	.8097*	.1705*			.0041		.00399		.00557	.00531	
	28454		.0641*		.06036		.00068			.00176		.00107
	28470	.1254*	.1073*	.00347		0011		.00109		.00323	.00086	
	28504	.4047*	.13382			.00928	.00514	.0014	.00776	.00073	.00229	
	28543	.09162	.0874*	.00784	.04626	.02007		.00234	.00384	.00275	.01133	
	28563	.3338*	.0877			.00682		.00058		.00098		
	28650	.8529*	1.0662*			.00364	.00184	.00165	.00063	.01063		

Table IV-2. Relative inverse lifetimes for some states of UI based on Ref. 32, Ref. 33 and Ref. 34. Energies are in cm^{-1}.

*indicates data is from Ref. 32

by Klose,[35] e.g., this gives a value of 1.30×10^7 sec^{-1} for the 28504 to 620 cm^{-1} transition. No absolute A value was available to normalize the relative A values in U^+. There is a state coincidence at 27499 cm^{-1} in U^o and U^+; so assuming a 50:50 ratio of U^o:U^+ N_1/N_2 will become 1 in Eq. (IV-4) if both transitions originate from these states. This evaluation of A values from the 27499 cm^{-1} state in U^+ establishes an absolute scale for A values in ionized uranium.

In the above manner the state energy levels were identified and the Einstein A coefficient for the various transitions was calculated. A summary of the lifetimes used is presented in Appendix B.

C. Collisional Data

In addition to the radiative data, the collisional cross sections are needed to describe the atomic states in the plasma. Atom-atom and atom-ion collisions can be neglected because the atoms are at thermal energies and due to their large mass are moving slowly compared to the orbital speed of bound electrons. Hence the electrons will adjust themselves to the changing force field in collisions with atoms without undergoing transitions.[26]

1. Ionization Cross-Sections

Direct experimental measurements of cross-sections for electron excitation and ionization in uranium are not available; thus, the necessary data had to be calculated. The ionization and excitation cross-sections by electron impact have been calculated from formulae proposed by Vriens[36] based upon the Gryzinski model corrected for enhancement due to ions[37]. Vriens corrects for the asymmetry in the original Gryzinski[38] cross-sections by allowing the incident electron to gain kinetic energy

equal to the potential energy it loses as it interacts with the atomic electron. The resulting formula for the ionization cross section[36] is

$$\sigma_i(E) = \frac{\pi e^4}{E + 2UI}\left[\left(\frac{1}{UI} - \frac{1}{E}\right) + \frac{2}{3}\left(\frac{1}{UI} - \frac{UI}{E^2}\right) - \frac{\ell n(E/UI)}{E + UI}\right], \qquad \text{(IV-7)}$$

where UI is the ionization potential of the state under consideration. In the present work, however, the factor $(E + 2UI)^{-1}$ in Eq. (IV-7) is replaced by E^{-1} as well as in the excitation cross-section formula presented later in order to account for the focusing effect of ions.[37]

The accuracy of these cross-sections compared to experimental cross-sections[39] is found to be about a factor of two. The excitation cross-sections presented in the next section are found to be aecurate to an order of magnitude. The large discrepancy in this case is due to the smaller energy differences possible in excitation events as opposed to ionization events.

Figure (IV-2) shows the calculated ionization cross-sections for the ground state of neutral and singly ionized uranium. The cross-section for neutral uranium peaks earlier and is larger than the corresponding cross-section for singly ionized uranium because of the larger ionization potential of singly ionized uranium. These characteristics are again observed for the cross-sections found for the higher energy states in neutral uranium shown in Fig. (IV-3).

2. Excitation Cross-sections

The excitation cross-section is more complicated in the Gryzinski model, since the excitation to the final state and the next higher energy level in addition to the ionization potential are necessary to describe

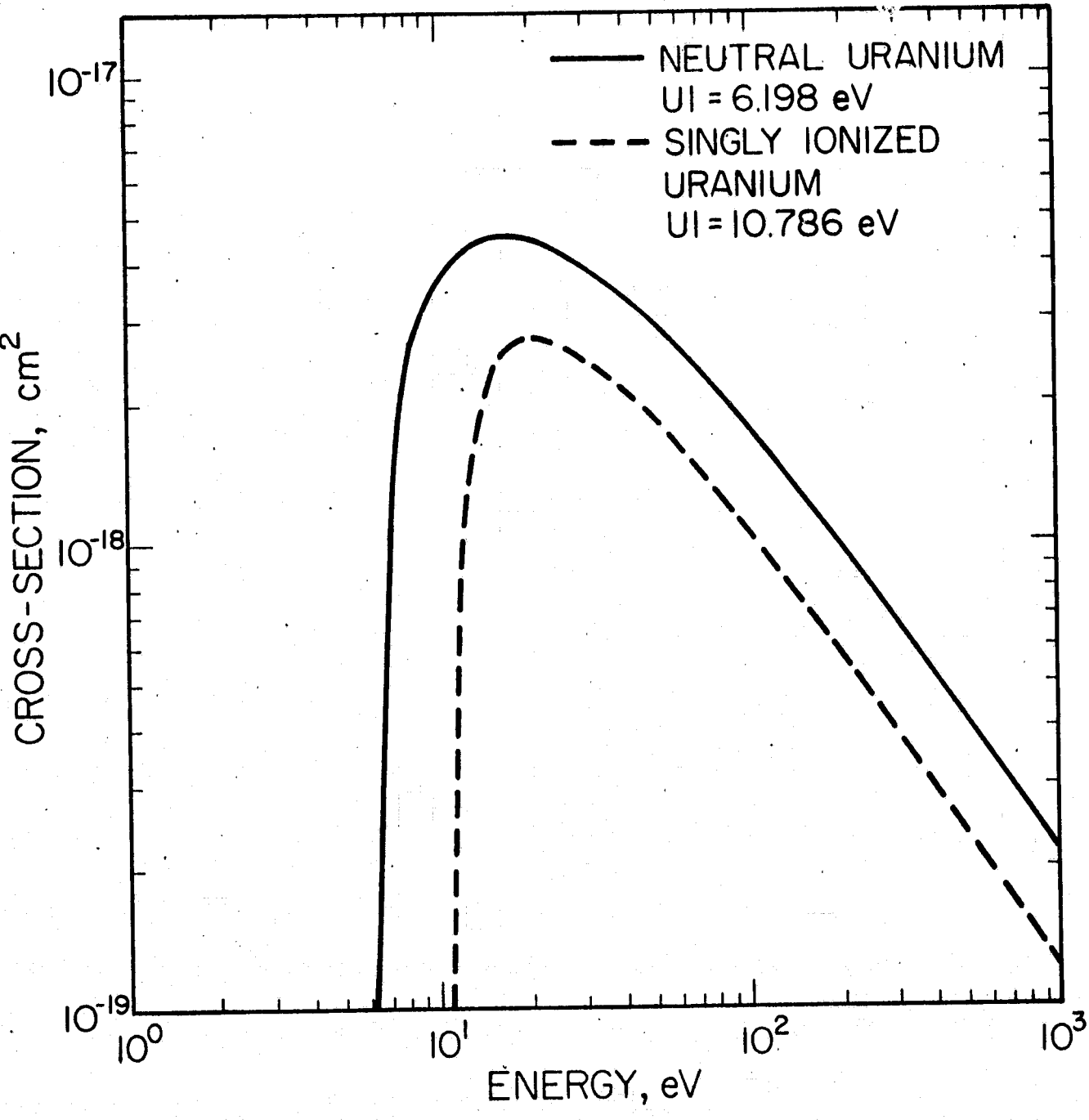

Figure IV-2 . Ionization cross-sections for the ground state of neutral and singly ionized uraniums.

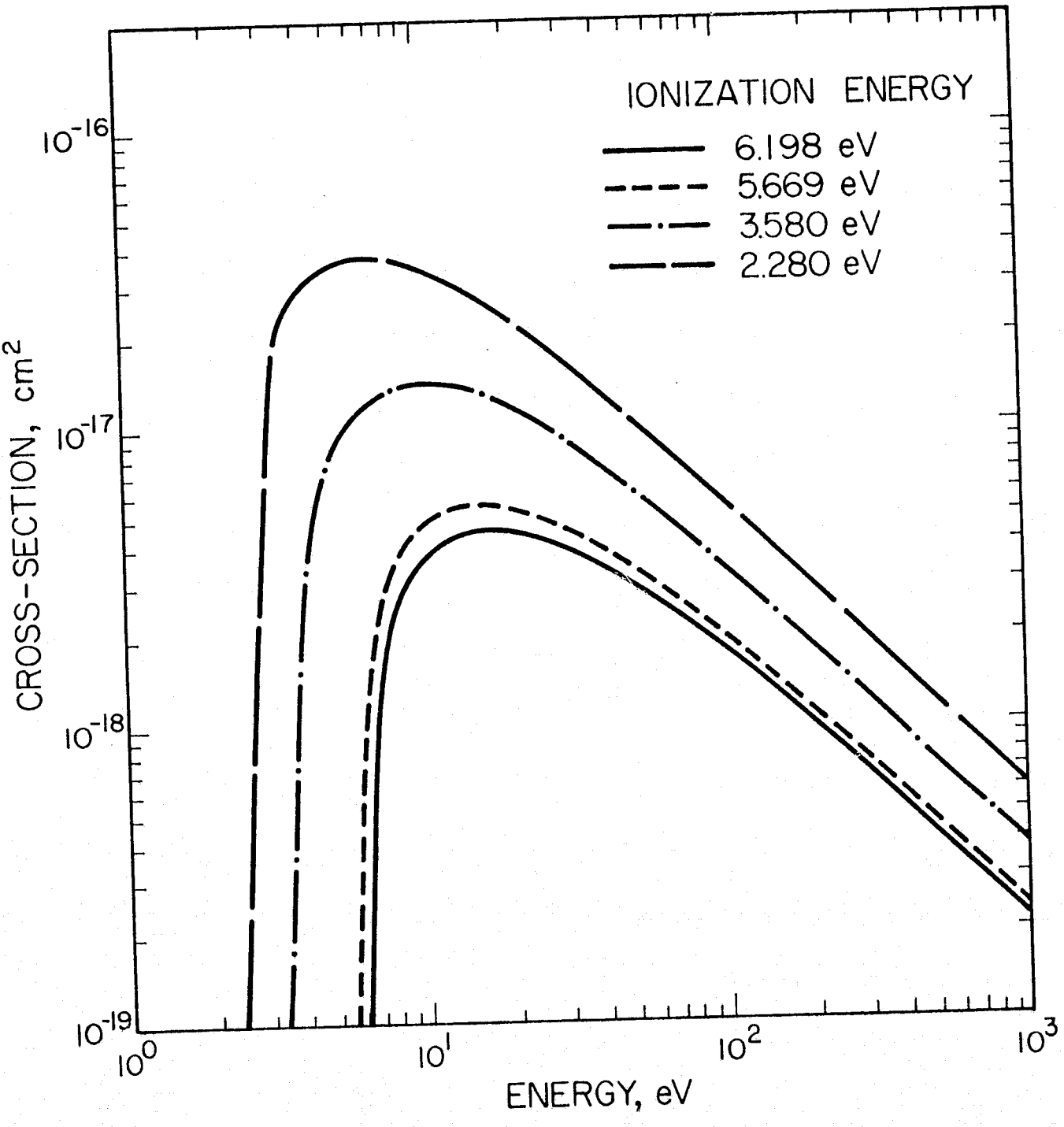

Figure IV-3 . Ionization cross-sections for various states in neutral uranium.

the interaction. The resulting cross-section can be written [36] as

$$\sigma_{ex}^{n}(E) = \frac{\pi e^4}{E + 2UI}\left[\left(\frac{1}{U_n} - \frac{1}{U_{n+1}}\right) + \frac{2UI}{3}\left(\frac{1}{U_n^2} - \frac{1}{U_{n+1}^2}\right)\right.$$

$$+ \left(\frac{1}{E + UI - U_{n+1}} - \frac{1}{E + UI - U_n}\right) + \frac{2UI}{3}\left(\frac{1}{\langle E + UI - U_{n+1}\rangle^2} - \frac{1}{\langle E + UI - U_n\rangle^2}\right)$$

$$\left. - \frac{1}{E + UI}\cos\left\{\sqrt{\frac{R}{E + U_n}}\,\ell n\left(\frac{E + UI - U_n}{U_n}\right)\right\}\ell n\,\frac{U_{n+1}(E+UI-U_n)}{U_n(E+UI-U_{n+1})}\right], \quad \text{(IV-8)}$$

where U_n is the excitation energy to state n, U_{n+1} is the excitation energy to state n+1 and R = 13.58eV. The rise from threshold to peak value is determined by the energy of the next higher state and over this energy range, $U_n \leq E \leq U_{n+1}$, U_{n+1} is replaced by E in Eq. (IV-8).

Because of the smaller energy transfers involved in excitation collisions, these cross-sections will generally be larger than for ionization. Also, as can be seen from Fig. (IV-2) the rise in the ionization cross-section from threshold to peak value takes place over an energy range of the order of electron volts. In contrast the rise from threshold to peak energy for the excitation cross-sections takes place over a smaller energy corresponding to the difference in energy between the n^{th} and the $n^{th}+1$ state. This sharp rise is evident from Fig. (IV-4) and Fig. (IV-5).

Figure (IV-4) shows cross-sections for excitation from the ground state to three different higher energy states in neutral uranium. The largest cross-section has the lowest excitation potential and the peak values of the cross-section decreases as the excitation potential increases. These trends are seen in Fig. (IV-5) which shows the cross-sections for various electron excitations to the 3.9959 eV energy level in neutral

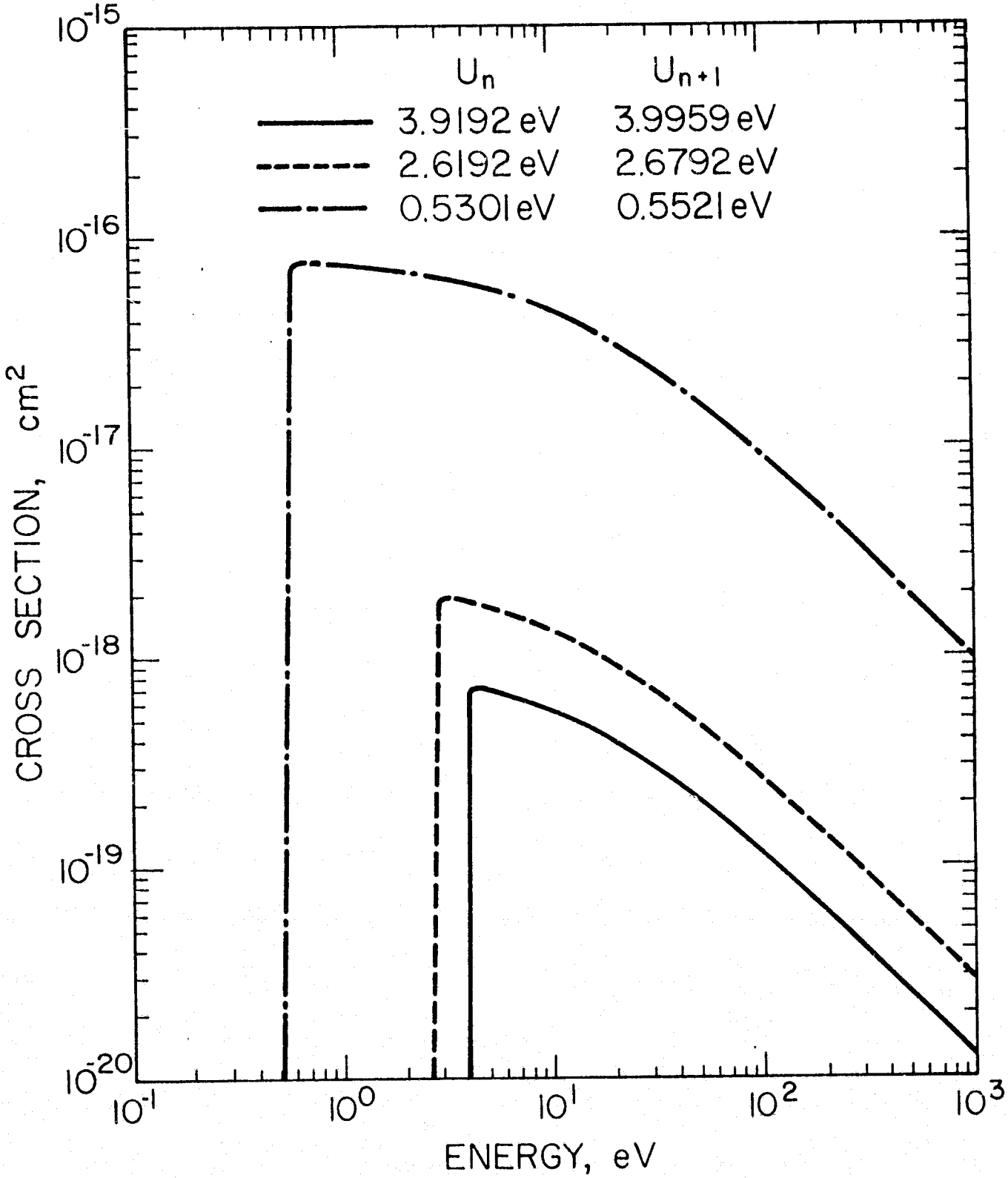

Figure IV-4 . Various excitation cross-sections from the ground state of neutral uranium.

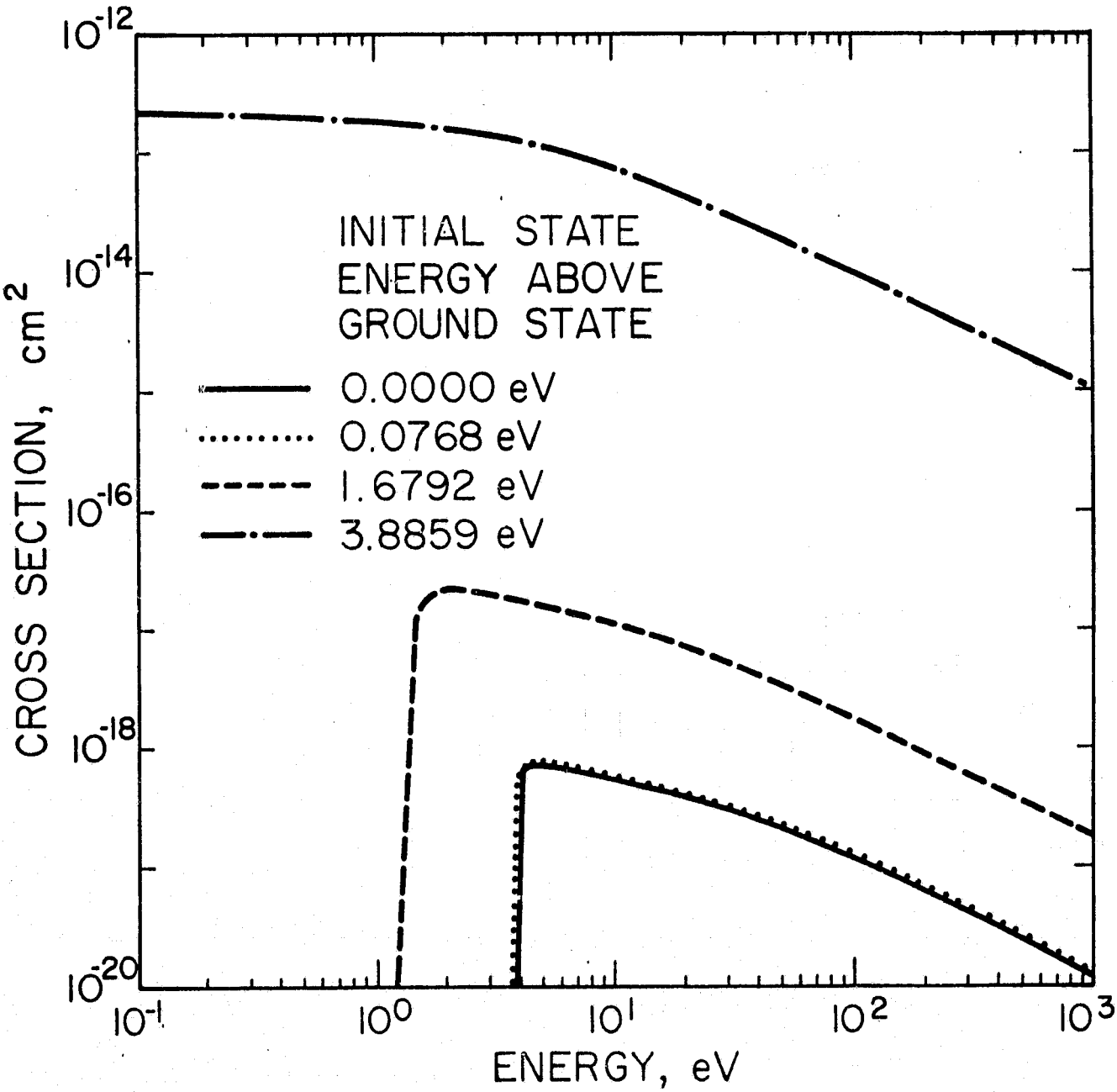

Figure IV-5 . Excitation cross-sections for various states to the 3.9192eV state in neutral uranium.

uranium. The increase in peak value of the cross-section due to the decrease in excitation potential is further enhanced by the decrease in ionization potential as seen by comparing the excitation cross-section from the ground state to the .5301 eV state in Fig. (IV-4) to the excitation cross-section from the 1.6792 eV state in Fig. (IV-5). Both of these cross-sections have approximately the same peak value although the excitation potential is doubled in the latter case. The difference in the ionization potential of the initial state compensates for the difference in excitation potential. With the atomic parameters now known, a model for the plasma can be implemented.

D. State Reductions

Due to limitations on the size of the computer program, all states in uranium cannot be treated explicitly. Hence, the number of states to be considered were reduced to a smaller number of "composite" states. To understand this reduction, consider the rate equation for state p

$$-\sum_{q} (R_{pq}+C_{pq})\ N_p + \sum_{q} (R_{qp}+C_{qp})\ N_q = D_p \ , \qquad \text{(IV-9)}$$

where q represents other states in the plasma, R the radiative terms in the rate equation, C the collisional terms in the rate equation, D the recombinational terms from the rate equation and N the atomic state densities.

For the model of uranium to accurately represent the actual plasma, the coefficients of the composite states in the rate equations must be equivalent to the coefficients of their constituent states. In the

present model, the composite transitions represent the average of all transitions from the constituent states. Hence, the A value and cross-sections of the composite state must be comparable to those of the constitutent states. In the present work, the composite state lifetime did not vary by more than a factor of two from the lifetimes of the constituent states. Also, the energy of the constituent states was within 200 cm^{-1} of the energy of the composite state. This ensures the cross-sections of the composite state will be equivalent to the cross-sections of the constitutent states. Figure (IV-5) illustrates this because the smallest two cross-sections are for states that are separated by 619 cm^{-1}. Figure (IV-6) shows a two level diagram where both the upper and lower levels represent composite states.

Using the above criteria the number of states was reduced from 169 to 62 in neutral uranium and from 95 to 46 in singly ionized uranium while still treating 822 optical transitions explicitly.

E. Electron Flux

In the preceding sections of this chapter global physical parameters were discussed. In this section the electron flux which determines local conditions in this analysis will be discussed. The calculations discussed in this section are taken from the work of C. Bathke[27]

1. Temperature Dependence

The first parameter we study is the temperature dependence of the electron flux for a given neutron flux. The reference neutron flux level used in this analysis is $2x10^{14}$ neutrons/cm^2-sec. The range of temperatures of interest is between 5000°K and 8000°K and the pressure is one atmosphere.

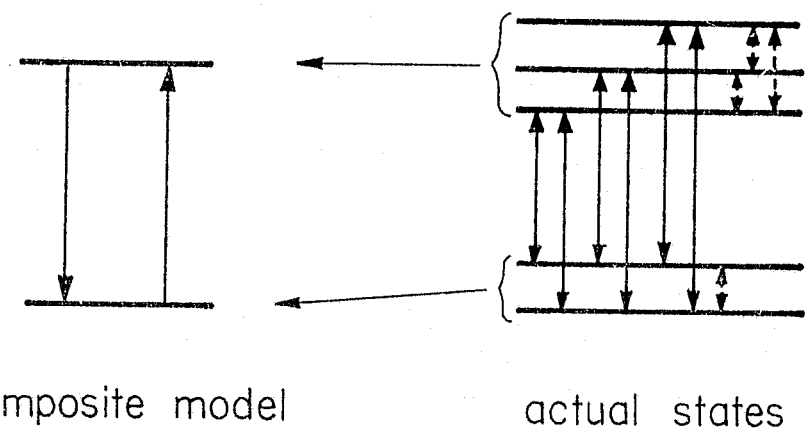

Figure IV-6. Schematic diagram of two level composite state representing five constituent states.

Figure (IV-7) shows the variation in electron flux with different temperatures. The non-Maxwellian component of the electron flux decreases as the temperature increases due to the corresponding decrease in the fission cross-section over this temperature range. The reduced fission cross-section causes the source of non-Maxwellian electrons to decrease, resulting in approximately an order of magnitude reduced in the high-energy electron-flux in going from 5000°K to 8000°K. This, coupled with the lower densities in the Maxwellian flux at low temperatures, implies that more radical non-Maxwellian excitation will occur in the low-temperature case.

2. Neutron Flux Dependence

A much more dramatic variation in the electron flux is seen when the exciting neutron flux is varied. In this study the range of variation is from 10^{12} to 10^{16} neutrons/cm^2-sec. Since the reaction rate for fission is proportional to the number of neutrons in the system, the change in the electron flux closely follows that of the neutron flux as can be seen in Fig. (IV-8).

The electron flux is so important because within the plasma all collisional reaction rates are calculated using it. The parametric study done here is of interest because it will be a direct test of the effectiveness of the non-Maxwellian tail of the electron flux in exciting the atoms in the plasma.

F. Data Processing

The preceding sections of this chapter have dealt with the various

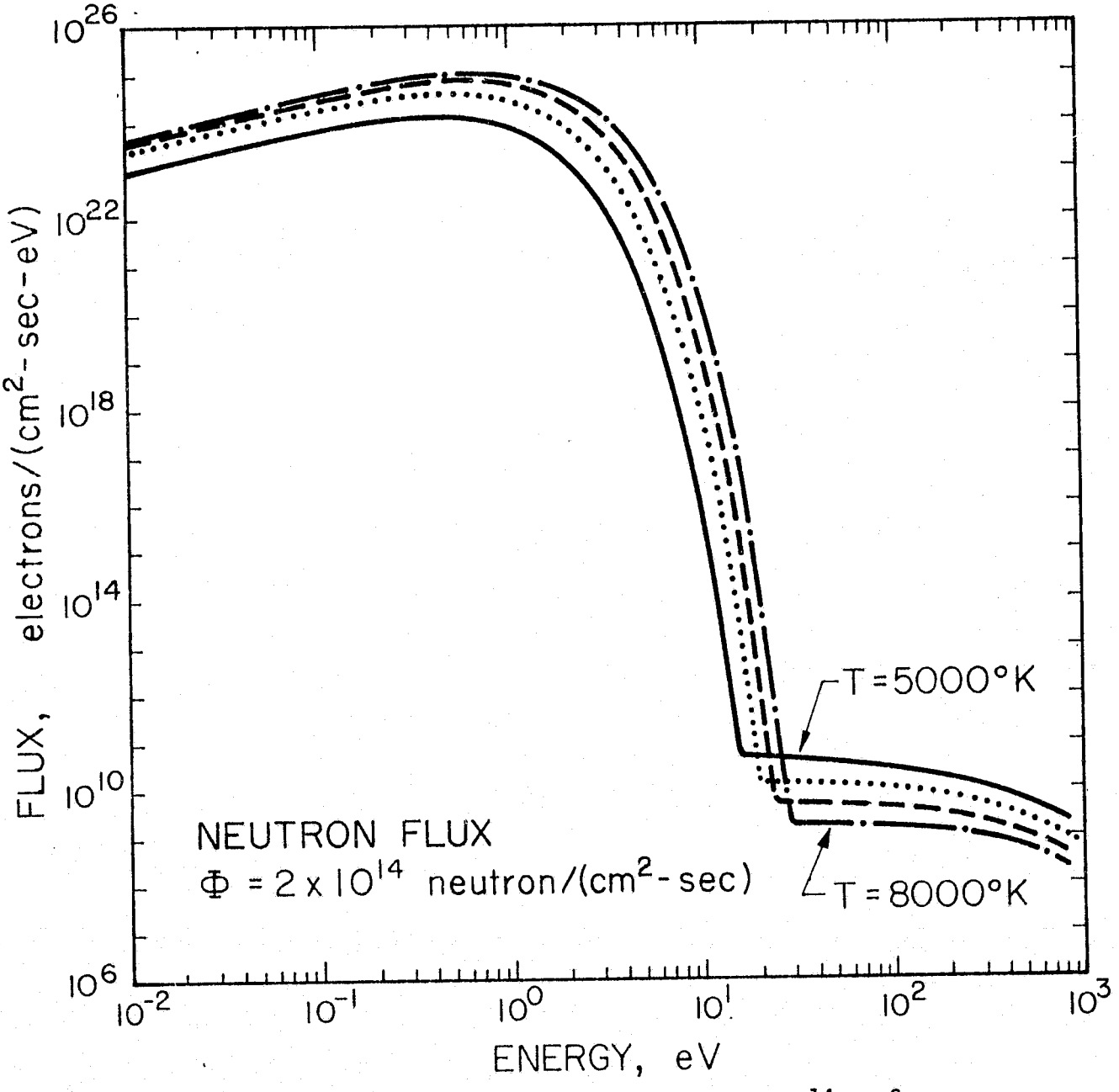

Figure IV-7. Electron flux for a neutron flux of 10^{14}n/cm^2-sec at temperatures of 5000°K, 6000°K, 7000°K and 8000°K.[27]

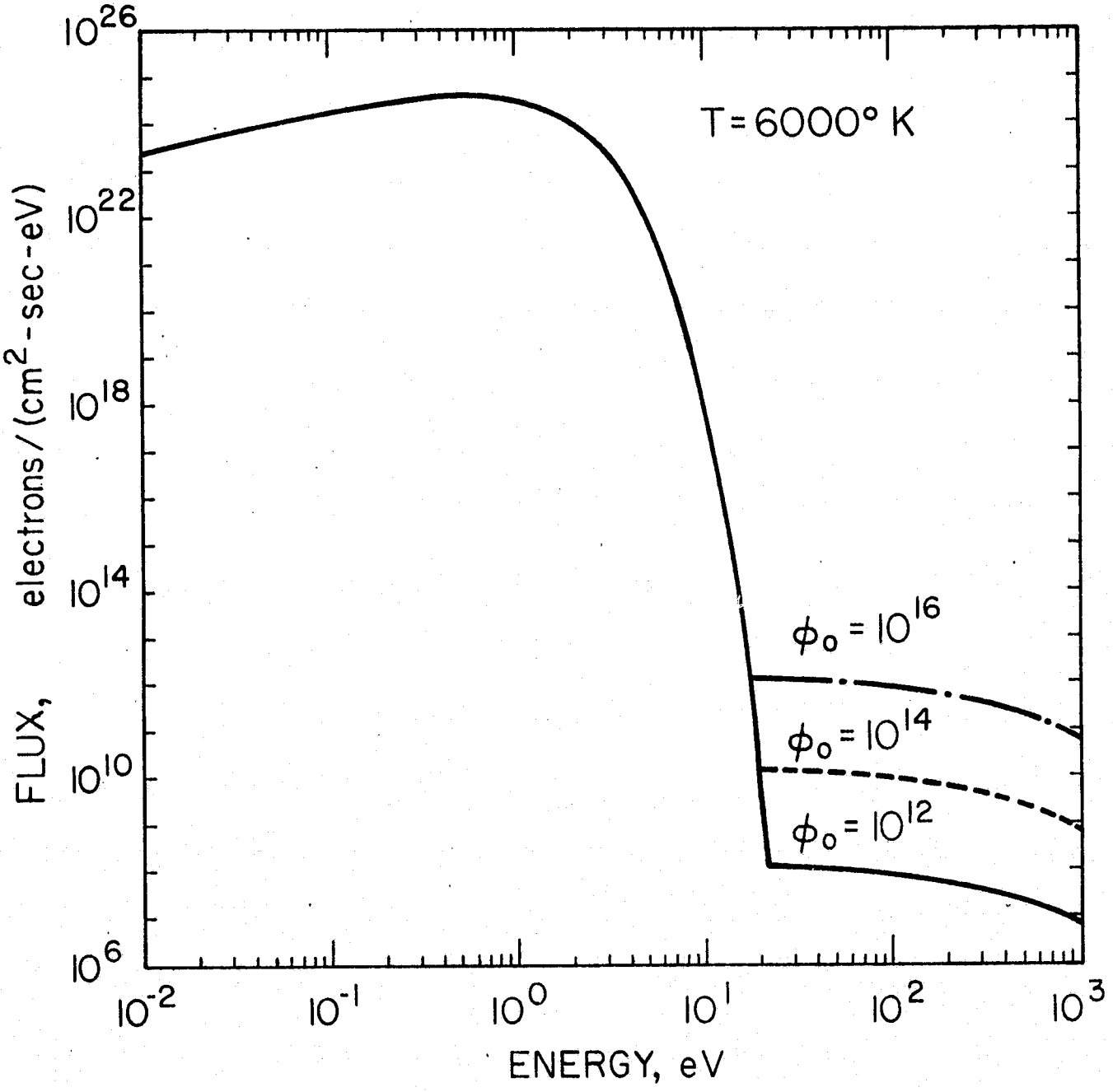

Figure IV-8. Electron flux at 6000°K for various neutron fluxes.[27]

physical phenomena that describe the plasma. In the present section the synthesis of these processes will be discussed.

Two types of coefficients are seen in the rate equation [Eq. II-11)]; those that vary with and those that remain constant with respect to the radiative-energy intensity. Collisional terms in the rate equations do not change with the radiative-energy intensity because the variable here is the electron flux. Thus within a given region these processes need only be calculated once. Throughout the plasma the state lifetimes for spontaneous decay, Einstein A coefficients also remain constant. Hence, these terms can be combined and saved for any calculations within a given region. This saves time when iterations are done in the code.

Absorption and stimulated emission depend upon the radiative-energy intensity and have to be calculated each iteration. These terms, combined with the constant terms, provide all of the coefficients employed in the rate equations.

Once the state densities are evaluated from the rate equations, the only parameter required to calculate the radiative-energy intensity is the line width. Due to the high pressure of the plasma a combined Doppler and collisionally broadened line widths are used[40,41]. Thus the line width, FWHM, is written as:

$$\Delta\nu = \frac{\pi\Delta\nu_D^2}{\nu} + \Delta\nu_{coll} \quad , \tag{IV-10}$$

where ν is the transition frequency, $\Delta\nu_{coll}$ is the collisionally broadened width and $\Delta\nu_D$ is the Doppler width given by

$$\Delta\nu_D = \sqrt{\frac{8kT\ 1n^2}{Mc^2}}\ \nu \quad , \tag{IV-11}$$

where k is Boltzmann's constant, T is the temperature of the plasma and M is the mass of the atom. The collisional width used in this work was developed by Linholm[42,43], who, by including the time dependence of the collision into the interruption broadening theory of collisions, accounted for close collisions. His results reduce to the interruption broadening results near line center or at low pressures. Also at high pressures or at frequencies in the wings, his result reduces to the statistical broadening result appropriate for these limits. Thus his model correctly describe the line shape in these limits. The Linholm collisional width is

$$\Delta\nu_{coll} = \frac{\pi e^2 f}{2m\nu_o} N \quad , \qquad \text{(IV-12)}$$

where e is the electron charge, m is the electron mass, f is the oscillator strength, and N is the density of the atomic species. The oscillator strength can be written

$$f = \frac{Ac^3}{8\pi^2\nu^2} \frac{m}{e^2} \quad , \qquad \text{(IV-13)}$$

where A is the transition probability. By substituting Eq. (IV-13) into (IV-12), the collisional width becomes

$$\Delta\nu_{coll} = \frac{Ac^3 N}{16\pi\nu^3} \quad . \qquad \text{(IV-14)}$$

To obtain the total line width Eq. (IV-11) and (IV-14) are substituted into (IV-10) to give

$$\Delta\nu = \frac{8\pi\ kT\ \ln 2}{Mc^2}\nu + \frac{Ac^3 N}{16\pi\nu^3} \quad . \qquad \text{(IV-15)}$$

The ratio of the collisional to Doppler contributions to the line width is obtained by dividing the first term in Eq. (IV-15) into the second

$$\frac{\Delta\nu_{coll}}{\Delta\gamma_D} = \sqrt{\frac{M}{2\pi kT}} \quad \frac{Ac^4N}{32\pi\nu^4} \quad . \tag{IV-16}$$

As can be seen here when the frequency of the transition is small or the density or transition probability is high, the collisional width becomes more predominant. Conversely, when the density or transition probability is low or the frequency is high then the Doppler width predominates this expression. Equation (IV-15) is the final parameter necessary to calculate the radiative-energy intensity.

G. Conclusion

In this chapter the distinction was made between global and local properties. Then the global properties were explained and used to give a model for the uranium plasma. This model is based on the modified Gryzinski cross-sections and experimentally measured radiation intensities. Thus, the model is limited by the accuracy of the theoretical cross-sections and the calculated lifetimes. In the absence of other data to incorporate into a model of uranium, this model is the most complete to date. Next, the electron flux, which defines the local plasma properties, was discussed. Finally, the combination of these properties in the transport code was explained.

CHAPTER V. RESULTS AND DISCUSSION

A. Physical Parameters and Convergence

Chapter II described the formalism that was incorporated into the computer code discussed in Chapter III. This chapter presents the results of these calculations. Unless otherwise specified, the plasma is at a uniform temperature and has a pressure of one atmosphere. The uranium plasma, consistent with projected gaseous core experiments, is cylindrical with a diameter and height both equal to one meter.

Before these results are presented, the convergence criteria used in the code must be discussed to understand the validity of the calculations. A choice of either the atomic state densities or the radiative-energy intensities could be used to determine convergence. If there is no radiation incident upon the surface of the cylinder, the directed radiative-energy intensity can be written

$$I(\nu,o) = \exp\left\{ \int_o^s \gamma(\nu,s')ds' \right\} \int_o^s f(\nu,s')ds' \exp\left\{ - \int_o^{s'} \gamma(\nu,x)\, dx \right\}. \qquad \text{(V-1)}$$

The source term, $f(\nu,s)$ is proportional to the upper state density and the attenuation, $\gamma(\nu,s)$ is proportional to the difference in the upper and lower state densities. Due to this complex dependence, the radiative-energy intensities are quite sensitive to changes in state densities and thus are used to establish convergence.

If the plasma is homogeneous so the source term and the attenuation are independent of position, Eq. (V-1) becomes

$$I(\nu,o) = \frac{f(\nu)}{\gamma(\nu)} \quad (e^{\gamma(\nu)s} - 1). \qquad \text{(V-2)}$$

The largest path length in the plasma is 141 cm. Assuming γ changes from -.05 to +.05 between iterations, the exponential, evaluated for the maximum path length in the plasma, in Eq. (V-2) changes from .0009 to 1153. Due to this large change, two convergence criteria were used. The first criterion is then no more than one percent, i.e., 8 of the transitions can diverge by more than 15%. This accounts for transitions that are changing from small absorptions to small gains. The second criterion is that no more than three percent, i.e., 25 of the transitions, can diverge between 5% and 15%. When both of these conditions are satisfied the solutions are assumed to be converged.

Details of the convergence for the case of a flux of 2×10^{14} neutrons/(cm^2-sec) and a uniform plasma temperature of 7000°K are shown in Table (V-1). Column one gives the number of the iteration; the second column, N15, gives the number of transitions that have diverged between 5% and 15%; and the third column, N15, gives the number of transitions that have diverged by more than 15%. The final column, N, represents the number of transitions that have converged to better than 5%. Initially, the convergence is slow but after the tenth iteration rate increases rapidly as the solutions stabilize. Finally, the rate decreases after a majority of the solutions have converged because only

	N5	N15	N
2	0	719	3
3	0	719	3
4	0	718	4
5	0	718	4
6	8	710	4
7	8	706	8
8	8	704	10
9	8	700	14
10	14	501	307
11	17	327	478
12	312	8	502
13	313	8	503
14	313	8	503
15	149	5	668
16	78	4	740
17	38	4	780
18	24	4	794

TABLE V-1. Convergence for a flux of 2×10^{14} neutrons/(cm^2-sec) and a gas temperature of 7000^0K

a few transitions have yet to converge. By the eighteenth iteration 96.5% of the transitions have converged to better than 5% in this case. Thus the observables calculated here should also be good to 5%.

This method was used in every calculation and Table (V-2) shows the final convergence for the uranium plasma when the temperature varied from 5000°K to 8000°K with the flux fixed at 2×10^{14} neutrons/(cm^2-sec). The 5000°K case converges so well because there are no inverted transitions, hence, the total radiative-energy intensities are small and do not make significant contributions to the rate equations. This effectively linearizes the problem because the atomic state densities are no longer dependent upon the radiation within the gas. As the temperature increases, the radiative-energy intensities increase, causing significant contributions to the rate equations and making the problem non-linear. Hence, the convergence becomes more difficult. In all cases the final solutions have converged to better than 5% for over 96.5% of the transitions in the plasma.

B. Radiative-Energy Current

In this section the radiative-energy current from a uranium plasma with a neutron flux of 2×10^{14} neutrons/(cm^2-sec) and a temperature variation of 5000°K to 8000°K will be discussed. Using the calculated atomic state densities, the radiative-energy current is computed from Eq. (II-29) where

$$\hat{\Omega} \cdot \hat{\Omega}' = \sin\theta \cos\phi \quad , \tag{V-3}$$

T, ^{0}K	N5	N15	N
5000	0	0	822
6000	5	3	814
7000	24	4	794
8000	12	7	803

TABLE V-2: Convergence for a flux of 2×10^{14} neutrons/(cm^2-sec)

and the current is evaluated at the mid-plane of the cylinder. The current is evaluated at a frequency corresponding to line center of each transition.

The Planck function,

$$J = \frac{2h\nu^3}{c^2} \left(e^{h\nu/kT} - 1 \right)^{-1} , \qquad \text{(V-4)}$$

describes the radiative-energy current from a system in thermal equilibrium. Equating Eq. (V-4) with the calculated radiative-energy current, the line "temperature", T_L, can be written:

$$T_L = \frac{h\nu}{k} \left[\ln\left(\frac{2h\nu^3}{Jc^2} - 1 \right) \right]^{-1} , \qquad \text{(V-5)}$$

where J is the calculated radiative-energy current. T_L when substituted into the Planck function will give the calculated radiative-energy current for the line at line center. Once the line temperature is calculated for all lines within the plasma, an effective temperature is defined by

$$T_{eff} = \langle T_L \rangle . \qquad \text{(V-6)}$$

Figure (V-1) illustrates this process. The solid curves represent the calculated radiative-energy current, J, from which the line temperature was calculated. These line temperatures are averaged to give the effective temperature. The current corresponding to the T_{eff} defined as $J_{T_{eff}}$

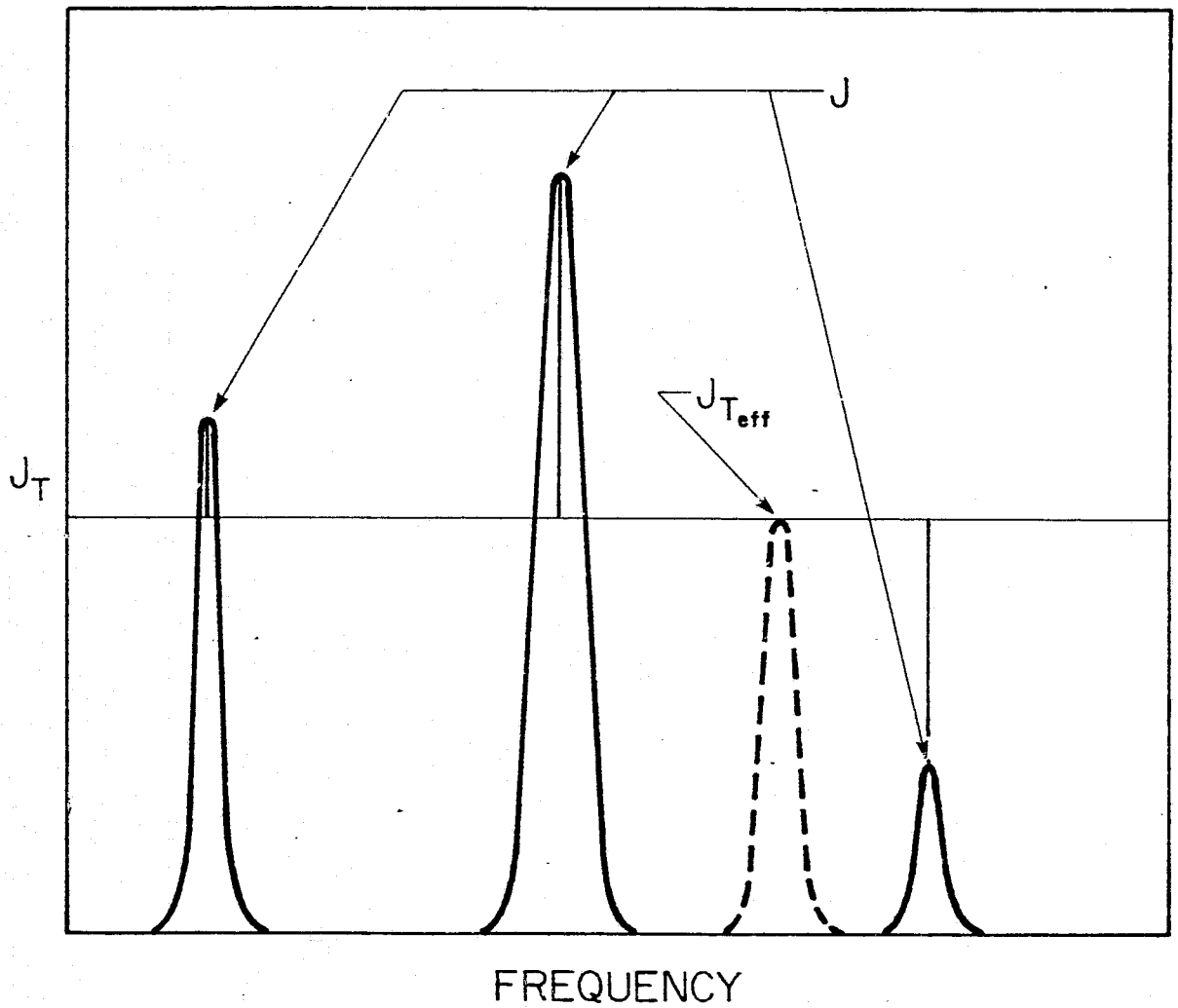

Figure V-1. Radiative-energy current versus frequency.

represents a weighted average as illustrated in the figure. T_{eff} is useful since the radiative-energy current from lines not included in this analysis can be computed by substituting the effective temperature and the frequency of the transition into Eq. (V-4). This is illustrated by the dashed curve in Fig. (V-1). Finally to solid line is the Planck function evaluated at T_{eff}.

Figures (V-2) through Fig. (V-5) show the J's plotted with respect to the Planck function at T_{eff} for a uranium plasma with a temperature variation of 5000°K to 8000°K and a flux of $2x10^{14}$ neutrons/(cm^2-sec). The horizontal curve is the Planck function at T_{eff} and the vertical lines are drawn from the Planck function to the radiative-energy current at line center as illustrated in Fig. (V-1). For 5000°K, no inversions are found within the plasma and T_{eff} is 9108°K. Much hotter effective temperatures are found at higher plasma temperatures, as in the 6000°K case where T_{eff} is 36,960°K. Along with the significant rise in T_{eff}, a number of inversions are found in this case [see Fig. (V-3)]. The most severe elevation in T_{eff} occurs at a plasma temperature of 7000°K where T_{eff} becomes 389,900°K [see Fig. (V-4)]. Finally, a T_{eff} of 180,800°K is calculated for the 8000°K plasma case [see Fig. (V-5)].

The T_{eff} variation for a flux of $2x10^{14}$ neutrons/(cm^2-sec) is shown in Fig. (V-6) where T_{eff}/T is plotted against T, the plasma temperature. To show that this variation can be predicted and explained, the simple three-state model illustrated in Fig. (II-2) is considered. The 3.9605-eV to .0769-eV transition in neutral uranium is assumed. In a homogeneous plasma radiative-energy current is

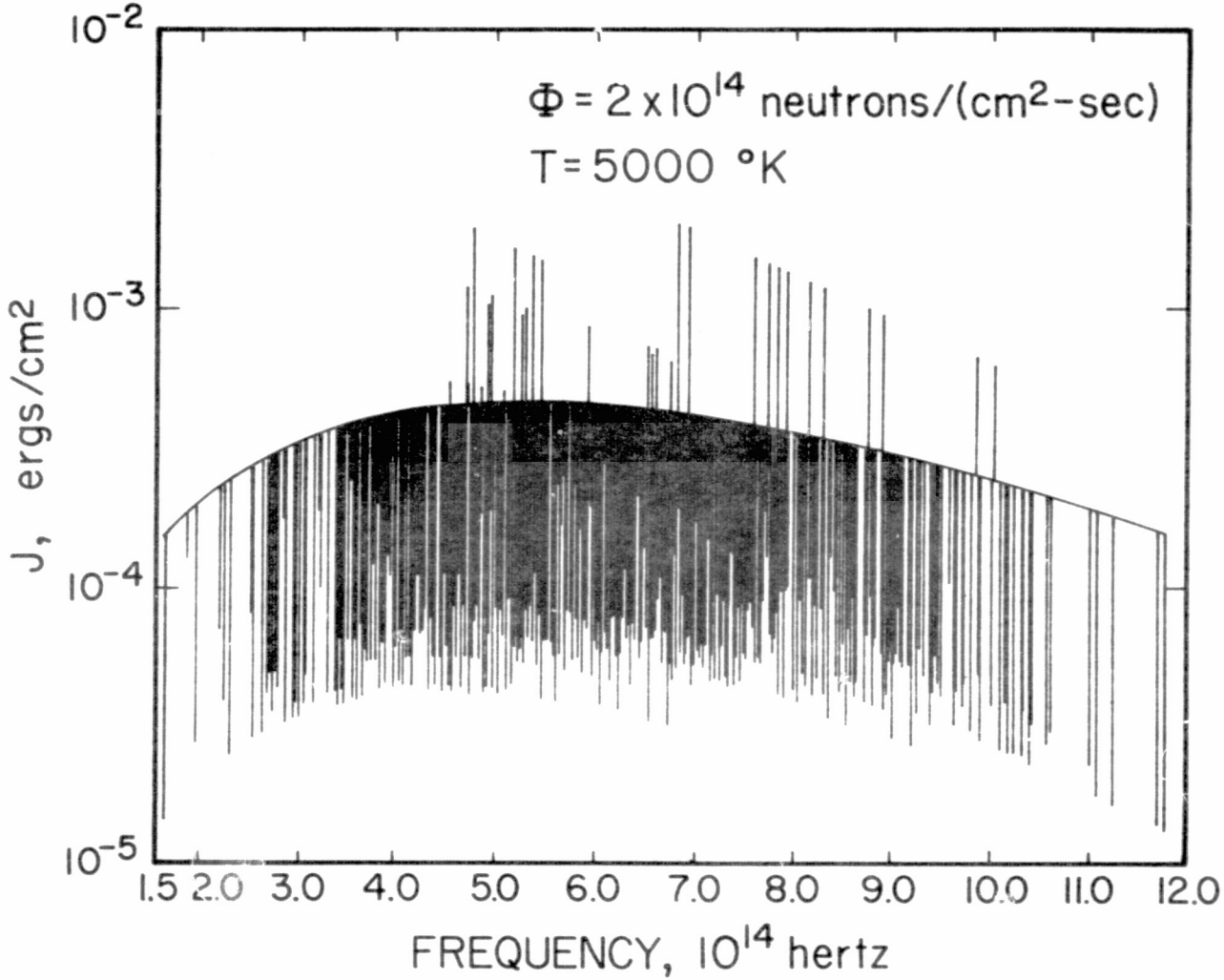

Figure V-2. Radiative-energy current versus frequency measured with respect to the Planck current at an effective temperature of 9108°K.

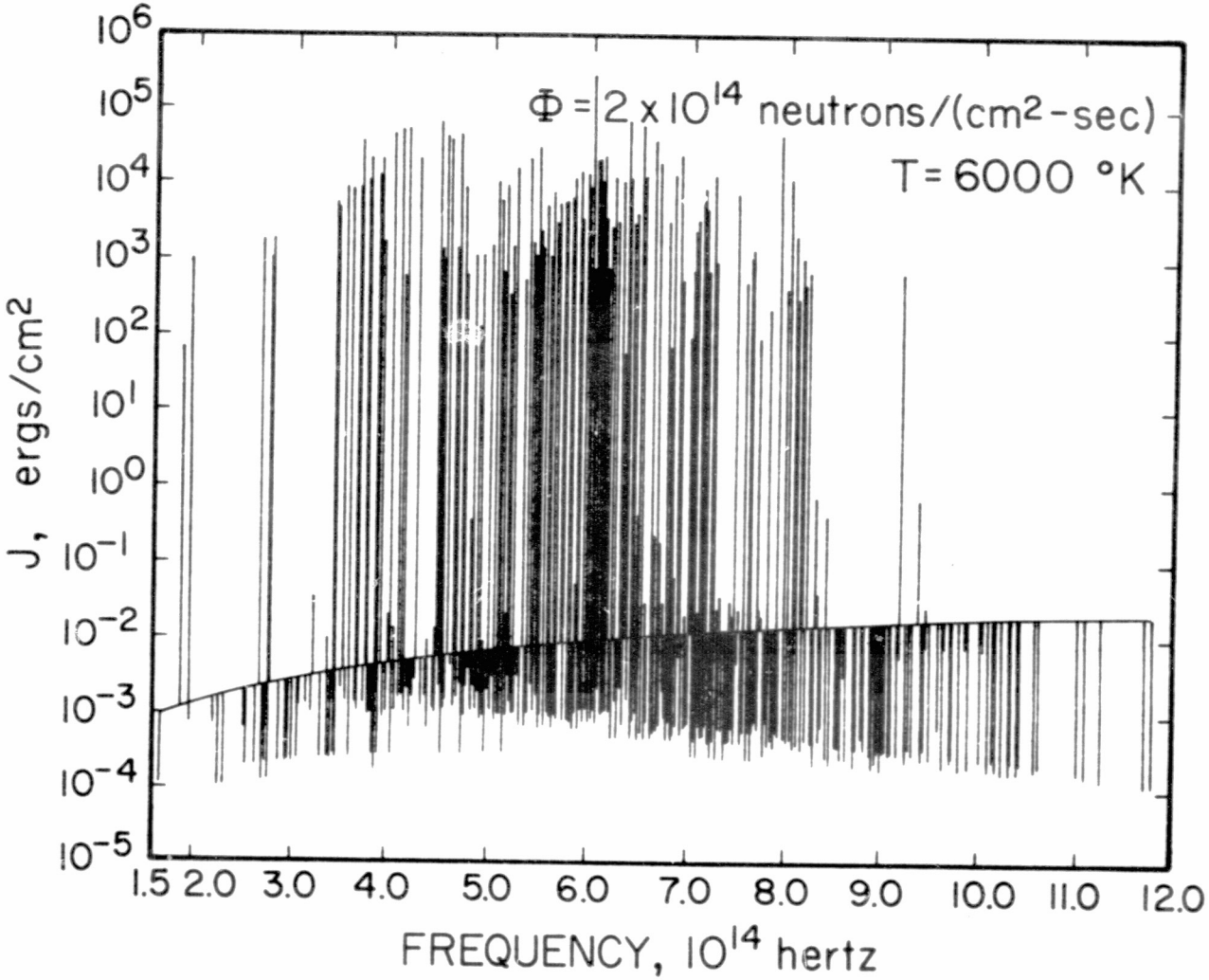

Figure V-3. Radiative-energy current versus frequency measured with respect to the Planck current at an effective temperature of 36,960°K.

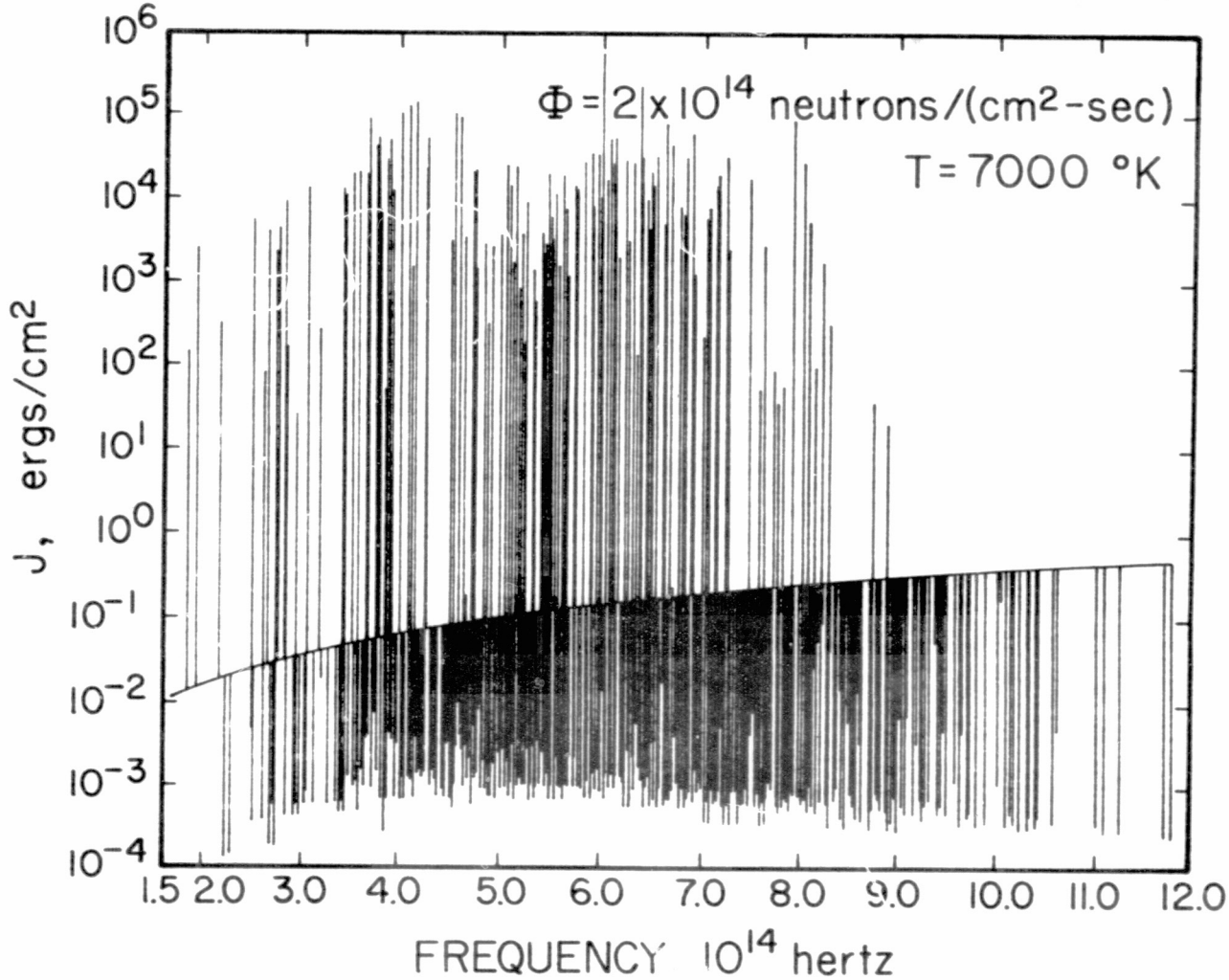

Figure V-4. Radiative-energy current versus frequency measured with respect to the Planck current at an effective temperature of 389,900°K.

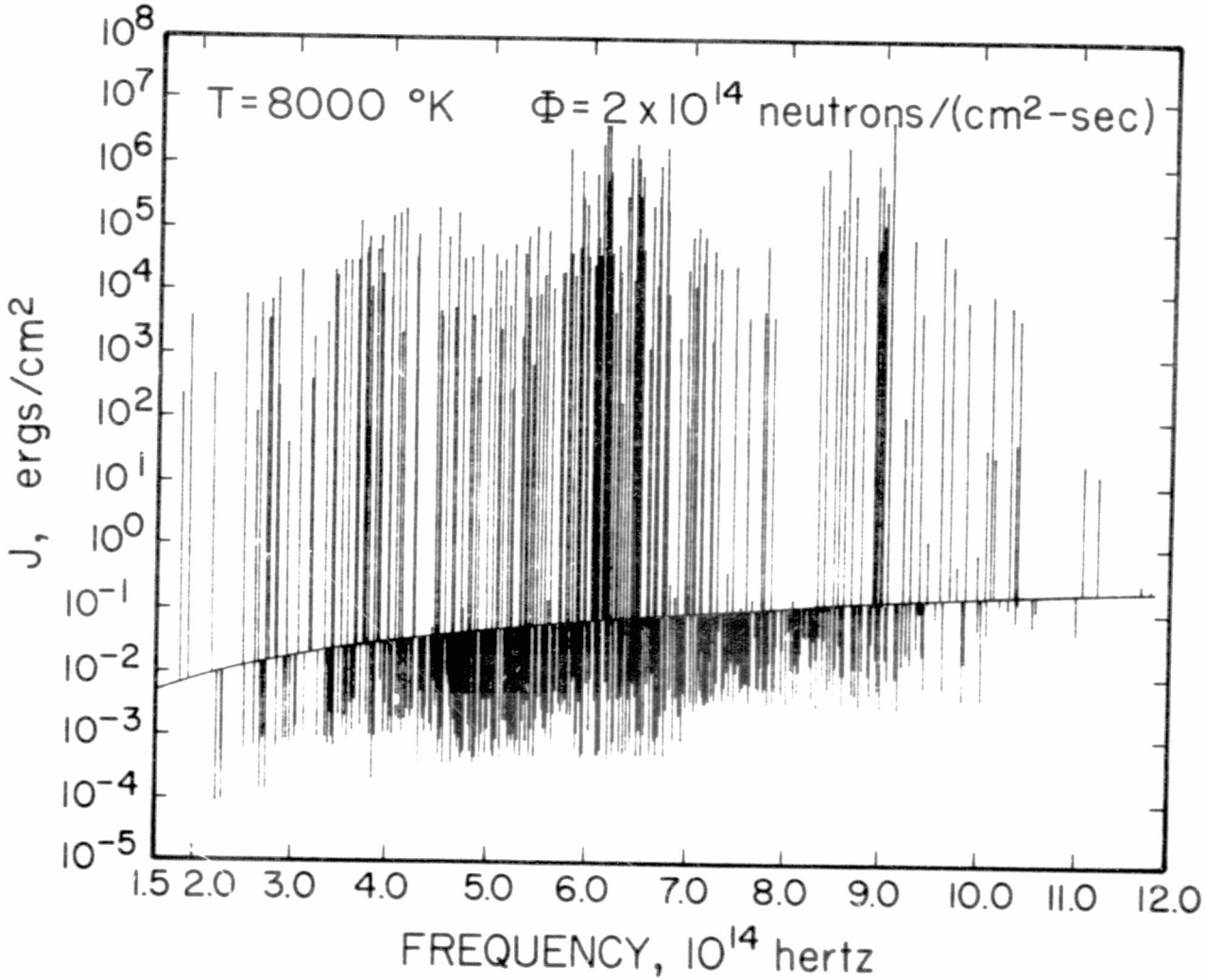

Figure V-5. Radiative-energy current versus frequency measured with respect to the Planck current at an effective temperature of 180,800°K.

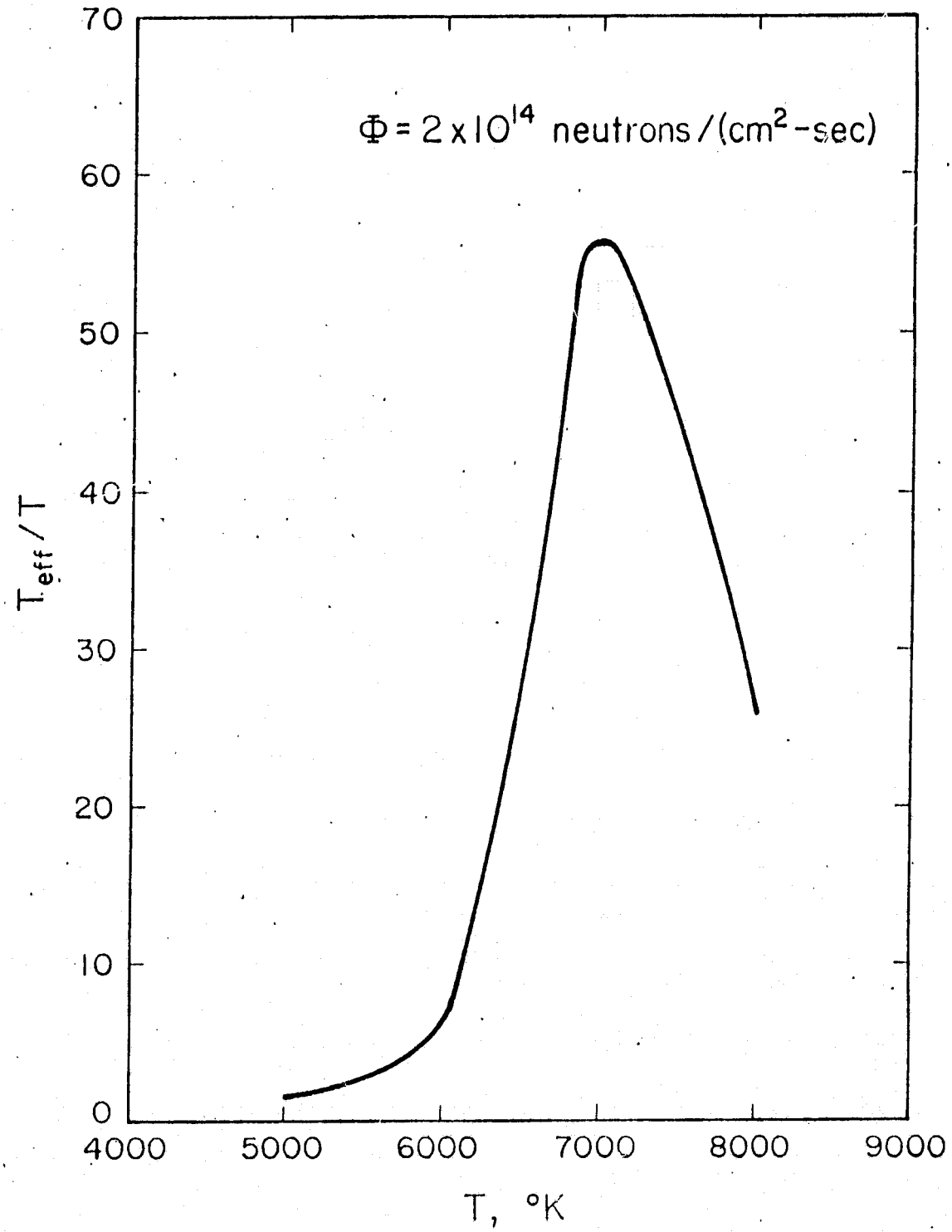

Figure V-6. T_{eff}/T for a flux of 2×10^{14} neutrons (cm^2-sec) over a temperature range of 5000°K to 8000°K.

$$J(x) = \hat{\Omega} \cdot \hat{\Omega}' \frac{f_L(\nu)}{\gamma_L(\nu)} \left(1 - e^{\gamma_L(\nu)x}\right) . \qquad \text{(V-7)}$$

If $\gamma_L(\nu)x$ is large then the radiative-energy current will be proportional to $f_L(\nu)/\gamma_L(\nu)$: Substituting this expression into Eq. (V-4) the line temperature becomes

$$T_L = \frac{h\nu}{k} \Big/ \ln\left(\frac{N_u}{N_L}\right) , \qquad \text{(V-8)}$$

where N_u is the upper state density and N_L is the lower state density.

Table (V-3) summarizes the state density and line temperature dependence on the plasma temperature for this case. This single transition will not exactly exhibit the variation found earlier for T_{eff} because the latter is an averaged quantity, but the line temperature shows similar trends. There is a rise in the line temperature as the plasma temperature varies from 5000°K to 7000°K and then the line temperature decreases as the plasma temperature varies to 8000°K. If the system were in thermal equilibrium, the line temperature would be equal to the plasma temperature. This can be seen by substituting the Boltzmann factor, $e^{h\nu/kT}$, for N_u/N_L in Eq. (V-8).

Two processes in the plasma cause the peaking effect observed in T_{eff}. The first is recombinational excitation within the plasma. In Table (V-3) the number of electrons in the upper state increases when the plasma temperature charges from 5000°K to 6000°K (since the non-Maxwellian tail in the electron distribution is inversely proportional to temperature [see Fig. (IV-7)], the non-equilibrium electron excitation

T, ^{0}K	N_u, cm^{-3}	N_L, cm^{-3}	T_L, ^{0}K	T_{eff}/T_L
5000	1.508×10^{15}	3.173×10^{17}	8415	1.683
6000	4.793×10^{15}	1.843×10^{17}	12334	2.056
7000	4.399×10^{15}	9.602×10^{16}	14598	2.085
8000	9.36×10^{14}	3.969×10^{16}	12011	1.051

TABLE V-3. Upper and lower state density and line temperature for a flux of 2×10^{14} neutrons/(cm^2-sec) calculated from a three state model.

is not caused by the non-Maxwellian tail, but by recombinational excitation). The second effect is the changing constituent densities within the plasma [see Table (VI-1)]. As the temperature increases, the number of ions and electrons in the plasma also increase causing more recombinational excitations to occur. If the number of neutrals remained constant or increased with temperature, the effective temperature would monotonically increase. The number of neutral atoms decreases as the plasma temperature increases, thus, the number of electrons in the excited state actually decreases [see Table (V-3)], as the temperature increases from 7000°K to 8000°K causing a drop in the effective temperature.

The total radiative-energy current carried in the lines calculated over frequency intervals of $1x10^{14}$ Hertz, is summarized in Table (V-4). A typical lasing line width of $1x10^{6}$ Hertz was used for lasing transitions in these calculations. Low frequency transitions are predominantly found in neutral uranium while high frequency transitions dominate in singly ionized uranium.

The transitions in the 1 to 2 x 10^{14} Hertz interval are all from transitions in neutral uranium and the transitions in the 11 to 12 x 10^{14} Hertz interval are from singly ionized uranium. The density effects can be seen directly in those two intervals. In the 1 to 2 x 10^{14} Hertz interval, the energy carried in the transitions decreases as the temperature increases. This is because the neutral uranium density decreases as the temperature increases [see Table (VI-I)]. The energy carried by transitions in the 11 to 12 x 10^{14} Hertz range increases with

T°K / Δν / 10^{14} Hertz	5000	6000	7000	8000
1 -2	2.27×10^{7}	2.38×10^{6}	1.49×10^{6}	8.76×10^{5}
2 -3	1.20×10^{8}	1.44×10^{8}	1.35×10^{7}	7.58×10^{6}
3 -4	2.24×10^{7}	2.31×10^{7}	1.30×10^{7}	6.78×10^{6}
4 -5	2.14×10^{7}	1.92×10^{7}	2.42×10^{7}	2.65×10^{7}
5 -6	5.02×10^{7}	2.87×10^{7}	5.28×10^{7}	7.13×10^{7}
6 -7	1.62×10^{7}	1.49×10^{7}	3.18×10^{7}	3.92×10^{7}
7 -8	2.15×10^{7}	4.18×10^{7}	9.10×10^{7}	1.40×10^{8}
8 -9	1.07×10^{7}	2.71×10^{7}	5.49×10^{7}	7.64×10^{7}
9 -10	4.28×10^{5}	2.20×10^{6}	8.78×10^{6}	1.87×10^{7}
10 -11	6.56×10^{4}	1.00×10^{6}	6.47×10^{6}	9.06×10^{6}
11 -12	1.19×10^{4}	2.26×10^{5}	1.76×10^{6}	4.42×10^{6}

TABLE V-4. Radiative-energy current carried in the lines within the plasma with the units of ergs/cm^2.

temperature because the density of singly ionized uranium increases with temperature. Within a particular frequency interval, the total radiative-energy current depends upon the number of lines in the interval and whether the transitions originate in neutral or singly ionized uranium.

C. Opacity Calculations

In this section the opacity of the plasma is calculated. This quantity is a measure of the absorption within the plasma and can be evaluated from

$$K_\nu = \frac{\gamma_\nu}{\rho} \quad , \tag{V-9}$$

where ρ is the plasma density and γ_ν is the absorption coefficient as given by Eq. (II-19) for the lines and Eq. (II-21) for the continuum between the lines. The opacity is essentially the mass absorption coefficient of the plasma. Thus, at a given density, the larger the opacity the less radiation will penetrate the plasma. Likewise as the opacity increases, the emitted radiation will come from a smaller volume of plasma near the surface.

All the opacities are calculated and then averaged over 1.55×10^{13} Hertz frequency intervals according to:

$$\langle K_\nu \rangle = \frac{K_\nu \Delta\nu}{\Delta\nu} \quad , \tag{V-10}$$

where $\Delta\nu$ is the line width and the sum is over all non-inverted lines

in the frequency interval plus the continuum between the lines. The dots in Fig. (V-7) are the result of such an averaging for a flux of 2×10^{14} neutrons/(cm^2-sec) and a plasma temperature of 5000°K.

Parks[9] calculated the opacity for a uranium plasma at a temperature of 5100°K and pressure of 3.58×10^{-4} atmospheres using experimental intensity data from the National Bureau of Standards [32,44]. The dashes in Fig. (V-7) represent his results corrected for the difference in densities of U° and U^{+}.

In his calculations there was a 40/60 mixture of neutral to singly ionized uranium while in the present calculations there is a 97.5/2.5 mixture. At low frequencies the transitions are principally found in U° while at high frequencies the transitions are mainly found in U^{+}. Since the opacity is the absorption divided by the density [Eq. (V-9)], Parks' opacities at high frequencies were divided by 24 and at low frequencies they were multiplied by 2.44 to correct for the difference in the mixtures. The cut-off between high and low frequencies was taken at the largest opacity at 8×10^{14} Hertz.

Figure (V-8) through Fig. (V-10) show the opacities for temperatures other than 5000°K. The effect of the changing constituent densities can be seen in these figures. As the temperature increases the U° density decreases. Consequently, the opacity decreases at low frequencies with increasing temperature. Similarly, the opacity at high frequencies increases as the temperature increases from 5000°K to 7000°K due to an increase in the density of U^{+}. Also a dip in the opacity at approximately

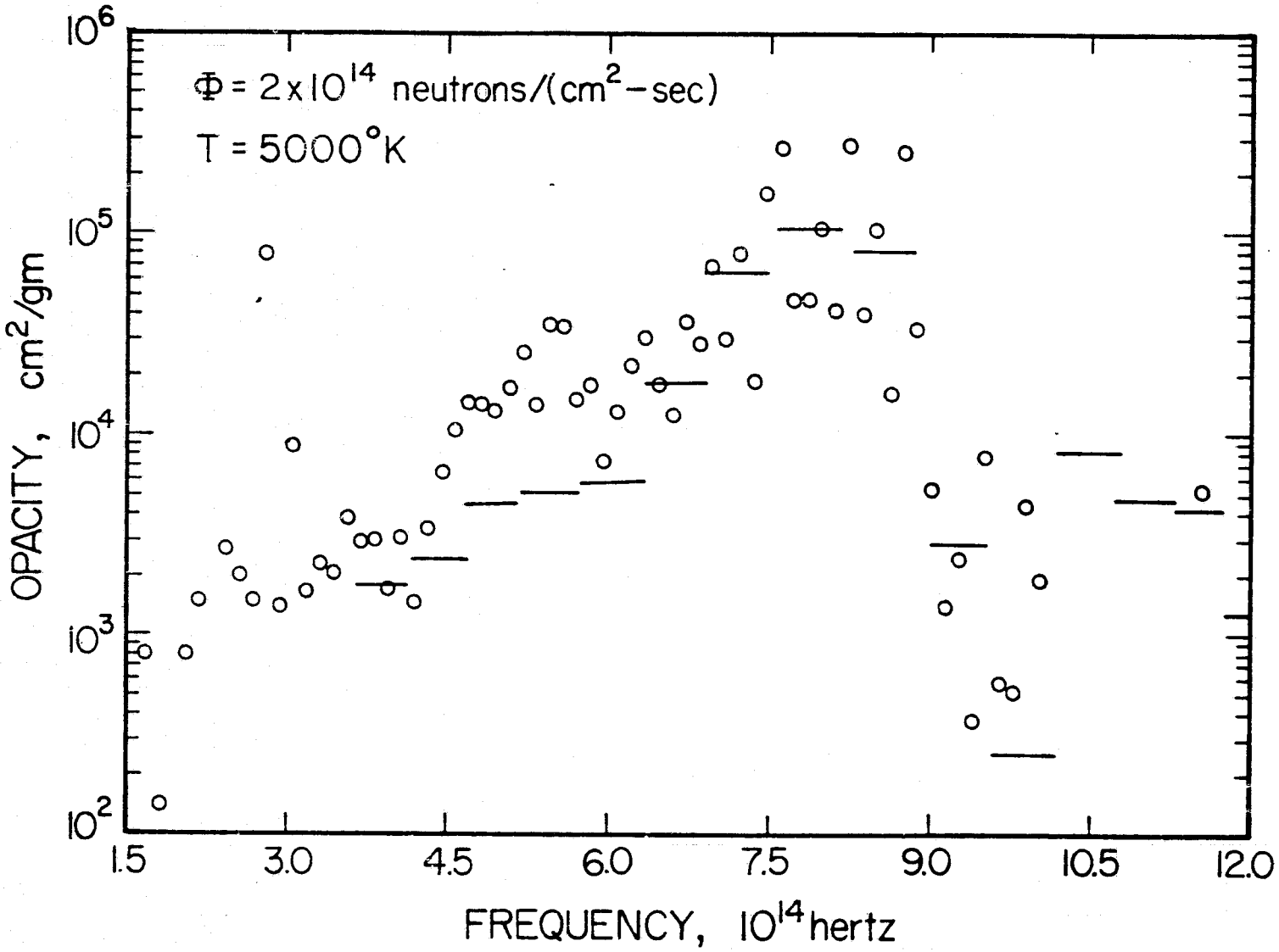

Figure V-7. Average opacity versus frequency for a plasma at a temperature of 5000°K. The dashes are taken from Parks[9].

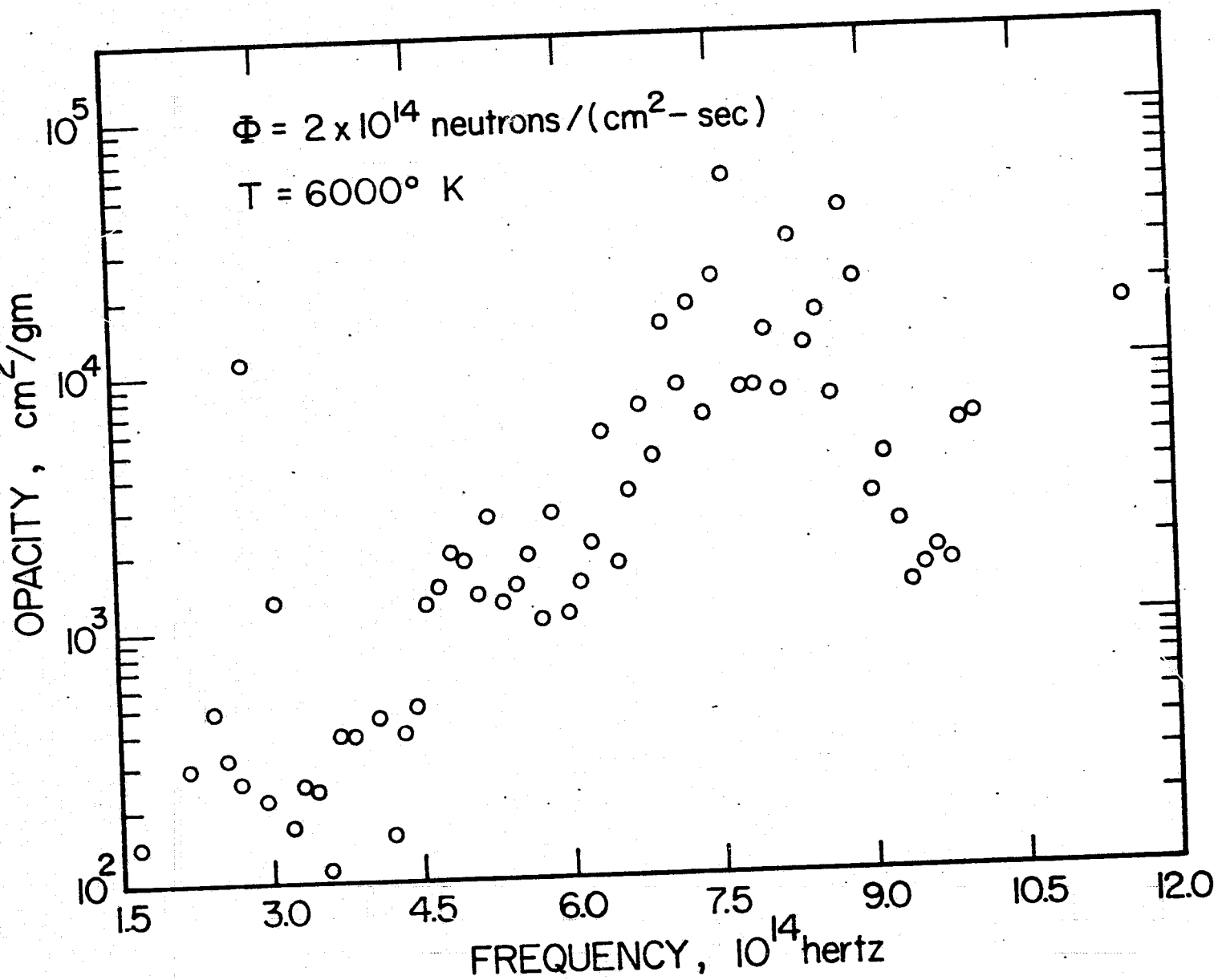

Figure V-8. Average opacity versus frequency for a plasma at a temperature of 6000°K.

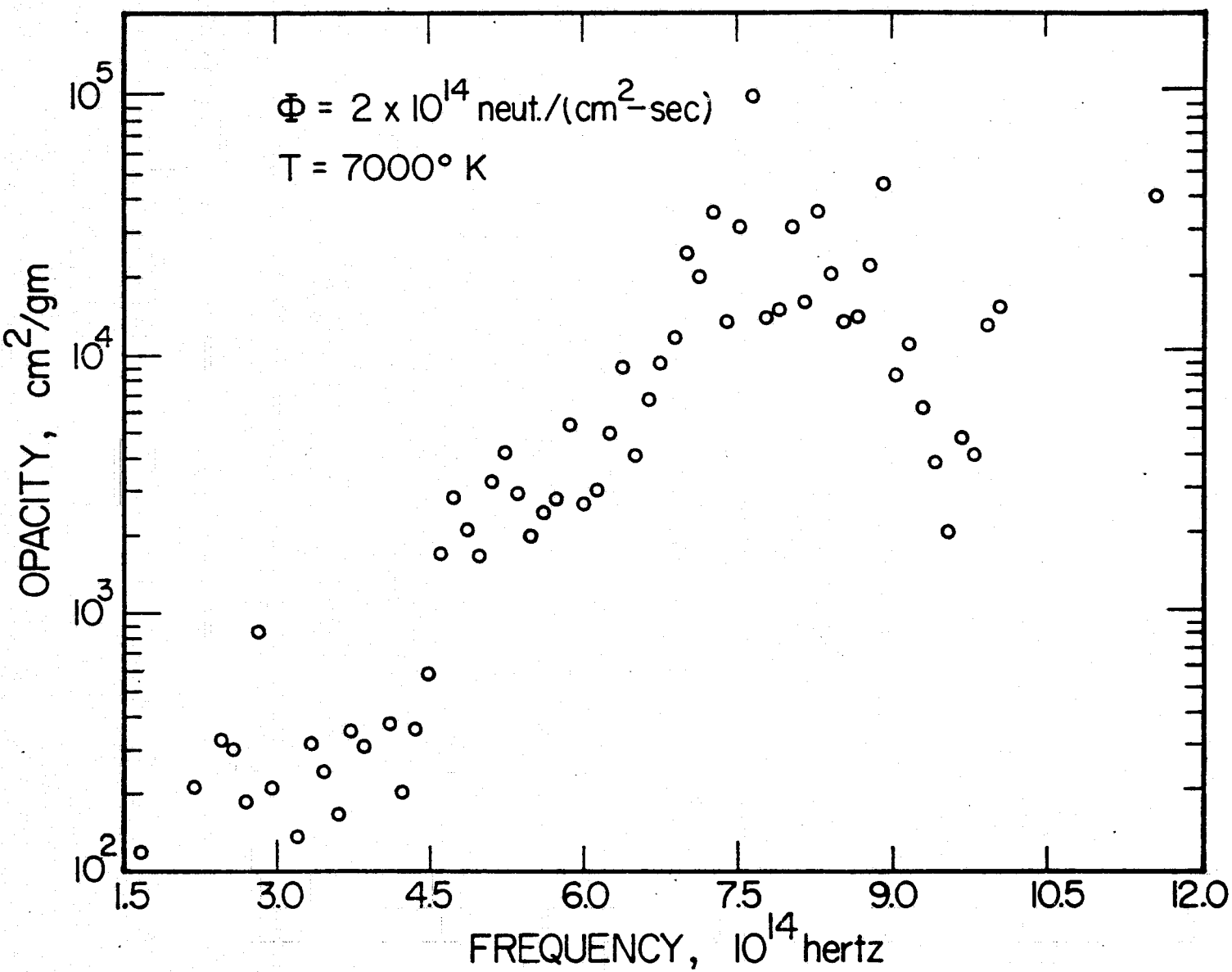

Figure V-9. Average opacity versus frequency for a plasma at a temperature of 7000°K.

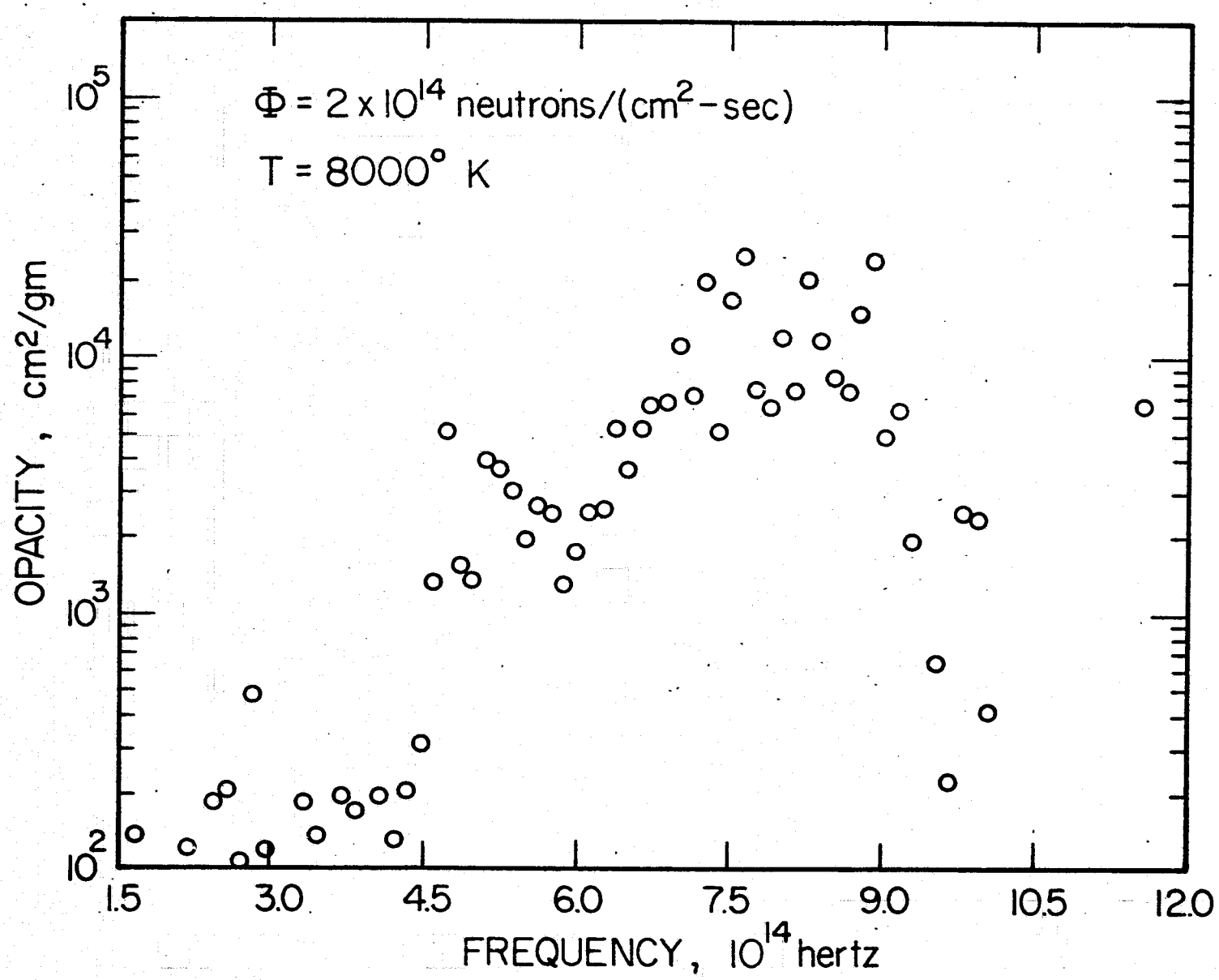

Figure V-10. Average opacity versus frequency for a plasma at a temperature of 8000°K.

$1.x10^{15}$ Hertz that is observed in Parks[9] calculations [see Fig. (V-7)] is also seen in the present 6000°K and 7000°K cases. The decrease in the opacity at high frequencies in the 8000°K case, Fig (V-10) is due to the increased excitation in singly ionized uranium which causes the magnitude of the absorption due to the lines to decrease [see Eq. (II-20)]. This is because the absorption is proportional to the differences between the lower and upper state densities.

D. Flux and Size Considerations

In the uranium plasma, the non-equilibrium effects are mainly due to recombination in the plasma. Hence, a change in the non-Maxwellian tail of the electron distribution function has no significant effect on the state densities in the plasma. Consequently, when the flux was varied from $2x10^{12}$ neutrons/(cm^2-sec) to $2x10^{16}$ neutrons/(cm^2-sec) at a plasma temperature of 6000°K, no significant changes in the radiative-energy current or the atomic state densities in the plasma occurred. Thus, the radiative-energy current calculated for one neutron flux in uranium is adequate for a range of neutron fluxes. Also, because the optical depth is small, less than a centimeter, the radiative-energy current does not change with a change in size of the plasma. Thus the total radiative-energy radiated by the plasma will be directly proportional to the surface area of the plasma. Then the radiative-energy current calculated here need only be multiplied by the surface area to obtain the total radiative-energy.

In this chapter the physical dimensions of the plasma were described and then the convergence criteria for the code were discussed. Next the results of the radiative-energy current calculations were presented, first introducing the concept of an effective temperature and then the actual energy carried in a frequency interval. Then the opacities of the plasma were presented along with a comparison to Parks[9] earlier results for a 5000°K plasma. Finally the effects of changing the size of the plasma and the neutron flux were discussed.

CHAPTER VI. CONCLUSIONS

A. Uranium Calculations

The results of this work show that non-equilibrium effects in the plasma cause larger radiative-energy currents at the lines than would normally be expected. United Aircraft's[8] assumption of a black-body spectrum is true for the interior of the plasma but there is an important contribution to the spectra due to bound-bound transitions in a sheath near the surface. The energy carried in these transitions is about 2% of the energy carried by the black-body spectrum in this frequency range. For calculating bulk quantities within the plasma a black-body spectra is sufficient; but if radiation processing or other frequency dependent processes are of interest, detailed analysis of the lines is necessary to correctly predict the emitted radiation.

In recent studies at United Technologies, Krascella[44] found that there was up to an order to magnitude difference between the integrated intensity and the black-body intensity at some temperatures, and Roman[45] found the ground state density in neutral uranium was depleted to a greater extent than was predicted by equilibrium calculations. He found the ground state density to be 8×10^{12} atoms/cm^3 and 2×10^{13} atoms/cm^3 in two instances compared to 10^{14} atoms/cm^3 predicted by equilibrium calculations. This depletion of the ground state is indicative of non-equilibrium excitation within the plasma as illustrated by the non-equilibrium radiation levels observed in these calculations.

Rogers et al.[46] predict a rise in the black-body radiative temperature corresponding to the outward heat flux above the gas temperature for the plasma core reactors they examined. Here a much greater rise in T_{eff} is observed than Rogers reported because he considered bluk quantities while the present work concentrates on line radiation where non-equilibrium effects would readily appear.

At high temperatures, 6000°K and above, approximately 20% of the transitions were inverted. These inversions were essentially due to recombinational effects. Due to the limitations of the model, exact inversions cannot be predicted. However, with the large ion and electron densities in the plasma, recombinationally driven inversions should be expected. Also observed was the effect of two constituents within the plasma. This is readily seen in the opacity calculations where the high frequency results were dominated by U^+ and the low frequency results were dominated by U°.

Finally due to the density of the plasma, line radiation comes from a narrow sheath on the plasma surface. This effect was assumed by Rogers[48] and Latham in their modeling where they allowed a 1.4 cm sheath that would account for all optical radiation. In the present calculations, 1.4 cm would be greater than a mean free path for any of the line transitions in the plasma.

The accuracy of these calculations depends primarily on the accuracy of the uranium model. Gryzinski[37] cross sections are used, but they have been successfully employed by other researchers previously (e.g.,

Lo[48] used the model for helium). However, comparisons of the calculated and experimental cross sections for cesium, which is similar to uranium in electronic structure, reveals that the calculated cross-section may be somewhat low. The uncertainty is estimated to be a factor of 2. This suggests that experimental measurements are badly needed. Also, the lifetimes of the atomic states should be measured directly to improve the accuracy of the results. Some progress is being made in this direction[33,50].

B. Implications to Uranium Plasma Program

The energy in line radiation represents a pertubation to the energy carried in the black-body spectrum of the plasma. Although only a pertubation, the radiative-energy current at a specific frequency corresponding to a line center can be orders of magnitudes larger than the current expected from equilibrium calculations.

In an uranium plasma, electron excitation may result from both direct excitation and recombination. Recombination will be the predominant cause of inversions in a plasma where the constituent atoms have small excitation and ionization potentials. This is because the Maxwellian electron flux will cause excitation from ground due to the small energy differences and non-equilibrium excitation will be caused by recombining electrons. Also, states that lie near the continuum and have large ionization potentials will be principally populated through recombination.when the electron states are close enough to the

continuum so the rate of recombination into these states is greater than the electron excitation rate.

As the plasma heats up and highly ionized uranium is present, or when a buffer or seed gas is introduced into the plasma the non-Maxwellian tail of the electron distribution function can be important in causing excitation. To illustrate this consider a 60:40 mixture of uranium to helium at a pressure of 1 atm. and a temperature of 5000°K. The corresponding electron flux has been calculated by Makowski[51]. The ground 2_1S and 2_1P state will be considered in this calculation, and they have densities of 7.82×10^9 and 1.26×10^9 electrons/cm^3, respectively. The line temperature [Eq. (V-8)] for the 2_1P to ground state transition is 4.82×10^6 °K which is much greater than the equilibrium value of 5000°K. Hence, recombination and the non-Maxwellian tail to the electron distribution function can produce high levels of radiation at a desired frequency corresponding to line transitions in the plasma.

C. Computational Method

The computational method developed to do these calculations is general. The rate equation formalism can treat both the non-linear problem present in this work as well as the "coronal" case. The radiative transport problem in cylinder can be used to calculate the radiation anywhere on the side of the cylinder. With modifications the computer code can treat radiation from any geometric configuration. Included here is the radiation from the end of a cylinder which would

allow the radiative-energy current from a typical laser configuration to be calculated. Also by using an appropriate electron energy structure, atomic lifetimes and electron excitation cross-sections, other plasmas can be treated.

D. Future Work

Due to gaps in knowledge about atomic cross-sections and lifetimes, experimental studies should be initiated to measure these. As data becomes available it should be incorporated into the uranium model so a calculation of exact inversions in the plasma can be made. Studies to determine the electron distribution function in uranium mixtures should be undertaken so the radiative-energy current can be calculated when a buffer or seed gas is present in the plasma. This would allow consideration of various radiation processing schemes to be evaluated.

Also, studies of different plasmas should be undertaken. Impurities in a fusion plasma could be investigated as well as the radiation due to a neutral gas blanket in a tokamak. The code could be used to investigate different lasing schemes both to see if lasing is possible and to check the accuracy of models used to explain the mechanism driving a particular laser.

APPENDIX A. RADIATIVE TRANSPORT CONSIDERATIONS

A. Review

In this appendix the expressions for the total radiative-energy intensity and the radiative-energy current are derived. Then analytic solutions for the one-region problem in a sphere and slab are obtained.

The equation for the directed radiative-energy intensity along path length s at the origin due to a directed radiative-energy intensity at s derived in Chapter II is

$$I(\nu,s) = I(\nu,o) \quad \exp\left\{ \int_o^s \gamma(\nu,s')ds' \right\} -$$

$$+ \exp\left\{ \int_o^s \gamma(\nu,s')ds' \right\} \quad \int_o^s f(\nu,s')\ ds' \quad \exp\left\{ -\int_o^{s'} \gamma(\nu,x')dx' \right\}, \quad \text{(A-1)}$$

where $f(\nu,s)$ is the volumetric source and $\gamma(\nu,s)$ is the attenuation coefficient within the volume.

When the angular dependence of the gain and the volumetric source are known, the total radiative-energy intensity at the origin is just the sum of the directed radiative energy flux from all directions, and can be written as

$$F_\nu(0) = \int_o^{2\pi} d\phi \int_{-1}^{1} d(\cos\theta)\ \ I(\nu,s[\theta,\phi]). \qquad \text{(A-2)}$$

This quantity is substituted into the rate equations to calculate the state densities.

To obtain the radiative-energy current in a direction $\hat{\Omega}'$ in terms of the directed radiative-energy intensity at $\hat{\Omega}$, the component of the directed radiative-energy intensity in the direction parallel to $\hat{\Omega}'$ must be obtained; this can be written as

$$I(\nu, s\,[\theta,\phi]) = \hat{\Omega} \cdot \hat{\Omega}'\; I(\nu,s)[\theta,\phi]). \tag{A-3}$$

Now the net radiative-energy current can be obtained by integrating Eq. (A-3) over all angles to give

$$J_\nu(0,\hat{\Omega}') = \int_0^{2\pi} d\phi \int_{-1}^{1} d(\cos\theta)\; \hat{\Omega} \cdot \hat{\Omega}'\; I(\nu,s[\theta,\phi]). \tag{A-4}$$

This quantity when evaluated at the surface for a given direction will give the signal measured by a detector some distance away from the plasma. Equation (A-2) and Eq. (A-4) can be found in any standard reference such as Ref. 5. To obtain the optical power radiated from the plasma the current normal to the surface should be integrated over all frequencies

$$P = \int J_\nu(o,\hat{\Omega}')d\nu. \tag{A-5}$$

Simple one region calculations will be carried out for a sphere and a slab analytically to illustrate the accuracy of this formulation

B. <u>One Region Problems</u>

1. Sphere

In this section the total radiative-energy intensity and the

radiative-energy current will be calculated in a sphere and a slab as illustrations of the use of this form.

If a spherical plasma of radius a with its center displayed a distance or up the z axis (see Fig. A-1) the path length can be written as

$$s = 2a \cos\theta \ . \tag{A-6}$$

Hence if there is not radiation incident upon the sphere and γ and f are constant with the plasma the directed intensity for a given frequency ν can be written as

$$I(\nu,\hat{\ }) = \frac{f}{\gamma} \left(e^{2a\gamma \cos\theta} - 1\right). \tag{A-7}$$

Substituting Eq. (A-7) into Eq. (A-4) with $\hat{\Omega} \cdot \hat{\Omega}' = \cos\theta$. The radiative-energy current becomes;

$$J_r(o,-\hat{k}) = \int_0^{2\pi} d\phi \int_{-1}^{1} d(\cos\theta) \cos\theta \ \frac{f}{\gamma} \left(e^{2a\gamma \cos\theta} - 1\right), \tag{A-8}$$

but $f = 0$ for $\cos\theta < 0$. Thus

$$J_r(o,-\hat{k}) = \frac{2\pi f}{\gamma} \int_0^{1} d(\cos\theta) \ \cos\theta \ \left(e^{2a\gamma \cos\theta} - 1\right), \tag{A-9}$$

which upon integration yields

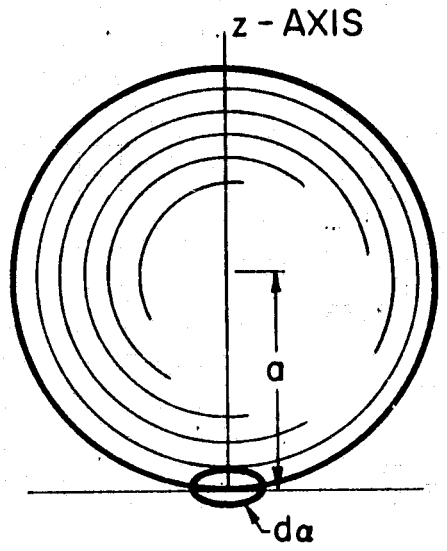

Figure A-1. Sphere displaced up the z axis a distance a.

$$J_\nu(o,-\hat{k}) = \frac{2\pi f}{\gamma}\left[\frac{e^{2a\gamma}}{2a\gamma} - \frac{e^{2a\gamma}}{(2a\gamma)^2} - \frac{1}{2} + \frac{1}{(2a\gamma)^2}\right] ,$$

$$J_\nu(o,-\hat{k}) = \frac{2\pi f}{\gamma}\left[\frac{2a\gamma-1}{4a^2\gamma^2}\ e^{2a\gamma} + \frac{1-2a^2\gamma^2}{4a^2\gamma^2}\right] . \qquad \text{(A-10)}$$

When the source is due to atomic line radiation

$$f = \frac{ANh\nu g(\nu)}{4\pi} , \qquad \text{(A-11)}$$

where A is the inverse lifetime, N the emitting state density, ν the frequency of the light from the atomic transition and $g(\nu)$ the line shape. Substituting this into Eq. (A-10) the radiative-energy current can be written

$$J_\nu(o,-\hat{k}) = \frac{ANh\nu g(\nu)}{8a^2\gamma^2}\left[(2a\gamma-1)\ e^{2a\gamma} + (1-2a^2\gamma^2)\right] . \qquad \text{(A-12)}$$

This result can also be obtained by considering the geometry in Fig. (A-1) and calculating the radiative-energy current going through a surface area $d\alpha$ in the x-y plane at the origin. The total radiative-energy current passing through $d\alpha$, $J_\nu(0\text{-}k)d\alpha$, will be the result of the product of the probability of emission of the radiation.

$$\text{prob of emission} = AN, \qquad \text{(A-13)}$$

times the attenuation

$$\text{attenuation} = e^{\gamma r} , \tag{A-14}$$

times the surface area seen at r of $d\alpha$

$$\text{observed surface area } \frac{d\alpha \cos\theta}{4\pi r^2} , \tag{A-15}$$

times the probability it is at the right frequency

$$\text{line shape} = g(\nu) , \tag{A-16}$$

times the energy of the transition

$$E = h\nu , \tag{A-17}$$

integrated over all space

$$J_\nu(o,-\hat{k})d\alpha = \frac{ANh\nu g(\nu)d}{4\pi} \int_0^{2\pi} d\phi \int_0^{1} d(\cos\theta) \int_0^{2a\cos\theta} \cos\theta \; e^{\gamma r} dr, \tag{A-18}$$

which upon doing the ϕ and r integrations yields

$$J_\nu(o,-\hat{k}) = \frac{ANh\nu g(\nu)}{2\gamma} \int_0^{1} d(\cos\theta) \; \cos\theta \; (e^{2a\gamma\cos\theta}-1) , \tag{A-19}$$

which is just Eq. (A-9). This illustrates the accuracy of the method

developed in Section A.

For the total radiative-energy intensity, Eq. (A-7) is substituted into Eq. (A-2) to obtain:

$$F_\nu(o) = \int_0^{2\pi} d\phi \int_0^1 d(\cos\theta) \; \frac{f}{\alpha} \; (e^{2a\gamma\cos\theta} - 1), \tag{A-20}$$

which upon integration yields

$$F_\nu(o) = \frac{2\pi f}{\gamma} \left[\frac{1}{2\gamma a} \; (e^{2\gamma a} - 1) - 1 \right]. \tag{A-21}$$

Another test of the accuracy of these results is to see if the total radiative-energy intensity is always greater than or equal to the radiative-energy current. To test this in the case of a spherical plasma divide Eq. (A-10) by Eq. (A-21) to obtain:

$$\frac{J_\nu(o,-\hat{k})}{F_\nu(o)} = \frac{1}{2\gamma a} \left[\frac{(2a\gamma-1)e^{2a\gamma} + 1 - 2a^2\gamma^2}{e^{2a\gamma} + 2a\gamma - 1} \right]. \tag{A-22}$$

If γ becomes very large this ratio goes to 1; if γ a becomes very small the ratio becomes $\frac{2}{3}$.

2. Infinite Slab

Another simple geometry that can be treated is a slab infinite in the x-y plane and with a thickness ℓ in the z direction (see Figure A-2) and having constant physical properties. In this case absorption must be considered for analytic results because otherwise infinite intensities would arise due to infinite path lengths. Therefore let $\gamma = -\alpha$ then

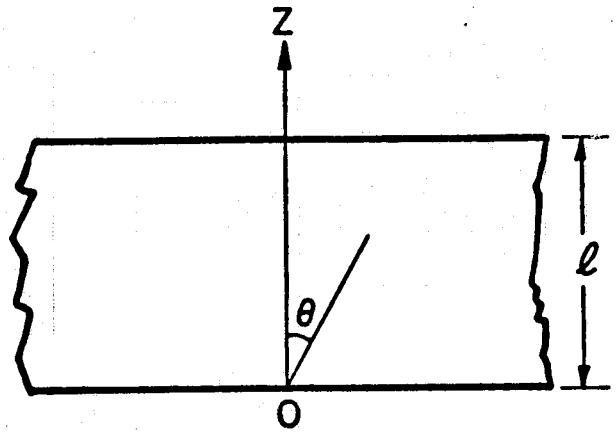

Figure A-2. A slab infinite in the x-y plane and with dimension ℓ in the z plane.

the path length can be written

$$s = \ell/\cos\theta, \tag{A-23}$$

substituting Eq. (A-23) into Eq. (A-1) where there is no incident intensity, the directed radiative-energy intensity becomes

$$I(\nu,0) = \frac{f}{\alpha}\left(1-e^{-\alpha\ell/\cos\theta}\right), \tag{A-24}$$

substituting Eq. (A-24) into Eq. (A-2) the total radiative-energy intensity becomes

$$F_\nu(o) = \frac{f}{\alpha}\int_0^{2\pi} d\phi \int_0^1 d(\cos\theta)\ \left(1-e^{-\alpha\ell/\cos\theta}\right), \tag{A-25}$$

which upon integration yields

$$F_\nu(o) = \frac{2\pi f}{\alpha}\left[1-E_2(\alpha\ell)\right]\ , \tag{A-26}$$

where $E_2(\alpha\ell)$ is the exponential integral defined by

$$E_2(\alpha\ell) = \int_1^\infty \frac{e^{-x\ell\alpha}}{x^2}\,dx\ . \tag{A-27}$$

Relationships and values for the exponential function can be found in Ref. 5.

Substituting Eq. (A-24) into Eq. (A-4) the radiative-energy current

becomes

$$J_\nu(o,-\hat{k}) = \frac{f}{\gamma} \int_0^{2\pi} d\phi \int_0^1 d(\cos\theta) \quad \cos\theta \quad (1-e^{-\alpha\ell/\cos\theta}), \qquad \text{(A-28)}$$

which upon integration yields

$$J_\nu(o,-\hat{k}) = \frac{2\pi f}{\alpha} \quad [\tfrac{1}{2} - E_3(\alpha\ell)], \qquad \text{(A-29)}$$

where $E_3(\alpha\ell)$ is the exponential integral defined by

$$E_3(\alpha\ell) = \int_1^\infty \frac{e^{-\alpha\ell x}}{x^3} \, dx \qquad \text{(A-30)}$$

To see that the total radiative-energy intensity is greater than the radiative energy current, take the ratio of Eq. (A-29) to Eq. (A-26) to give

$$\frac{J_\nu(o,-k)}{F_\nu(o)} = \frac{\frac{1}{2} - E_3(\alpha\ell)}{1-E_2(\alpha\ell)} , \qquad \text{(A-31)}$$

but $E_2(\alpha\ell) < 2E_3(\alpha\ell)$ so

$$\frac{J_\nu(o,-k)}{F_\nu(o)} < \frac{\frac{1}{2} - E_3(\alpha\ell)}{1 - 2E_3(\alpha\ell)} , \qquad \text{(A-32)}$$

$$\frac{J_\nu(o,-\hat{k})}{F_\nu(0)} < \frac{1}{2} \quad . \tag{A-33}$$

so that the total radiative-energy intensity is always greater than or equal to the radiative-energy current. This is because the current is just the component of the total radiative intensity normal to the surface.

The accuracy of the preceding analysis depends upon Eq. (A-6), Eq. (A-7), Eq. (A-23), and Eq. (A-24). These are verified in Ref. 5 by substituting the formulae found on page 283 into the expression on page 22. These results can be used in cases where the energy spectrum of the electron flux does not significantly charge over the volume of the gas. Then these analytical results can be used instead of a transport calculation if the geometry is the same as used in either of the examples.

APPENDIX B. URANIUM DATA

In this appendix the optical data for neutral and singly ionized uranium is tabulated[32,33,34]. All state energies are in cm^{-1} (1eV = 8066.1 cm^{-1}).

The tables are grouped according to the species of atom, the first three deal with neutral uranium and the second three with singly ionized uranium. Relative inverse lifetimes for all identified states are found in the first table of each group. All relative lifetimes in U^{o} are compared to the relative A value of one for the 26226 cm^{-1} to 0 cm^{-1} transition in neutral uranium which has an absolute lifetime[35] of 9.785×10^{7} sec^{-1}, while the values for U^{+} are normalized to the $2.190 \times 10^{8} sec^{-1}$ inverse lifetime for the 26191 cm^{-1} transitions.

The second table in each group contains the composite state relative A coefficients to be used in the calculations, while the final table in the group enumerates the sum of the A values that give the average A values of the composite state.

TABLE B-1. Relative A Coefficients for Neutral Uranium.
State energies are in cm^{-1}.

Initial State \ Final State	0	620	3801	3868	4276	4453	5762	5991	6249	7006	7104	7326	7646	8119	10347	10686	13128
15463	.00178	.00094			.00047	.00108	.00096	.00014									
14644	.00642	.00281							.00157			.00166		.00047			
15632	.00457		.00101						.00296	.00137		.00237		.00370	.00152		
15638	.00145	.0004	.00203				.00159		.00255	.00239		.00356		.00319			
15721	.00146	.00127			.00075	.00266	.00213		.00316		.00348	.00103					
16122		.00554				.0039	.00744	.00995									
16506	.00097	.00109	.00091		.00096				.00037	.00040				.00054			
16900	.01511		.00082		.0006				.03065	.27026		.03290		.03578	.01449	.00731	
16930	.00054	.00166			.0006	.00020	.00101		.00106	.00113							
17070	.00221	.00549	.00341		.00057		.00095			.00374		.00386		.00421			
17262	.00169	.00367			.00098			.00192	.00028	.00230		.00153		.00100			
17468		.00105				.00004	.00062	.00094			.00139						
17894		.00013					.00019	.00019									
17908	.00011	.00024			.00007	.00038	.00032	.00038	.00039								
17969				.00035		.00108		.00065									
18754	.00053	.00105	.0011				.00058		.00089	.00164							
18406	.00232	.00457			.00205	.00079		.00036	.00376	.00215							
18531				.00046		.00243					.00111						
18759	.0041	.00404	.00089		.00044		.00258		.00040				.00468	.00489			
18933	.0073	.00168			.00161	.00018	.00033	.00144	.00331	.00103							
19126		.00084		.00044		.00009		.00040									
19192		.00112				.00019	.00089	.00143			.00089						
19472	.00014	.00002			.00024	.00016		.00003		.00035							
19489			.00289										.00089	.00754	.00164	.00121	.00068
19552		.00123		.00117		.00065	.00007	.00036			.00035						
19548	.00259		.000329		.00075					.00042		.00041			.00053	.00113	
19783	.00179	.00112	.00060				.00040		.00005	.00088		.00010		.00086			
19885	.02285		.00088		.00037				.00055	.00064		.00041	.00068	.0004		.00179	
20114	.00172	.00081			.00043	.00040	.00007	.00020	.00062	.00069							
20219	.00077	.00031	.00095		.00063		.00053			.00038		.00504		.00107			
20312		.00117			.00875				.00169	.00055							
20392				.00056		.00016		.00005									
20420	.00057	.00055	.00026		.00046		.00015			.00024		.00053		.00047			
20464	.00116		.00144		.00192							.00066		.00065	.00093	.00060	
20529			.00657										.00050	.00034	.00477	.00493	
20569		.00309		.00182		.00419	.00010										
20621					.00091		.00019		.00033	.00035							
20662		.00023	.00136		.00658		.00012					.00009		.00117			
20766	.00015		.00082		.00111				.00012	.00010		.00065	.00116	.00042	.00130	.00135	
20852	.00012	.00029			.00179	.00043	.00050		.00045								
20943	.00085	.00050			.00144		.00055			.00004		.00041		.00005			

TABLE B-1. (continued)

Initial State \ Final State	0	620	3501	3868	4276	4453	5762	5991	6249	7006	7104	7326	7646	9119	10347	10686	13128
21062				.00065		.001		.00019			.00009						
21079	.00018	.00036			.00165	.00220	.00021		.00271								
21265	.00833	.0073	.00313		.00435		.00293		.00348			.00039		.00213			
21585	.03888	.00591	.06233		.00474		.02658	.00075	.01617	.00742							
21637	.08329	.02394			.00085	.00048		.00115	.00026	.00079							
21766	.00033	.00036	.00019		.00034		.00088		.00023	.00000		.00007		.00005	.00064		
21768	.00247		.00583		.00023				.00009						.00093		
21941				.00016		.00157		.00105			.00081						
22038		.00002		.00108		.00107	.00277	.00112									
22056	.00136	.00883	.00114		.00370			.00138	.00888	.00158							
22368	.01106		.00860						.00388	.00022		.00037	.00093	.00050	.00026	.00034	
22378	.00004	.00008			.00009	.00019	.00064	.00179	.00089	.00010							
22464	.00072	.00974	.00165		.00307		.00284		.00249	.00060		.00046	.00104	.00033			
22583	.00146	.00877	.00458		.00139		.00067		.02299			.00016					
22633	.00002	.00053	.00416		.00024				.00108	.00091		.00012	.00012	.00054	.00029		
22754	.07285	.01306	.00461		.00097		.00016		.00097			.00023		.00012			
22790			.00109									.00165	.00046	.00006	.00057		
22862	.01558	.00986	.00782		.00252		.01169		.00128	.01625				.00187			
22919	.1011		.03922		.00921				.09397	.01525		.00045	.04477	.00029			
23058	.02942		.02611		.00009				.03318	.02432		.02387	.00878			.01228	
23187						.00108	.00171	.00081			.00007						
23197	.00067		.00069		.00149				.00138	.00372			.00013	.00058			
23325	.00012	.00001			.00050	.00102	.00023	.00084	.00079	.00038							
23430		.00048				.00067	.00145	.00147			.00053						
23433	.01433	.01224			.00801	.02227	.01441	.02160		.02695							
23544	.06995		.00442		.00009	.00035			.00499	.00023		.00046	.00008	.00009	.00017		
23572	.04749	.1019	.03412		.00064				.00084	.00103		.00166					
23849	.01587		.00024		.00108				.00107	.00131		.00056		.00026	.00013	.00033	
24067	.2721		.00333		.00160				.00469			.00463	.00375	.00074			
24186	.06465		.00926		.01841				.00097	.00065		.09063		.26804		.01270	
24334	.0224		.00533		.00222				.00798			.00456		.00173	.00139		
24433	.03664	.03932	.00424		.01065		.01741		.03735	.00172		.02325		.00093			
24560	.00058		.00228		.00586	.00029			.00159	.00228		.00270		.00953	.00104	.00039	
24581			.00565									.00277	.00230	.01031	.00023		.00076
24671	.00292	.1167	.00674		.01580		.10269		.05793	.06474		.00083		.00126			
24757		.02127		.02044			.00503	.02329			.01877						
25319	.1254	.1467			.02391			.00902	.03994	.04775		.06943		.00287			
25349	.5169	.87145	.01836		.03833		.01568		.31357	.03191		.00104	.00231	.00065			.00039
25389			.00013									.01315		.03151			
25463	.1418	.08758	.00449		.02579		.01348		.05296	.00448							

TABLE B-1. (continued)

Initial State \ Final State	0	620	3801	3868	4276	4453	5762	5991	6249	7006	7104	7326	7646	8119	10347	10686	13128
25627															.00057	.00020	.00058
25672	.2240		.00977		.00660				.07437				.04428	.07859	.00860		
25826	.7112	.03737	.04799		.00039			.00671	.04288	.01817				.09681			
25918			.00048									.00100	.0022	.00112	.00035	.00019	.00049
25938	.3058	.05444	.04297		.01739		.05065					.07370		.02050			
26104	.06236	.02164	.00878		.00592		.00401		.00305	.00725		.02805					
26226	1.0000	.51332	.08091							.14962							
26313			.00859									.11694	.00519	.00884	.01634	.00712	.00321
26454			.00549									.00554	.01588	.00916	.01170		.00617
26550	.1549	.09340	.00534				.00386		.00845	.01239							
26608	.00032		.0123		.00205				.00619	.00359			.00172	.00326	.00588	.00123	
26792	.05759	.02402	.00212		.00164		.00039		.02117	.01629							
26921	.2209	.22611	.05759		.02814	.01632	.04062	.04503	.01442	.03674							
26979			.03703									.02400	.00012	.00088	.00129		.00013
27324	.00589		.00064		.00421				.00607	.00155		.00039	.00410		.00161	.00824	
27478			.09839									.00093		.00672	.00320		.00052
27499	.06136	.06726			.00094		.01479		.00446	.00249				.00162			
27616	.1315	.1471	.00636		.00592		.00381		.00151	.00306							
27682	.03086	.01477			.00504	.00639	.00743	.00065	.00195	.00238							
27744	.06267	.09834	.02047		.02510				.00091								
27791	.02527	.1266			.01759	.00089			.00593	.00012							
27818			.07442									.00575	.00571	.00386	.00041	.00228	.00176
27687	1.407		.00576						.05094	.00341				.00584			
27941	.1646	.5192	.04466		.05112				.01433	.00679							
27966	.1436		.05762						.01140	.01029		.00849		.01932	.03075		
28053	.1806	.25229	.07585				.00297		.00286	.00167		.00016		.02542			
28099	.1827	.09581	.00058						.00170	.02994							
28119	.3214	.01766	.02190		.00354				.01848	.00145		.00466		.00463	.01766		
28153			.09099		.05592				.00495	.00115		.01686			.06382	.40117	
28286	.1556		.01034		.02473				.03093	.02855		.00960	.00182		.00116	.00605	.00697
28444	.8097	.1705			.00410		.00399		.00557	.00530							
28454		.0641		.06036		.00068			.00176		.00107						
28470	.1254	.1073	.00347		.00110		.00109		.00323	.00086							
28504	.4047	.13387			.00928	.00514	.00140	.00776	.00732	.00229							
28543	.09162	.0874	.00784	.04626	.02007		.00234	.00384	.00275	.01133							
28563	.3338	.08770			.00682		.00058		.00098								
28650	.8529	1.0662			.00364	.00184	.00165	.00063	.01063								
28799	.00441		.04739		.05808				.00814			.00310	.00281	.01170	.03959		
28875	.1806	.5939	.03963		.08440		.00785		.02771	.00657		.00375					
29126	.00516	.1265	.00472		.02408		.00022		.01852	.00121							

TABLE B-1. (continued)

Initial State \ Final State	0	620	3801	3868	4276	4453	5762	5991	6249	7006	7104	7326	7646	8119	10347	10656	13128
29233		.1811				.07993	.02535		.00410	.00396							
29414			.02836			.1670						.05443	.01593	.08160	.08505	.14706	
29559	.02378	.21543	.00216						.05215			.00738		.00567			
29791		.08795	.1212		.02962	.00462	.00627		.00414	.03025		.01573	.00090	.00746			
29838	1.66273		.6133		.38725				.02055	.01982			.10401		.06659		
29866	.02764	.04577	.02758		.01772		.00271		.02256					.00182			
29958	.25831		.1262		.00148				.02059				.00955	.01512			
30222						.1148											
30451	.00671	.06249	.3439		.06347		.04446		.02733	.00339		.00825	.00817				
30499		.1075		.05145		.00853	.00033	.00353									
30587	.00293		.1397		.00729				.00140	.00934		.02550		.01263		.01838	
30637	.1086		.04967		.12702		.03504			.01242		.02614		.00620			
30676	.02682		.04126		.2823		.04877		.01980	.00347				.00448			
30986			.1362									.03122	.01586	.02184		.02193	
30993	.00883	.01333			.00490	.2474	.04124	.00512	.00667								
31221		.03787		.07579		.01409	.1417										
31270													.06007		.04586	.03152	.07822
31276	.00900		.04080		.1473				.03397			.04901	.00154	.09013	.00388		
31279			.4689									.22424	.00584	.31284	.38838		
31301			.07132		.03096				.00124	.00031		.00493	.00535		.002406		
31445			.1324									.00283	.00212	.02604	.070857		
31552			.06278		.04318		.01022		.00097	.01352		.00300					
31946	.09091				.10496	.36627	.71612	.06009	.12976								
32017	.00370		.04468		.05218				.00870	.01883		.01542	.00053	.04923	.00732	.00252	
32098	.2208		.12882		.1065				.05004	.01367		.02678	.00557	.05915	.00431	.01125	
32318	.00405				.06754	.05384		.03895	.02194								
32492	.00812	.00429			.1531		.02920		.2011								
33412	.00407	.4523			.08902		.00960		.00224	.01668		.01341		.01624			
33571	.03625		.17039		.11180				.03153	.1866			.02961	.00224	.03306	.01215	
33640	.03189	.3997	.18937						.05950	.00641		.08134		.1162			

TABLE B-2. Radiative Relative A Coefficients for U°.
State energies are in cm^{-1}.

Initial State \ Final State	0	620	3801*	4276	4453	5762	5991	6249	7006*	7526	7646	8119	10347	10686	13128
13463	.00178	.00094		.00047	.00108	.00096	.00014								
14644	.00642	.00281						.00157		.00165		.00047			
15778	.00746	.00721	.00304	.00075	.00305	.01116	.00995	.00868	.00724	.00696		.00688	.00152		
16506	.00097	.00109	.00091	.00096				.00037	.00041			.00034			
16900	.01511		.00082	.0006				.03065	.27026	.03291		.03578	.01449	.00731	
17207	.00444	.01187	.00341	.00216	.00024	.00258	.00287	.00134	.00830	.00540		.00521			
17924	.00011	.00038	.00035	.00007	.00146	.00051	.00133	.00039							
18397	.00285	.00562	.00156	.00205	.00322	.00058	.00037	.00465	.00491						
18846	.0114	.00572	.00089	.00205	.00018	.00292	.00144	.00372	.00103		.00468	.00489			
19263	.00013	.00198	.00044	.00024	.00044	.00089	.00188		.00113						
19618	.00438	.00235	.00498	.00075	.00066	.00048	.00036	.00046	.00165	.00051	.00089	.00161	.00218	.00234	.00068
19885	.02285		.00088	.00037				.00055	.00064	.00041	.00068	.00040		.00179	
20215	.00249	.00230	.00095	.00980	.00040	.00060	.00020	.00231	.00163	.00504		.00107			
20406	.00057	.00055	.00081	.00046	.00016	.00015	.00005		.00024	.00053		.00047			
20556	.00116	.00332	.01119	.00850	.00419	.00022				.00075	.00050	.00217	.00570	.00553	
20852	.00112	.00080	.00147	.00525	.00143	.00125	.00019	.00091	.00058	.00106	.00116	.00047	.00130	.00135	
21172	.00850	.00766	.00313	.00600	.00220	.00314		.00619		.00039		.00213			
21611	.12217	.02985	.06233	.00558	.00048	.02658	.00189	.01693	.00820						
21878	.00280	.00039	.00727	.00057	.00264	.00365	.00217	.00032	.00082	.00007		.00005	.00158		
22515	.10302	.05025	.02839	.01196		.01536	.00138	.04050	.01865	.00122	.00197	.00283	.00026	.00034	
22600	.00007	.00061	.01198	.00285	.00019	.00064	.00018	.00197	.00102	.00177	.00058	.00060	.00086		
22989	.13052		.06533	.00930				.12715	.03957	.02433	.05356	.00029		.01228	
23285	.00079	.00049	.00068	.00199	.00297	.00339	.00302	.00216	.00470		.00013	.00058			
23691	.33392	.11414	.03745	.01025	.02227	.01441	.02160	.00553	.02798	.00629	.00375	.00074			
23697	.08582		.00466	.00117	.00035			.00606	.00155	.00101	.00008	.00035	.00031	.00033	

TABLE B-2. (continued)

Initial State \ Final State	0	620	3801*	4276	4453	5762	5991	6249	7006*	7326	7646	8119	10347	10686	13128
24430	.10158	.15602	.02024	.04486		.12010		.09624	.06710	.11471		.27023		.01270	
24558	.02298	.02127	.03370	.00808	.00029	.00503	.02329	.00957	.02106	.01003	.00230	.03157	.00266	.00039	.00076
25451	1.0081	1.1057	.03262	.09464		.02916	.00903	.48084	.08414	.08258	.04428	.11297	.00860		
25645			.00061							.00204	.00253	.00177	.00092	.00038	.00146
25997	2.017	.60514	.17187	.01778		.05065	.00671	.04288	.16779	.07370		.11731			
26209	.06236	.02164	.01737	.00592		.00401		.00305	.00725	.14499	.00519	.00884	.01634	.00712	.00321
26531	.00032		.01779	.00205				.00619	.00359	.00554	.01760	.01242	.01758	.00123	.00617
26754	.43339	.34352	.06505	.02978	.01632	.04488	.04503	.04403	.06542						
27392	.09811	.08203	.13656	.01018	.00639	.02222	.00065	.01249	.00641	.02532	.00422	.00922	.00610	.00824	.00066
27787	.36304	.37204	.15887	.04861	.00089	.00381		.01976	.01347	.01425	.00571	.02319	.03115	.00228	.00176
27914	1.5716	.5192	.10228	.05117				.06527	.01020			.00584			
28192	1.6500	.53627	.19967	.08829		.00696		.06450	.06807	.03128	.00182	.03004	.08263	.40722	.00697
28556	.95992	.48037	.16532	.09535	.00582	.00541	.01160	.01758	.03615	.00510	.00281	.01170	.02959		
28763	1.0335	1.6601	.03963	.08804	.00164	.00951	.00063	.03834	.00657	.00375					
29425	.02829	.61098	.15643	.05370	.25145	.03185		.07891	.03541	.07754	.01683	.09473	.08505	.14706	
29838	1.6627		.6133	.38725				.02055	.01982		.10401		.06659		
30015	.28594	.04577	.15378	.01920	.1148	.00271		.04316			.00955	.01693			
30718	.15390	.18332	.76218	.48502	.25593	.16985	.00865	.05520	.02022	.09111	.02404	.04515		.04030	
31344	.00900	.03787	.38309	.22144	.01409	.15192		.03619	.01363	.05976	.06908	.11617	.07300	.03152	.078222
31613	.09091		.4689	.10496	.36627	.71612	.06009	.12976		.22723	.00584	.31284	.38838		
32231	.23675	.00429	.17351	.37932	.05384	.02920	.03895	.28178	.03271	.04220	.00620	.10838	.01163	.01377	
33541	.07221	.852	.35976	.20082		.00960		.09326	.20969	.09476	.02961	.13667	.03306	.01215	

TABLE B-3. U° Relative $\sum A$ Coefficients

State energies are in cm^{-1}.

Initial State \ Final State	0	620	3801*	4276	4453	5762	5991	6249	7006*	7326	7646	8119	10547	10686	13128	<A> x10^8
13463	.00178	.00094		.00047	.00108	.00096	.00014									.00526
14644	.00642	.00281						.00157		.00165		.00047				.01265
15778	.00249	.00240	.00152	.00075	.00152	.00372	.00995	.00289	.00241	.00232		.00344	.00152			.01808
16506	.00097	.00109	.00091	.00096				.00037	.00041			.00034				.00493
16900	.01511		.00082	.0006				.03065	.27026	.03291		.03578	.01449	.00731		.39913
17207	.00148	.00297	.00341	.00072	.00012	.00086	.00144	.00067	.00208	.00280		.00261				.01176
17924	.00011	.00019	.00035	.00007	.00073	.00025	.00041	.00039								.00146
18397	.00143	.00208	.00078	.00205	.00161	.00058	.00037	.00232	.00164							.00842
18846	.0057	.00286	.00089	.00103	.00018	.00146	.00144	.00186	.00103		.00468	.00489				.01904
19263	.00014	.00067	.00044	.00024	.00015	.00089	.00063		.00057							.00233
19618	.00219	.00117	.00125	.00075	.00066	.00024	.00036	.00046	.00055	.00025	.00089	.00081	.00109	.00117	.00068	.00587
19885	.02285		.00088	.00037				.00055	.00064	.00041	.00068	.00040		.00179		.02795
20215	.00124	.00077	.00095	.00327	.00040	.00030	.00020	.00117	.00054	.00504		.00107				.00874
20406	.00057	.00055	.00041	.00046	.00016	.00015	.00005		.00024	.00053		.00047				.00194
20556	.00116	.00166	.00280	.00425	.00419	.00011				.00038	.00050	.00072	.00285	.00276		.01057
20852	.00037	.00040	.00073	.00131	.00072	.00042	.00019	.00030	.00014	.00053	.00116	.00024	.00130	.00135		.00360
21172	.00425	.00383	.00313	.00300	.00220	.00157		.00309		.00039		.00213				.01925
21611	.06109	.01493	.06233	.00279	.00048	.02658	.00095	.00822	.00410							.13382
21878	.00140	.00018	.00182	.00028	.00132	.00182	.00108	.00016	.00041	.00007		.00005	.00788			.00546
22515	.01717	.01005	.00473	.00239		.00384	.00138	.00675	.00466	.00030	.00098	.00071	.00026	.00034		.04498
22600	.00003	.00030	.00600	.00095	.00019	.00064	.00018	.00099	.00051	.00088	.00029	.00030	.00043			.00459
22989	.06526		.03267	.00465				.06358	.01978	.01216	.02678	.00029		.01228		.22618
23285	.00039	.00024	.00068	.00100	.00099	.00113	.00100	.00108	.00118		.00013	.00058				.00514
23691	.11131	.05707	.01872	.00342	.02228	.01441	.02160	.00276	.01399	.00315	.00375	.00074				.19281

TABLE B-3. (continued)

Initial State \ Final State	0	620	3801*	4276	4457	5762	5991	6249	7006*	7326	7646	8119	10347	10686	13128	<A> x10^8
23597	.04291		.00233	.00058	.00035			.00303	.00077	.00050	.00008	.00017	.00015	.00035		.04975
24430	.03386	.07801	.00675	.01496		.06005		.03208	.02237	.03824		.09008		.01270		.32739
24558	.01149	.02127	.00843	.00404	.00029	.00503	.02329	.00479	.01053	.00334	.00230	.010522	.00089	.00039	.00076	.03360
25451	.25202	.36858	.01087	.02366		.01458	.00903	.12021	.02805	.04129	.04428	.03766	.00869			.07565
25645			.00031							.00102	.00126	.00089	.00046	.00016	.00049	.00317
25997	.67233	.20171	.05729	.00889		.05065	.00671	.04288	.08390	.07370		.05867				1.06680
26209	.06236	.02164	.00868	.00592		.00401		.00305	.00725	.07249	.00519	.00884	.01634	.00712	.00321	.15034
26531	.00052		.00889	.00205				.00619	.00359	.00554	.00880	.00621	.00879	.00123	.00617	.04426
26754	.14446	.11451	.02168	.01489	.01632	.01496	.04503	.01468	.02181							.35467
27392	.03270	.04101	.04552	.00339	.00639	.01111	.00065	.00416	.00214	.00844	.00211	.00307	.00203	.00824	.00033	.83912
27787	.09076	.12401	.03972	.01620	.00089	.00381		.00494	.00449	.00712	.00571	.01159	.01558			.20720
27914	.7858	.2596	.05114	.05117				.03214	.00510			.00584				1.10981
28192	.33	.13407	.03993	.02207		.00348		.01075	.01134	.00782	.00182	.01502	.02754	.20361	.00697	.51756
28556	.19198	.09607	.03306	.01905	.00291	.00135	.00580	.00293	.00904	.00310	.00281	.01170	.03959			.29584
28763	.51675	.83005	.03963	.04402	.00184	.00475	.00063	.01917	.00657	.00375						1.40993
29425	.01414	.15275	.03911	.02685	.08382	.01062		.01973	.01180	.02585	.00841	.03158	.08505	.14706		.32647
29838	1.6627		.6133	.38725				.02055	.01982		.10401		.06659			2.81238
30015	.14297	.04577	.07689	.00960	.1148	.00271		.02158			.00955	.00847				.22565
30718	.03078	.06111	.12703	.09700	.12797	.03397	.00432	.01360	.00505	.02278	.01202	.01129		.02015		.32077
31344	.00900	.03787	.07662	.07381	.01409	.07596		.01206	.00692	.01494	.01727	.05809	.01825	.03152	.07822	.21122
31613	.09091		.4689	.10496	.36627	.71612	.06009	.12976		.11362	.00584	.31284	.38838			1.40328
32231	.05919	.00429	.08675	.09483	.05384	.02920	.03895	.07045	.01635	.02110	.00510	.05419	.00582	.00689		.34553
33541	.02407	.426	.17988	.10041		.00960		.03109	.06990	.04738	.02961	.04556	.03306	.01215		.68610

TABLE B-4. Relative A Coefficients for Singlely Ionized Uranium.
State energies are in cm^{-1}.

Initial State \ Final State	0	289	915	1749	2295	4421	4585	4706	5260	5402	5526	5667	5791	6283	6445	8394
18200	.00605	.00162	.00192		.00251											
20572	.00451		.00183					.00139		.0020		.00124				
20962	.00499		.00234					.00623		.00024		.00134				
21021	.00674		.00237					.00674		.00017		.00018			.00056	
21320	.01239		.00981							.00064		.00832			.00016	
21711		.01020		.00654			.00169		.00354				.00026			
22101	.00032	.00038			.00100	.00077						.00027			.00048	
22165	.00555	.01034	.00159	.00120	.00092	.00491	.00944			.00260		.00047	.00403			
22430	.00270	.01985	.01706			.00870				.00099		.01118			.00036	
22642	.01245	.05108	.00399		.00430	.00293						.02838	.00044		.07049	
22868		.00981	.00316									.01258			.00072	
22917	.01864	.00294	.04905	.01134	.00459	.00570	.01905								.01015	
23241	.01297	.00646	.00577	.00126	.00661	.00175	.00055			.00781			.01513	.00817	.00056	
23315	.02201	.06837	.01292		.00027					.000728		.01123		.01761		
23554	.13167	.01595	.01364	.00407	.00713	.00108					.00651		.00047	.00070	.00067	
23636		.02218		.00726	.00582		.00211		.00042					.00459		
23778	.02137		.01577	.01503	.00329	.00257							.00082		.01253	
23912	.00361	.00791	.01494			.00377				.00139		.01333			.00128	
24010	.04624	.00972	.00492	.00908	.02133	.00733	.00008						.00130		.00131	
24153	.02323	.03693	.00253	.00032	.01236	.00305							.00135	.00095		
24160		.02354		.01582	.00742	.03423			.00357					.00790		.00470
24288	.11178	.03470	.00092	.01049	.01236		.00549				.00258			.00066	.00080	
24306	.01497	.00269	.00897		.00022	.00410				.00082		.00077			.00100	
24342	.02832		.01508					.01216		.00163					.00621	
24453	.03881	.00019	.01136		.00428	.00452				.00084		.00069			.00103	
24608	.13103	.07989	.00986	.01050	.00183		.00379						.00070	.01251	.00150	
24684	.24648	.06503	.00038		.00586	.00176				.00278		.00209	.00577		.00262	
25164		.04737		.01804		.00315	.00530		.00135		.00072		.00398	.00022		.00111
25357	.03397	.15349		.16678	.02199	.06828										
25714	.00082	.03701	.02686	.17207	.01331	.00403	.00864		.00088	.00168			.00518	.00115		
25968	.07213		.07651		.01092			.01841	.00640	.03636		.04521		.00043		
25986	.44247	.04236		.05519			.00738	.00357	.00015		.00184		.00173	.00042		
26191		1.0000		.3096	.00795	.00152	.01842		.00117		.00149		.00501	.00576		
26415		.16154		.02658	.01963	.00493	.01087				.00639		.00296			.00199
26717		.44334		.05729	.00294		.01821							.01059	.00868	
26887							.00132		.00291					.00279		.00093
27126	.00018	.00086	.08400		.01278					.00518		.00105	.00525		.00082	
27290	.00017		.01953					.00614		.00033		.00217			.00055	
27357	.03931	.03156	.08898	.01328	.03157	.00677	.01880						.00628	.00287	.00678	
27390			.05767	.02680							.01404					

TABLE B-4. (continued)

Initial State \ Final State	0	289	915	1749	2295	4421	4585	4706	5260	5402	5527	5667	5791	6283	6445	6394
27499	.02684	.01491	.00197	.09629	.04205	.00822	.00665				.05974	.00397	.00076	.00022		
27930	.02350	.12754	.14669	.02680	.11957	.02070	.01774		.00069		.00571		.00711	.00459		.00545
28154	.23431		.62061	.00455	.38475	.01626	.11714						.00257	.00310		
28508	.05460		.06783	.01717	.08404	.00269	.01704				.00205			.00221		
28578		.01526	.03459	.09122		.01808										
28758	.02480	.03171	.05868		.00381	.00150	.01268				.00475			.00038		
29207	.00922	.02877	.05868	.05737	.06076	.02578					.00532			.00575		
29477		.04684		.02773	.00258	.02123	.01704		.00098		.02743		.00348	.00570		
29828	.02297	.06234	.01083	.02874	.00005	.00272					.00178		.00143	.00116		.00220
29932				.07868			.04357	.03290	.08192					.00796		
29936	.02834	.06407	.00718	.04922		.01514	.00988				.00647		.00009	.00237		
30061	.04745	.08084	.00571	.08039	.00628	.03644	.03499							.00232	.00013	
30086	.00916	.02219	.00882	.00022	.00352	.03928	.00065				.00501			.006615		
30240	.36416	.12304	.02672	.06908	.00907	.00006	.01883				.00324			.01717	.00028	
30264			.05941			.02464				.00267	.00087		.02730			
30342				.11996			.201		.19264		.00091			.03522		.00631
30469	.00143		.02086			.00229										
30550		.08805	.02060	.00165	.00840		.00276				.00927		.00895	.00760	.00030	
30860		.16207	.04607	.06837	.02312	.01768	.01735	.01743		.01422				.07602	.00855	
30863		.02703		.00335	.05418				.04642				.00023			.00053
30942				.1523			.1307		.12098		.00184			.04491		.00609
31084	.00271	.08579		.03077	.03438	.02186	.00205				.00573		.00049	.00796	.00027	.00355
31219		.27626		.02409	.00331		.00328				.00959		.01934	.01967		
32211					.1372		.00118				.16879		.10113	.00275		.02157
32535					.49839		.00110				.29286		.15078	.00229		.06109
33104		.12788		.09897	.05740	.01552	.02651		.05418		.00755		.01029	.00339		.00207
33475		.07034		.07255	.06310				.04953		.01442			.05750		.00655
33749	.01140	.13205		.01000	.01223		.00458						.00250			
34049		.00906		.14006	.00731	.02075	.02040		.06601					.01076		.09405
34439	.09716	.29306			.00026	.00097	.00077				.00619		.00432			
34708		.24164		.33175	.07210		.02863		.09477					.03136		.05540
34886	1.0906	1.2651	.23678	.20837		.00025	.00986									
34924		20441			.06096		.00019		.00305		.00038		.0375	.00039		.00001
35685		.49781	.23813	.19199	.00892											
35790		.2238		.08767	.41889		.01908		.00025		.01009		.02335			
36789		.41373		.22663	.14759				.06888		.00481					
37308							.00779		.28886		.24525					
39109	1.3096	.05016		.41466	.26978											
39508							.11014		.16184		.1187			.00112	.03102	

TABLE B-5. Radiative Relative A Coefficients for U^*.
State energies are in cm^{-1}.

Initial State \ Final State	0	289	915	1749	2295	4421	4585*	5330*	5596*	5791	6283	6445	8394	<A> x10^8
18200	.00605	.00162	.00192		.00251									.02652
20851	.00483		.00218				.00479	.0002	.00050			.00056		.03006
21516	.01239	.01020	.00981	.00654			.00169	.00209	.00832	.00026		.00016		.05864
22101	.00032	.00038			.00100	.00077			.00027			.00048		.00702
22298	.00413	.01510	.00933	.00120	.00092	.00680	.00944	.00180	.00583	.00403		.00036		.11160
22780	.01545	.02701	.02652	.01134	.00445	.00432	.01905	.02838	.00044			.00054		.32361
22868		.00981	.00316					.01258				.07049		.08164
23370	.05555	.03026	.01077	.00276	.00467	.00141	.00055	.00427	.00887	.00780	.00883	.00562		.27891
23778	.01249	.01505	.01535	.01114	.00456	.00317	.00211	.00091	.01333	.00082	.00459	.00691		.11680
24183	.06042	.02622	.00279	.00893	.01782	.01267	.00278	.00357	.00258	.00132	.00317	.00106	.00470	.24769
24367	.02737	.00144	.01180		.00230	.00431	.01216	.00110	.00073			.00241		.11591
24818	.18876	.06410	.00512	.01427	.00384	.00245	.00455	.00206	.00140	.00348	.00637	.00206	.00111	.48594
25680	.03564	.09525	.05168	.16942	.01541	.03616	.01352	.01133	.04521	.00518	.00079			.71728
26091	.42247	.52118		.18240	.00795	.00152	.00979	.00066	.00167	.00337	.00309			2.06537
26303		.30244		.04194	.01128	.00493	.01454		.00639	.00296	.01059	.00868	.00199	.84973
27088	.00017		.01953				.00373	.00162	.00217		.00279	.00055	.00093	.04035
27357	.02211	.01577	.05815	.04546	.02879	.00750	.01273	.00518	.01919	.00517	.00181	.00261		.39334
28042	.12891	.12754	.38365	.01567	.25216	.01848	.06744	.00069	.00571	.00484	.00384		.00545	2.06903
28614	.03970	.02348	.05370	.05419	.02392	.00743	.01486		.00340		.00130			.39794
29504	.01609	.04599	.03476	.03795	.02113	.01641	.01704	.00098	.01151	.00246	.01261		.00220	.39305
30061	.02832	.05570	.02028	.05213	.00490	.02887	.02440	.04224	.00412	.01370	.00481	.00013		.40855
30291	.36416	.12304	.02672	.09452	.00907	.00006	.10992	.19264	.00208		.02620	.00028	.00631	1.30065
30627	.00143	.05754	.02073	.00250	.03129	.00229	.00276	.04642	.00927	.00459	.00760	.00030	.00053	.22189
30901		.16207	.04607	.11033	.02312	.01768	.05516	.06760	.00184		.06047	.00855	.00609	1.94307
31152	.00271	.18103		.02743	.01884	.02186	.00266		.00776	.01292	.01382	.000272	.00355	.61006
32373					.31780		.00114		.23083	.12591	.00152		.04133	1.57597
33290		.09911		.08576	.06025	.01552	.02651	.05186	.01099	.01029	.03044		.00136	.67540
33749	.01140	.13205		.01000	.01223		.00458			.00250				.37839
34471	.09616	.17186		.14006	.02284	.01086	.00712	.03453	.03282	.02091	.00558		.04703	.69497
34797	1.0906	.75337	.23678	.27006	.07210	.00025	.01925	.09477			.03136		.05540	4.01523
35738		.36081	.23813	.13983	.21390		.01908	.00025	.01009	.02335				1.88352
37049		.41373		.22663	.14759		.00779	.17887	.12503					1.53699
39309	1.3096	.05016		.41466	.26978		.11014	.16184	.1187		.00111		.03102	2.70158

TABLE B-6. $U^{\bullet}$ Relative $\sum A$ Coefficients

State energies are in cm^{-1}.

Initial State \ Final State	0	289	915	1749	2259	4421	4585*	5330*	5596*	5791	6283	6445	8394
18200	.00650	.00162	.00192		.00251							.00056	
20851	.1448		.00981	.00654			.01436	.00060	.00155			.00016	
21516	.01239	.01020	.00981	.00654			.00109	.00419	.00832	.00026		.00048	
22101	.00032	.00038			.00100	.00077			.00027			.00036	
22298	.00825	.03019	.01866	.00120	.00092	.01361	.00944	.00359	.01165	.00403		.00108	
22780	.03109	.05402	.05304	.01134	.00869	.00863	.01905		.02838	.00044		.07049	
22868		.00981	.00316						.01258		.02648	.00124	
23370	.06665	.09078	.03232	.00532	.01401	.00282	.00055	.00859	.01774	.01560	.00459	.01381	
23778	.01498	.03009	.03070	.02228	.00912	.00634	.00211	.00182	.01333	.00082	.00950	.00210	.00470
24153	.18125	.1090	.00837	.03572	.05346	.03801	.00557	.00357	.00258	.00265		.00824	
34367	.0821	.00289	.03541		.00460	.00862	.01216	.00329	.00146		.01273	.00412	.00111
24818	.37751	.19230	.01024	.02855	.00768	.00491	.00909	.00411	.00281	.01045	.00158		
25680	.10692	.19050	.10337	.33885	.04622	.07231	.02905	.04532	.04521	.00518	.00619		
26091	.42247	1.04236		.36479	.00795	.00152	.02936	.00132	.00333	.00674	.01059	.00868	.00199
26303		.60488		.08387	.02257	.00493	.02909		.00639	.00296	.00279	.00055	.00093
27088	.00017		.01953				.00746	.00325	.00217		.00363	.00782	
17357	.06633	.04732	.23262	.13637	.08640	.01499	.02546	.00518	.07676	.01550	.00769		.00545
28042	.25781	.12754	.7673	.03134	.50432	.03695	.13488	.00069	.00571	.00968	.00260		
28614	.06940	.04696	.16110	.10838	.08785	.02228	.02972		.00680		.00420		.00220
29504	.03219	.13796	.06951	.11384	.06338	.04923	.01704	.00098	.03453	.00491	.01927	.00013	
30061	.08496	.16710	.08112	.20851	.00980	.11560	.12199	.08448	.01235	.02739	.05239	.00028	.00631
30291	.36416	.12304	.02672	.18904	.00907	.00006	.21983	.19264	.00416		.00760	.00030	.00053
30627	.00143	.11508	.04146	.00500	.06259	.00229	.00276	.04642	.00927	.00918	.12093	.00855	.00609
30901		.16207	.04607	.22067	.02117	.01768	.16549	.13521	.00184		.02764	.00027	.00355
31152	.00271	.36205		.05486	.03768	.02166	.00533		.01552	.02583	.00304		.08266
32373					.63559		.00228		.46165	.25181	.05089		.00272
33290		.19822		.17152	.12050	.01552	.02651	.10371	.02197	.01029			
33749	.01140	.13205		.01000	.01223		.00458			.00250	.01115		.09405
34471	.09716	.50653		.14006	.06852	.02172	.02135	.06905	.00656	.04182	.01115		.09405
34797	1.0906	1.50674	.23678	.54012	.07210	.00025	.03849	.09477			.03136		.05540
35738		.72161	.23813	.27966	.42781		.01903	.00025	.01009	.02335			
37049		.41373		.22663	.14759		.00779	.35774	.25006				
35309	1.3096	.05016		.41466	.26978		.11014	.16184	.1187		.00111		.03102

APPENDIX C. THREE STATE RATE EQUATIONS

The formalism for solving the rate equations for a three state plasma, will be developed here because it is used in the simple examples used in the text.

For a three state gas the rate equations can be written

$$\frac{dN_1}{dt} = R_{12}\, N_2 + R_{13}\, N_3 + R_{C1} - (R_{21} + R_{31} + R_{I1})\, N_1 , \qquad \text{(C-1a)}$$

$$\frac{dN_2}{dt} = R_{21}\, N_1 + R_{23}\, N_3 + R_{C2} - (R_{12} + R_{32} + R_{I2})\, N_2 , \qquad \text{(C-1b)}$$

$$\frac{dN_3}{dt} = R_{31}\, N_1 + R_{32}\, N_2 + R_{C3} - (R_3 + R_{23} + R_{I3})\, N_3 , \qquad \text{(C-1c)}$$

where R_{ij} is the rate that state j goes to state i (both collisionally and radiatively), R_{Ci} is the recombination rate into state i and R_{Ii} is the ionization rate from state i.

In the steady state problem and when the total number of atoms of the species is known (N_o) Eq. (C-1b) be rewritten

$$R_{21}(N_o - N_1 - N_2) + R_{23}\, N_3 - (R_{12} + R_{32} + R_{I2})\, N_2 = R_{C2} , \qquad \text{(C-2)}$$

combining terms and letting

$$A_2 = R_{12} + R_{23} + R_{I2} + R_{21} , \qquad \text{(C-3a)}$$

$$B_2 = R_{23} - R_{21} , \qquad \text{(C-3b)}$$

$$C_2 = R_{C2} + R_{21}\, N_o . \qquad \text{(C-3c)}$$

Eq. (C-2) can be rewritten as

$$-A_2 N_2 + B_2 N_3 = -C_2 \cdot \qquad \text{(C-4)}$$

Similarily Eq. (C-1c) can be rewritten

$$B_3 N_2 - A_3 N_3 = -C_3 \cdot \qquad \text{(C-5)}$$

Therefore, the state densities are

$$N_2 = \frac{C_3B_2 + C_2A_3}{A_2A_3 - B_2B_3} , \qquad \text{(C-6a)}$$

$$N_3 = \frac{C_2B_3 + C_3A_2}{A_2A_3 - B_2B_3} , \qquad \text{(C-6b)}$$

$$N_1 = N_o - (N_2 + N_3) \cdot \qquad \text{(C-6c)}$$

To show how these are used let state 3 be the 3.9605 eV state in neutral uranium and state 2 account for all upper state interactions with state 3. Also the interaction with the ground state will be that of the 1.6691 eV state. The rates used will be for a neutron flux of 2×10^{14} neutrons/(cm^2-sec) and a temperature of 8000°K. Hence, the total neutral uranium density is 2.58×10^{17} atoms/cm^3. The other rate constants will be found in Table (C-1) and give values of 2.56×10^{17} atoms/cm^3 for N_1, 1.15×10^{15} atoms/cm^3 for N_2 and 9.63×10^{14} atoms/cm^3 for N_3.

	A, sec^{-1}	B, sec^{-1}	C, $(sec\text{-}cm^3)^{-1}$
2	1.932×10^{13}	1.226×10^{13}	1.0461×10^{28}
3	1.666×10^{13}	1.231×10^{13}	1.8598×10^{27}

Table C-1. Rate constants for Eq. (C4) and Eq. (C5) for a flux of 2×10^{14} neutrons/$(cm^2\text{-sec})$ and a temperature of 8000°K.

REFERENCES

1. C. Bathke and G. H. Miley, "Non-Equilibrium Uranium Plasmas and Applications," IEEE Conference Record--Abstracts, 2nd International Conf. on Plasma Science, Ann Arbor, p. 79 (1975).

2. D. R. Bates, A. E. Kingston and R. W. P. Whirter, "Recombination Between Electrons and Atomic Ions I. Optically Thin Plasmas," Proc. Roy. Soc. 267, 297 (1962).

3. D. R. Bates, A. E. Kingston and R. W. P. McWhirter, "Recombination Between Electrons and Atomic Ions II. Optically Thick Plasmas," Proc. Roy. Soc. 270, 155 (1962).

4. N. L. Krascella, "Theoretical Investigation of the Spectral Opacities of Hydrogen and Nuclear Fuel," Air Force Systems Command Report RTD-TDR-63-1101 prepared by United Aircraft Research Laboratories (1963).

5. H. H. Helmick, G. A. Jarvis, J. S. Kendall and T. S. Latham, "Preliminary Study of Plasma Nuclear Reactor Feasibility," LA-5679 (1974).

6. R. C. Stoeffler and J. S. Kendall, "Conceptual Design Studies and Experiments Related to Cavity Exhaust Systems for Nuclear Light Bulb Configurations," United Aircraft Research Lab Report L-910900-15 (1972).

7. W. Bernard, H. H. Helmick, G. A. Jarvis, E. A. Plassmann and R. H. White, "Research Program on Plasma Core Assembly," LA-5971-MS (1975).

8. R. J. Rogers, T. S. Latham and H. E. Bauer, "Analytical Studies of Nuclear Light Bulb Engine Radiant Heat Transfer and Performance Characteristics," United Aircraft Research Lab Report K-910900-10 (1971).

9. D. E. Parks, et al., "Optical Constants of Uranium Plasmas," NASA CR 72348, N.T.I.S., Springfield, VA 22151 (1968).

10. E. L. Maceda and G. H. Miley, "Non-Maxwellian Electron Excitation in Helium," Proc. 27th Annual Gaseous Electronics Conf., Houston, Texas (1974).

11. G. R. Shipman, R. A. Walters and R. T. Schneider, "Population Inversions in Fission Fragment Excited Helium," Trans. Am. Nuc. Soc., 17, p. 3 (1973).

12. G. Cooper, "Recombinational Pumped Atomic Nitrogen and Carbon Afterglow Lasers," Ph.D. Thesis, Nuclear Engineering Program, University of Illinois, Urbana (1976).

13. T. Holstein, "Imprisonment of Resonance Radiation in Gases," Phys. Rev., vol. 72, p. 1212 (1947).

14. T. Holstein, "Imprisonment of Resonance Radiation in Gases," Phys. Rev., vol. 83, p. 1159 (1951).

15. T. J. Love, Radiative Heat Transfer, Charles E. Marrill Pub. Co., Columbus, (1968).

16. G. C. Pomraning, The Equations of Radiation Hydrodynamics, Pergamon Press, New York (1973).

17. T. L. Eddy, E. Pfender and E. R. G. Eckert, "Spectroscopic Mapping of the Nonequilibrium Between Electron and Excitation Temperatures in a Latin Helium Arc," IEEE Trans. Plasma Sci., PS-1, p. 32 (1973).

18. T. L. Eddy, "The Continuum Emission Coefficient Relation for the Multi-thermal Equilibrium Model of Non-LTE Plasmas," Bull. APS, 20, p. 248 (1975).

19. K. Thom, R. J. Schneider and F. C. Schwenk, "Physics and Potentials of Fissioning Plasmas for Space Power and Propulsion," XXVth Congress International Astronuatical Federation, Amsterdam (1974).

20. R. T. Schneider and K. Thom, "Fissioning Uranium Plasmas and Nuclear Pumped Lasers," Nuc. Tech., 27, p. 34 (1975).

21. J. R. Williams and J. D. Clement, "Exploratory Study of Several Advanced Nuclear-MHD Power Plant System,s" Final Status Report, NASA Grant NGR-11-003-145, Georgia Inst. of Tech. (1973).

22. R. J. DeYoung, M. A. Akerman, W. E. Wells and G. H. Miley, "Studies of Radiation-Induced Laser Plasmas," IEEE Conf. on Plasma Science, Ann Arbor, Mich. (1975).

23. G. H. Miley, "Nuclear Radiation Effects on Gas Lasers," Laser Interactions and Related Plasma Phenomena, 2, p. 43, Schwartz and Hora, Eds., Plenum Press (1972).

24. A. Maitland and M. H. Dunn, Laser Physics, North-Holland Publishing Co., London (1969).

25. G. Bekefi, Radiation Processes in Plasmas, John Wiley and Sons, New York (1966).

26. M. Mitchner and C. H. Kruger, Partially Ionized Gases, John Wiley & Sons, New York (1973).

27. C. Bathke, "Calculation of the Electron Energy Distribution Function in a Uranium Plasma by Analytic and Monte Carlo Techniques," Ph.D. Thesis, Nuclear Engineering Program, University of Illinois, Urbana (1976).

28. V. V. Sobulev, A Treatise on Radiative Transfer, p. 9, D. Van Nostrand Co., Inc., New York (1963).

29. J. Guyot, "Measurement of Atomic Metastable Densities in Noble Gas Plasmas Created by Nuclear Radiation," Ph.D. Thesis, Nuclear Engineering Program, University of Illinois, Urbana (1971).

30. W. S. C. Chang, Principles of Quantum Electronics, Addison-Wesley Publishing Co., Reading, Mass. (1969).

31. M. Hercher, "An Analysis of Saturable Absorbers," Applied Optics 6, P. 947 (1967).

32. W. F. Meggers, C. H. Corliss and B. F. Scribner, Tables of Spectral Line Intensities, NBS Monograph 32 p. 1, Washington (1961).

33. D. W. Steinhaus, L. J. Radzienski, R. D. Cowan, Et al., "Present Status of the Analysis of the First and Second Spectra of Uranium (UI and UII) as Derived from Measurements of Optical Spectra," LA-4501 (1971).

34. D. W. Steinhaus, M. V. Phillips, J. B. Moody, et al., "The Emission Spectrum of Uranium Between 19,080 cm^{-1} and 30,261 cm^{-1}, LA-4944 (1972).

35. J. F. Klose, "Mean Life of the 27887 cm^{-1} Level in UI," Phys. Rev. A., 11, p. 1940 (1975).

36. L. Vriens, "Electron Exchange in Binary Encounter Collision Theory," Proc. Phys. Soc., 89, p. 13 (1966).

37. A. Burgess and I. C. Percival, Adv. Atom. Molec. Phys., 4, p. 109 (1968).

38. M. Gryzinski, "Classical Theory of Atomic Collisions I, Theory of Inelastic Collisions," Phys. Rev., 138, p. A336 (1965).

39. V. I. Ochkur and A. M. Petrun'kin, "The Classical Calculation of the Probabilities of Excitation and Ionization of Atoms by Electron Impact," Soviet Phys.-Optics and Spectroscopy, 14, p. 245 (1963).

40. S. G. Rautian and w. I. Sobel'man, "The Effect of Collisions on the Doppler Broadening of Spectral Lines," Soviet Phys. Uspekhi, 9, p. 701 (1967).

41. A. E. Siegman, An Introduction to Lasers and Masers, McGraw-Hill Book Co., NY (1971).

42. R. G. Breene, "Line Shape," Rev. Mod. Phys., 29, p. 94 (1957).

43. R. G. Breene, The Shift and Shape of Spectral Lines, Pergamon Press, NY (1961).

44. C. H. Corliss and W. R. Bosman, Experimental Transition Probabilities for Spectral Lines of Seventy Elements, NBS Monograph 53, Washington (1962).

45. N. L. Krascella, "The Spectral Properties of Uranium Hexafluoride and its Thermal Decomposition Products", NASA CR-145047, Washington (1976).

46. W. C. Roman, "Plasma Core Reactor Simulations Using RF Uranium Seeded Argon Discharges", NASA CR-2719, Washington, (1976).

47. R. J. Rogers, T. S. Latham and N. L. Krascella, "Analysis of Low-Power and Plasma Core Cavity Reactor Experiments," United Aircraft Research Laboratories Report R75-911908-1, (1975).

48. R. J. Rogers and T. S. Latham, "Analytic Design and Performance Studies of the Nuclear Light Bulb Engine," United Aircraft Research Laboratories Report L-910900-16, (1972).

49. R. Lo, "Energy Distributions of Electrons in Radiation Induced Helium Plasmas," Ph.D. Thesis, Nuclear Engineering Program, University of Illinois, Urbana, Illinois, (1972).

50. L. R. Carlson, S. A. Johnson, E. F. Warden, C. A. May, R. W. Solar and J. A. Paisner, "Determination of Absolute Atomic Transition Probabilities Using Time Resolved Optical Pumping", Preprint UCRL-78662, Livermore (1976).

51. M. Makowski, "Calculation of Electron Energy Distributions for Uranium and Helium Mixtures", Master's Thesis, Nuclear Engineering Program, University of Illinois, Urbana, Illinois (1977).

52. Shih-I Pai, Radiation Gas Dynamics, p. 11-12, Springer-Verlag, New York (1966).

53. M. Abramowitz and I. A. Stegan, Handbook of Mathematical Functions: with Formulae, Graphs and Mathematical Tables, p. 228-230, NBS, Applied Math. Series 55, Washington (1964).

54. Hottel and Sarofin, Radiative Transfer, McGraw-Hill Book Co., New York (1967).

VITA

Edward Louis Maceda was born in [redacted]. He received the B.S. degree in Physics from Manhattan College at Bronx, New York in 1970. He enrolled at the University of Illinois at Urbana-Champaign in the Department of Physics where he held a position as a teaching assistant for two years. Upon receiving the M.S. degree in Physics in 1972, he transferred to the Nuclear Engineering Program at the University of Illinois where he became a research assistant.

As a Ph.D. candidate in the Nuclear Engineering Program, he has co-authored a number of papers which have appeared in such journals as the A.N.S. Transactions. He is also a member of the American Nuclear Society and the American Physical Society.